SENSING AND MOLECULAR COMMUNICATION USING SYNTHETIC CELLS: THEORY AND ALGORITHMS

A Dissertation
Presented to
The Academic Faculty

By

Arash Einolghozati

In Partial Fulfillment
of the Requirements for the Degree
Doctor of Philosophy
in
Electrical and Computer Engineering

School of Electrical and Computer Engineering
Georgia Institute of Technology
August 2016

SENSING AND MOLECULAR COMMUNICATION USING SYNTHETIC CELLS: THEORY AND ALGORITHMS

Approved by:

Dr. Faramarz Fekri, Chair, Advisor
Professor, School of Electrical and Computer Engineering
Georgia Institute of Technology

Dr. Christopher J. Rozell
Associate Professor, School of Electrical and Computer Engineering
Georgia Institute of Technology

Dr. Raghupathy Sivakumar
Professor, School of Electrical and Computer Engineering
Georgia Institute of Technology

Dr. Howard Weiss
Professor, School of Mathematics
Georgia Institute of Technology

Dr. Steven McLaughlin
Professor, School of Electrical and Computer Engineering
Georgia Institute of Technology

Date Approved: July 18, 2016

To my mother, father and my sisters,

without whom this would be impossible.

TABLE OF CONTENTS

LIST OF FIGURES

SUMMARY

Molecular communication (MC) is a novel communication paradigm in which molecules are used to encode, transmit and decode information. MC is the primary method by which biological entities exchange information and hence, cooperate with each other. MC is a promising paradigm to enable communication between nano-bio machines, e.g., biosensors with potential applications such as cancer and disease detection, smart drug delivery, toxicity detection etc.

The objective of this research is to establish the fundamentals of diffusion-based molecular communication and sensing via biological agents (e.g., synthetic bacteria) from a communication and information theory perspective, and design algorithms for reliable communication and sensing systems. In the first part of the thesis, we develop models for the diffusion channel as well as the molecular sensing at the receiver and obtain the maximum achievable rate for such a communication system. Next, we study reliability in MC. We design practical nodes by employing synthetic bacteria as the basic element of a biologically-compatible communication system and show how reliable nodes can be formed out of the collective behavior of a population of unreliable bio-agents. We model the probabilistic behavior of bacteria, obtain the node sensing capacity and propose a practical modulation scheme. In order to improve the reliability, we also introduce relaying and error-detecting codes for MC.

In the second part of the thesis, we study the molecular sensing problem with potential applications in disease detection. We establish the rate-distortion theory for molecular sensing and investigate as to how distortion can be minimized via an optimal quantizer. We also study sensor cell arrays in which sensing redundancy is achieved by using multiple sensors to measure several molecular inputs simultaneously. We study the interference in sensing molecular inputs and propose a probabilistic message passing algorithm to solve the pattern detection over the molecular inputs of interest.

CHAPTER 1

INTRODUCTION AND RELATED WORK

The use of molecular signaling as a means of communication is inspired from naturally occurring communication between bacteria in a process called Quorum Sensing (QS) [1]. It has been understood that bacteria use concentration of small signal molecules to understand the state of the environment (e.g., bacteria's population density) and to synchronize their actions [1–5]. This mechanism enables bacteria to behave collaboratively for performing the tasks that would be impossible otherwise. From a macro-level perspective, QS can be viewed as a way that bacteria propagate information spatially by relaying it to other bacteria in the vicinity. Some examples for these coordinated tasks are light production and attacking the host by bacteria.

Molecular communication and sensing have been shown to play major roles in intercell communication inside the human body as well. One of the most prominent examples is the transfer of small micro-RNA (miRNA) molecules throughout the body [6–8]. In particular, it has been observed that specific patterns over certain miRNA types can be used to detect diseases such as cancer and heart failure. In the cancer case, it has been proposed that tumors propagate their corrupt genetic information via transfer of molecules (e.g., miRNAs) to the healthy tissues [9]. These phenomena call for a thorough study for molecular communication and sensing from a theoretical and practical perspective.

Recent developments in synthetic biology and nano/bio technology have motivated the researchers from various disciplines to study the fundamentals of molecular communication systems and the design of synthetic circuitry using primitive bio agents (e.g., bacteria) [10–15]. This alongside with system biology enables researchers to engineer microorganisms for certain objectives [16]. Moreover, primitive bio agents can be designed to behave collaboratively for performing the tasks that would be impossible otherwise [17, 18].

Synthetic biology, despite in its infancy, provides engineering solutions to redesign biological systems that improve human health, address environmental issues, and provide renewable energy [14, 19–21].

Emergence of new applications in biomedicine [22–24], e.g., smart drug administration [25] and monitoring systems [26] as well as several prospective industrial and security related applications including surveillance for biological and chemical attacks [10] require network designs that are 1) capable of operation in micro-scale 2) bio-compatible, 3) cheap to deploy, 4) highly reliable, and possibly 5) self-organized [15, 27]. In many of the above applications, communication between different network components is essential to achieve their true capability which necessitate the development of alternative networking paradigms. One of the most promising candidates for constructing networks that satisfy the requirements mentioned above is adaptation and engineering of specific types of bacteria that are capable of sensing, computation, actuation, and above all, communication with each other [1, 28].

In this research, we are interested in both theoretical and practical aspects of molecular communication and sensing. The thesis has two parts, one studies the communication problems and the other investigates the sensing problems. We first study the fundamental problems in communication between two nodes in MC. In particular, we are interested in Diffusion-Based Molecular Communication (DbMC) in which the molecules diffuse freely to reach their destination. DbMC is the most common form of molecular communication in nature [10]. The transmitter is considered to be a nano-device or a bio-engineered cell capable of emitting molecules and releasing them into the medium to change the concentration according to information bits. Similarly, the receiver is capable of absorbing the molecules or chemical signals by using molecular bindings. The diffusion process has a profound impact on transmission of information that makes the diffusion channel very different from the classical models developed for electromagnetic-based communication. The molecules that are produced by the transmitter stay in the medium and affect the later

transmissions. We study fundamental problems such as the maximum achievable rate of information exchange (i.e., capacity) by considering all the components in such a diffusion-based molecular communication.

Further, from a practical point of view, networks of engineered bacteria can be deployed in the environments such as human body, where other forms of wireless communication methods may be infeasible, to sense the density of a particular chemical, communicate it to other nodes, and possibly take appropriate actions [11, 29]. In order to design practical communication nodes, we employ genetically modified bacteria [17, 18] that can detect specific types of molecules and respond accordingly as the basic element of the communication nodes. Reliability is one of the most critical issues in MC, especially for the sensitive applications such as bio-sensors. We propose as to how design reliable MC nodes out of the primitive unreliable agents. We also study relaying and error-control-coding to further address this issue in MC.

The second part of this thesis investigates molecular sensing via synthetic cells. Among the most promising applications of molecular sensing is the design of biological sensors who measures and reports the existence and/or the intensity of specific types of molecules in the environment [11]. We establish the rate-distortion theory in the context of molecular sensing and show how redundancy can be employed to limit the distortion is molecular inference. We identify the sources of distortion and obtain the optimal quantizer for such a bio-sensor. We also discuss the sensor cell arrays in which multiple sensors can act simultaneously to detect environmental signals. In particular, we study the problem of detecting specific patterns of micro-RNA molecules in the environment via multiple RNA sensors.

In Fig. 1.1, molecular communication between two bio-nodes, each consisting a population of bio agents, has been depicted[1]. In the following, we introduce the building blocks of such communication and sensing system that will be discussed in this thesis and also

[1]Courtesy of Precision Biosystems Lab, Mechanical Engineering department at Georgia Institute of Technology
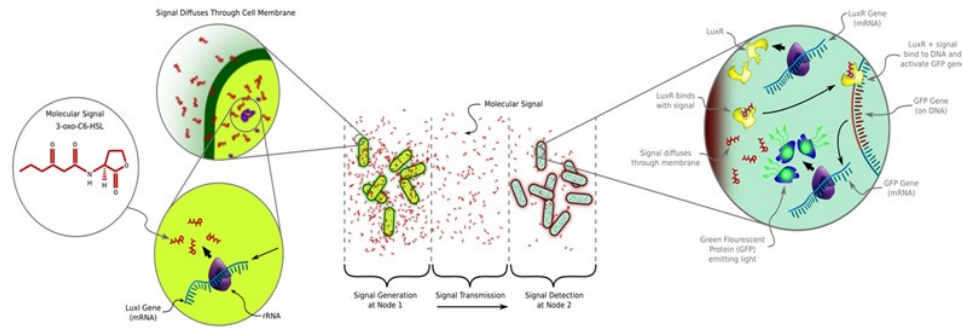
Figure 1.1. Two-node molecular communication via populations of synthetic bacteria

review the relevant prior literature.

Diffusion Channel in MC: In diffusion-based molecular communication, molecular signals propagate the channel freely via diffusion, as shown in Fig. 1.1, from the transmitter to reach the receiver node. Molecular random walk and the diffusion process [30] have been studied in the biological context by [31]. In [32], an end-to-end model for communication through a diffusion channel has been proposed. Authors in [33] have introduced a simplified binary symmetric channel model for MC and the channel capacity by considering the molecular degradation has been discussed in [34].

In this thesis, we model the memory in the diffusion channel via a Markov chain and treat it as a discrete noiseless channel. We obtain the capacity of the diffusion channel for a binary signaling under certain assumptions and show the limiting effect of lingering of molecules on the capacity. We also study the effect of model parameters, such as the range of the input concentration, on the capacity [35].

Inspired by this research, authors in [36] have proposed a model to capture the channel memory and molecular noise by modeling the molecular diffusion as an ideal gas transfer. In [37], a LTI-Poisson model is used to obtain the diffusion channel capacity. In order to mitigate the molecular lingering, different methods such as choosing appropriate pulse lengths and shut-off periods [38], using enzymes to reset the channel [39], and alternative use of molecule types [40] have been proposed. In [41], a stochastic model for bacterial

electron transfer has been described.

Ligand Reception: In molecular communication, the receiver agents are capable of absorbing the molecules or chemical signals by using ligand-receptor bindings and producing an appropriate response. In bacteria, the receptors are transmembrane proteins on the surface of the cells [42, 43]. The details of such a sensing process is shown in Fig. 1.1 and will be explained at length in Chapter 4. In such a setup, populations of synthetic bacteria are employed as transmitter as well as the receiver. Upon the arrival of signal molecules from the channel, complex molecules are formed by the probabilistic binding of the signal molecules with ligand receptors which in turn, transcribe the genes responsible for the output production. The final translated output is usually in the form of Green Fluorescent Protein (GFP). The theoretical analysis of the ligand reception process in molecular communication is a novel subject of study. In [44], a noise model has been proposed for the ligand-binding reception and a sampling-based receiver has been described in [45].

In this thesis, we present two models accounting for the uncertainty in estimation of concentration of molecules by the ligand receptors in a biological agent. We focus on the the steady state and obtain the sensing capacity of the ligand reception using these models. We also obtain the capacity-achieving distribution on the molecular input and show that the optimal distribution is approximately binary [46]. This observation will be used further on to design the optimal transmitter.

Inspired by this research, it has been proven in [47] that discrete distributions can achieve the capacity of ligand reception. In [48], the capacity of ligand reception has been obtained in the transient mode in which the binding/unbinding has yet to reach an equilibrium. Authors in [49] have proposed different methods for a receiver in the MC to recover the transmitted information distorted by both ISI and noise. In [50], two techniques for the detection of the molecular pulses, amplitude and energy detection, have been analyzed. In [51], authors study the estimation and detection problems for diffusion-based communication in the presence of ISI and reception noise and a combined model for diffusion and

6

ligand reception is proposed in [52]. Authors in [53], in order to improve the decoding performance, have introduced memory to keep track of the transmitted symbols. Optimal receiver design has also been discussed under various assumptions [54, 55]

Two-Node Communication Design: In [10, 11], fundamentals of molecular communication in nano-networks have been discussed. They include the channel description, node and protocol design, and experimental validation setup. In [56], several challenges that differentiate molecular communication with conventional wireless communication have been studied and a frameworks to study MC systems is also introduced in [57]. The transmitter and receiver nodes in MC can be formed by modifying cells genetically [58] or by designing artificial cells [59]. In [60], the idea of lab-on-a-chip has been analyzed for molecular communication and a nonlinear model for molecular communication systems has been developed in [61].

In this thesis, we introduce using synthetic bacteria to form MC nodes and show that forming reliable communication is possible by using a population of unreliable biological agents. This scenario has been shown is Fig. 1.1 where population of primitive synthetic bacteria form the communication nodes. As such, the collective behavior of such agents can be used to transmit or receive signaling molecules [15, 62, 63]. We model the reception/transmission noise in such nodes and study the two-node communication using such nodes. We show how the noise is accumulated at each stage and obtain the maximum rate of transferring information [38, 64, 65].

Inspired by this research, authors in [66] have proposed a cooperative architecture for MC. Source addressing and access control [67], Stop-and-Wait (SW) and Automatic Repeat reQuest (ARQ) [68], and resource allocation problem [69] have been discussed for a bacterial communication network. Authors in [70] have discussed chromosome transfer in bacterial networks and plasmid transfer in a nano sensor network is discussed in [71]. In [72], a swarm of nano-robots is proposed to be used in biomedicine applications. In [73], a bacteria inspired mitigation of selfish users in social networks has been proposed and

in [74], a probabilistic model for quorum sensing of bacteria is investigated.

Modulation Techniques: In molecular communication, information can be encoded in various forms such as the concentration, type or timing of molecules. Encoding the information in the timing of emission of molecules has been introduced in [75, 76] where the propagation from the transmitter to the receiver is governed by Brownian motion. Capacity under such circumstance, for both with and without drift, has been obtained in [77–80]. In [81], a new class of time-coding has been introduced with identical signaling quanta.

Although Brownian motion of particles is basically the same process as diffusion, natural organisms do not directly sense the Brownian motion of a single particle [31]. Instead, they measure average diffusion of many small molecules by following the changes in concentration. Arguably, the most dominating form of the communication at the micrometer scale in nature is diffusion based molecular communication, i.e., embedding the information in the alteration of the concentration of molecules and rely on diffusion to transfer the information to the destination [35]. Encoding information in the variations of concentration of molecules has been modeled in [32, 82]. Modulation techniques based on type of molecules have been proposed in [83] and extended in [84]. Another approach for information encoding in MC is to directly send genetic contents between different nano machines [85]. Although in such approaches, more information can be potentially transferred in the network, the encoding/decoding complexity is a huge drawback.

In this thesis, we propose *M*-ary modulation in which the information is encoded in discrete levels of concentration of molecules and decoded via measuring the GFP level at the receiver [38]. We show that unlike the conventional wireless communication, reliability cannot be improved arbitrarily by increasing the SNR. This suggests using other methods alongside with the node design to increase the reliability in MC.

Inspired by this research, authors in [86] have analyzed the error performance of pulse-based modulation. In [87], authors have proposed modulations techniques based on type and concentration of molecules and analyzed their performance.

Reliability in MC: Due to huge randomness in production, diffusion and reception of molecules, reliability is one of the most critical problems in MC [88]. Attenuation of the molecular concentration (i.e., the signal) as it travels through the medium via the diffusion process is another major problem in achieving reliability in MC [89]. It has been shown that the signal attenuation in molecular communication is faster than the conventional wireless communication [90]. Therefore, communication to long distances remains a challenge especially whenever other types of molecules are present at the medium.

Relaying is one of the methods to improve the communication reliability in MC. This is inspired by QS through which bacteria reach a consensus by relaying their inaccurate estimates back and forth. From a macro-level perspective, QS can be viewed as a way that bacteria propagate information spatially by relaying it to the bacteria in their vicinity. We are motivated by this observation to study and design a relaying scheme in which information is transmitted from a source to a destination in a network, through the help of relay nodes. The design of repeaters in Calcium junction channels is discussed in [91]. Authors in [92] considered the multi-user problem in molecular communication and compared it with its conventional counterparts.

In this thesis, we introduce two forms of relaying in MC namely, sense-and-forward and decode-and-forward. In the former, we consider continuous symbols and study the effect of relaying on the capacity [93]. In the latter, we study the more practical case of using discrete symbols and demonstrate the effect of relaying on the probability of error [94]. We investigate using the same or a different type of molecule for the relaying path as for the direct path and identify the regimes at which one would outperform the other.

Inspired by this research, authors in [95] have analyzed a multi-hop architecture in molecular communication and extended the Amplify-and-Forward Relaying in [96]. Relaying with time-dependent concentration is discussed in [97] and network coding in molecular relaying is proposed in [98].

Error-Control Coding for MC: Another approach to enhance the reliability in MC is

to use error-control coding [99, 100]. Different capacity-approaching codes such as Turbo codes [101] and low density parity check (LDPC) codes [102] have been designed for the conventional communication systems. However, the encoding/decoding complexity of such codes deem them impractical for MC. One of the biggest challenges here is to develop codings schemes with transmitter and receiver nodes requirements in terms of complexity. Coding schemes for molecular communication has been briefly discussed in the literature. In [103], a new distance measure for molecular communication has been studied and a family of ISI-free codes has been introduced in [104]. Authors in [105] apply convolutional coding schemes, by making use of memory units and XOR gates, to improve the probability of error in molecular communication. The use of Hamming codes for molecular communication is discussed in [106] in which logic gates are used for encoding and decoding.

In this thesis, unlike the above schemes, we advocate using error detection schemes [100]. We focus on error detection rather than error correction for two reasons. First, often a node acts as a sensor that reports its readings (e.g., existence of a chemical in the environment [99]) to a destination repeatedly over time. In such a context, we need a reliable error-detection capability to avoid erroneous readings. However, discarding erroneous transmissions can be tolerated as the nodes are repeatedly sensing the environment and sending the information of interest. Hence, a natural repetition code is built into the application. The second reason is due to the limitations of biological agents to implement operations such as arithmetics and table lookup. Thus, error detection appears to be desirable to obviate the complexity imposed by error-correcting codes, especially at the receiver using ML decoding, and allow the system to be implemented in all-bio domain without requiring electronic components.

We model the binary DbMC over a completely asymmetric channel where one of the bits can be transmitted without any error while the other can undergo a random error by the channel. To obtain an optimal detection scheme, we model the detection problem via an

erasure channel and propose algorithms to obtain the optimal codewords efficiently for two different optimality measures. Then, we consider an error-free sub-family of such codes, namely constant weight codes, and propose an implementation specific to the molecular communication [107].

Rate Distortion and Optimal Quantization: Optimal Quantization techniques in the context of conventional communication have been discussed extensively in the classical literature. Max in [108] described the optimal choice of quantizing intervals and the reconstruction points that result in minimum average quantization error for an arbitrary signal distribution. Uniform quantization (i.e., having uniform quantization levels) is the most common and practical quantization method [109]. Authors in [110] showed that the uniform quantization is asymptotically optimal with the number of quantization levels. Universal quantizers have been introduced for the cases where the input distribution is unknown beforehand [109]. A universal quantizer in the minimax sense (i.e., minimizing the distortion for the distribution that yields the maximum error) is introduced in [111] and the idea is extended in [112, 113].

In the world of biology, distortion and error are usually mitigated through redundancy (e.g., number of sensors). In this research, we study the distortion in sensing and estimation of the concentration of molecular signals by ligand receptors in biological agents. The sensing distortion is caused by both the the random measurement of the molecular signal and the quantization of the final receiver output. We propose an optimal random quantization technique that minimizes the overall distortion and compare its performance with a uniform quantizer [114]. The exact distribution of molecules in the environment is often unknown. Hence, in collaboration with my colleague A. Abdi, we introduce the optimal universal quantizer in the minimax sense for a molecular sensor.

micro-RNA Sensor Cell Arrays: DNA microarays have long been a practical solution for detecting/estimating environmental genetic targets [115–119]. Several signal

11

processing and machine learning methods have also been developed for these technologies [120–132]. In particular, authors in [120,121] have proposed using Compressive Sensing (CS) techniques to make more efficient microarrays capable of simultaneous estimation of various targets. In [121] a graphical model is used to solve the CS decoding problem for a microarray. Sparse nonnegative recovery through a sparse measurement matrix, where the matrix is the binary adjacency matrix of a bipartite graph with constant column sum, has been presented in [120].

As explained earlier in this chapter, irregular patterns over specific miRNAs have been linked to certain types of cancer and cardiac diseases. In this research, we introduce a general framework to sense environmental miRNAs and detect certain irregular patterns. We use a sensor cell (i.e., biosensor) array comprising of various genes whose expression can be suppressed through miRNAs of interest. Interference and noise are major issues in miRNA sensing via such a cell array. In particular, every miRNA may have a footprint on multiple biosensors and each biosensor in the array may be affected by multiple miRNAs. We present a probabilistic model capturing this phenomenon and solve the detection problem via a factor graph. Since certain patterns rather than the exact values of the input miRNAs are needed, for disease detection, fewer observation are required to achieve the same level of pattern-detection accuracy relative to directly measuring the concentration. Finally, we use Belief Propagation, a message-passing algorithm, to infer the presence of irregular patterns [133].

CHAPTER 2

MOLECULAR RECEIVER WITH LIGAND RECEPTORS

In this chapter, we discuss the reception model for the biological agents inside the MC nodes as depicted in Fig. 1.1. The functionality of agents inside the transmitter and receiver nodes, which can be synthetic bacteria or man-made nano-machines, is similar differing only in the input and output type. In design of such bio agents, we are inspired by the Quorum Sensing (QS) in bacteria through which bacteria can reach a consensus to perform a task, e.g., producing light in bioluminescent bacteria, collectively.

In Fig. 2.1, we have shown the main stages in production of the output, Green Fluorescent Protein (GFP), in response to a molecular input, Acyl Homoserine-Lactone (AHL), in a typical synthetic E. coli bacterium [17]. We can identify the three main stages as

1. AHL molecules binding to the receptor proteins LuxR

2. Complex molecule formation that transcribe corresponding genes

3. GFP production.

In this chapter, we focus on the receptor binding and assume the next stages to be deterministic. Hence, our results would be applicable to any molecular receiver with ligand receptors [46]. Specifically, we answer two questions: 1- What is the maximum rate by which a bio agent can sense information from the environment via ligand receptors? 2- What is the corresponding capacity-achieving molecular distribution?

2.1   Modeling the Ligand Receptors

In molecular sensing, the receiver measures the concentration of molecules, using a set of binding sites, i.e., ligand receptors, that become active once they trap a molecule. The simplest reaction between a ligand and its receptor can be written as a two-way process [43]:

$$\text{Ligand} + \text{Receptor} \leftrightarrow \text{Complex}$$
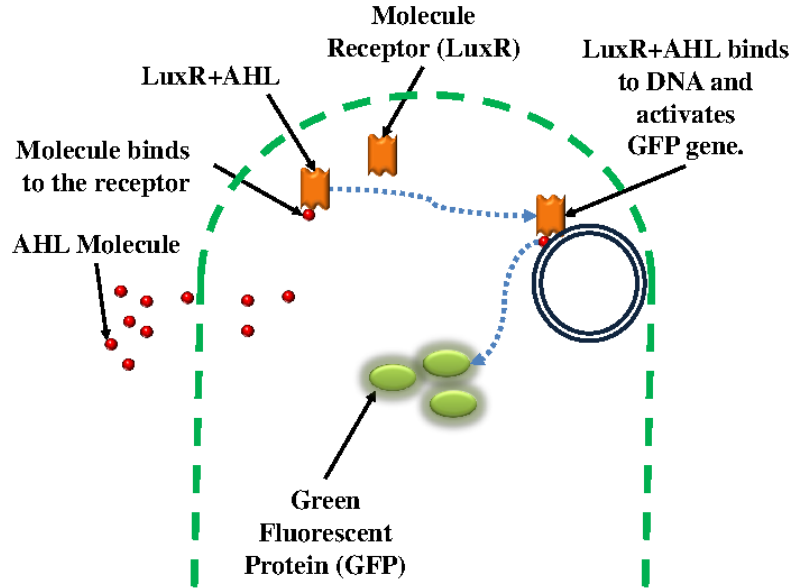
Figure 2.1. The main stages in GFP production of bacteria by reception of AHL molecules

In most cases, the focus is on the equilibrium behavior of the ligand reception in which the rate of removal of the ligand by the cell is equal to rate at which new ligands are supplied by diffusion [43]. Each binding site can trap one molecule at a time and cannot accept any more until the reaction to the previously trapped molecule is completed. As the concentration of molecules increases, the probability that a molecule is trapped and hence the number of active sites increases. This way, the receiver can estimate the concentration in the medium by observing the activated receptors.

Assume a receiver equipped with *N* binding sites/receptors as shown in Fig. 2.1. At every moment, a receptor is either active (a molecule is trapped in it) or inactive (empty). We assume all the receptors are identical, observe the same concentration, and act independently. The process of determining the concentration of molecules at the receiver is as follows: the molecules arriving from the channel produce a time-varying concentration *A(t)* at the receiver vicinity. The higher the concentration around the receiver, the higher the probability that a molecule is trapped in a receptor. The receiver periodically samples the environment and based on the number of bound receptors infers the concentration of molecules at the receiver vicinity.

We denote by p the probability that a single molecule being bound to an empty ligand-receptor when the concentration $A(t) = A$. In other words,

Figure 2.2. Molecular receiver with ligand receptors

$$p = \mathbf{P}\left(\text{Binding} \mid A \,\&\, \text{the receptor is empty}\right)$$

$$(2.1)$$
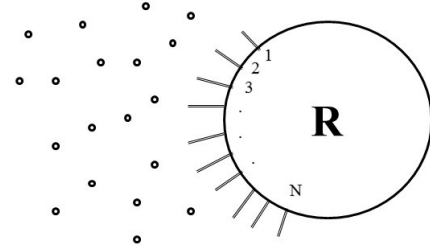
For the general case, the function that maps the concentration of molecules to the probability of the absorption is assumed to be a monotonically increasing one, $[0, \infty] \rightarrow [0, 1]$. In Chapter 4, we will consider a specific function modeling the ligand reception in bacteria. Moreover, $p \in [0, 1]$ is a realization of a random variable P.

We associate an indicator random variable X_i, $i \in \{1, 2, ..., N\}$ to each receptor where X_i's are Bernoulli distributed with parameter p, i.e., $\mathbf{P}(X_i = 1) = p$. Let $X^{(N)}$ be the vector containing the outputs of all the receptors. The vector $X^{(N)}$ is the input used to estimate p. It is known that $\sum_{i=1}^{N} X_i$ is the sufficient statistics for estimation of p. This implies that the receiver functionality is to aggregate the values of all the receptors at every sampling instant. Let $\hat{P}$ be the best unbiased estimator for p. Since $\hat{P} = \frac{1}{N} \sum_{i=1}^{N} X_i$, the expected value and variance of $\hat{P}$, given p, can be easily derived as $\mathbf{E}[\hat{P}] = p$ and $\mathrm{Var}[\hat{P}] = \frac{1}{N} p(1 - p)$.

Clearly, $\hat{P}$ depends on the value that P takes. In other words, we have

$$\mathbf{P}\left(\hat{P} = \frac{i}{N} \,\middle|\, P = p\right) = \binom{N}{i} p^i (1 - p)^{N-i}. \tag{2.2}$$

We use the shorthand $\mathbf{P}(i|p)$ for $\mathbf{P}\left(\hat{P} = \frac{i}{N} | P = p\right)$ in (2.2). Hence, by computing $\hat{P}$, the receiver has an estimate for p which in turn is a function of A. In other words, the receiver maps back the estimate $\hat{P}$ to a level of concentration $\hat{A}$.

We are interested in calculating the maximum information rate, i,e., the sensing capacity, with which the receiver with functionalities as described above can obtain from the environmental molecular signals. We observe that except for the relation between P and $\hat{P}$,

all the other relations are deterministic and one-to-one. Therefore to study the capacity of the ligand receptors, it is sufficient to consider only the mutual information between P and $\hat{P}$. This implies that

$$C = \max_{f_P(p)} I(\hat{P}; P) = \max_{f_P(p)}[H(\hat{P}) - H(\hat{P}|P)] \tag{2.3}$$

where C is the ligand reception capacity and $f_P(p)$ is the probability distribution function of P. In addition, $H(\hat{P})$ is the entropy of the discrete random variable $\hat{P}$ which takes values from the set $\left\{\frac{i}{N}, \ i \in 0, 1, ..., N\right\}$. Using (2.2) and the definition of mutual information, we have

$$C = \max_{f_P(p)} \sum_i \int_p \mathbf{P}(i|p) \log\left(\frac{\mathbf{P}(i|p)}{\int_p \mathbf{P}(i|p)f_P(p)dp}\right) f_P(p) \ dp \tag{2.4}$$

Therefore, in order to calculate the capacity, we need to obtain the optimal input distribution $f_P(p)$ that maximizes (2.4).

Note that the capacity of the receiver with ligand receptors depends on the model assumed for functionality of the receptors. In the following, we study two models to describe the process of estimating the concentration of molecules. First, the ideal receptor model is discussed. Then, we extend this model to better capture the functionality of the receiver using a Markov chain model.

2.1.1 Ideal Receptors

An ideal receptor is defined as a memoryless receptor which at each sampling time is ready to receive molecules. Once bound, the receptor remains as such until the next sampling time. This means that the parameter $\hat{P}$ would be directly an estimate for the probability in (2.1). Therefore,

$$I\left(P; \hat{P}\right) = I\left(P; \sum_{i=1}^{N} X_i\right) = I\left(P; X^{(N)}\right). \tag{2.5}$$

In this case, the problem of finding the capacity-achieving distribution in (2.3) resembles the corresponding problem in source coding which is discussed in [134]. There, the problem is to find the distribution that maximizes the mutual information between an observed

16
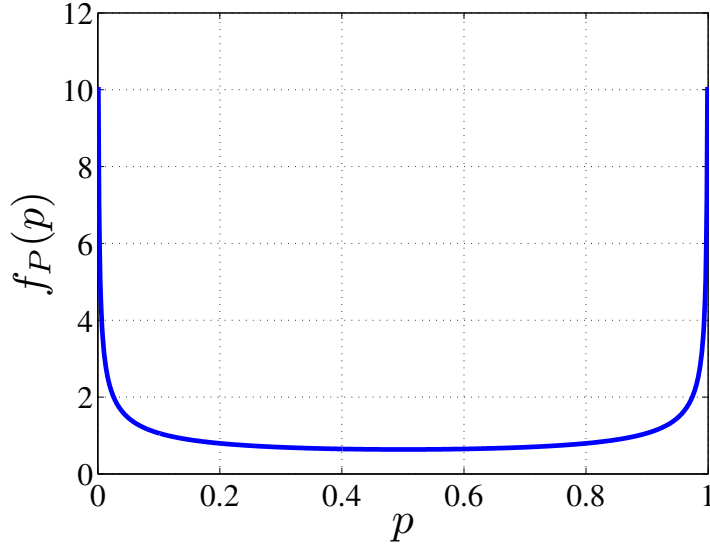
Figure 2.3. Capacity-achieving distribution for p

sequence and its unknown source parameter θ. It is shown that the capacity-achieving distribution is Jeffreys Prior which is proportional to the square root of the determinant of the Fisher information $\mathcal{I}$:

$$f_P(\theta) \propto \sqrt{\mathcal{I}(\theta)}.$$

In our setup, we intend to maximize the mutual information between the sequence $X^{(N)}$ and the unknown parameter p. By comparison to the source coding problem we have:

Lemma 1. *The capacity achieving distribution on P that maximizes the mutual information $I(P, X^{(N)})$ follows the Jeffery's prior [134].*

It is easy to verify that the Fisher information contained in N independent Bernoulli trials with parameter θ is

$$\mathcal{I}(\theta) = \frac{N}{\theta(1 - \theta)}.$$

Therefore, the Jeffrey's prior for a Bernoulli random variable is given by the Arcsine distribution:

$$f_{\Theta}(\theta) = \frac{1}{\pi \sqrt{\theta(1 - \theta)}}, \quad 0 < \theta < 1. \tag{2.6}$$
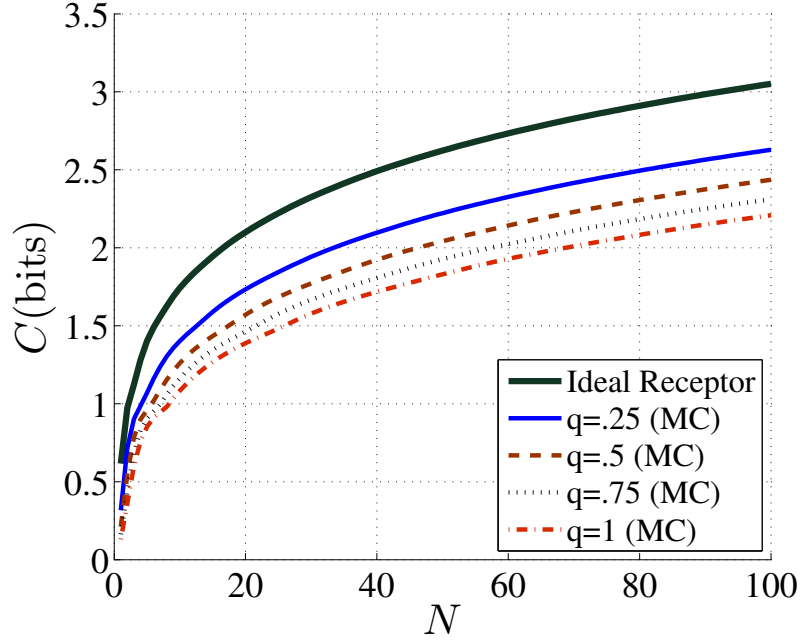
Figure 2.4. Capacity versus the number of receptors

As shown in [134], this results in the sensing capacity to be increasing logarithmically with the number of receptors N as described by

$$C = \max I(\theta; X^N) = \ln(N) + \frac{1}{2} \ln(\frac{\pi}{2e}) + o(1) \tag{2.7}$$

The capacity-achieving distribution is shown in Fig. 2.3. The resulting distribution for P shows that, in order to achieve the capacity, the transmitter should produce molecules in a way that approximately, makes P close to either 1 or 0, in each transmission. Intuitively, when p is chosen to become closer to $\frac{1}{2}$, the variance $p(1-p)$ of the Bernoulli output of each receptor is maximized which would reduce the mutual information in (2.3). The numerical results for the capacity of the ligand receptors versus the number of receptors N is shown in the outermost plot in Fig. 2.4. Expectedly, the capacity is monotonically increasing with respect to N but the added value of each receptor decreases with N .

2.1.2 Markov Chain Model for Receptors

In [135], a more realistic model to address the lingering of molecules in receptors is introduced. In the ideal model introduced in the previous section, the unbinding of a bound

18
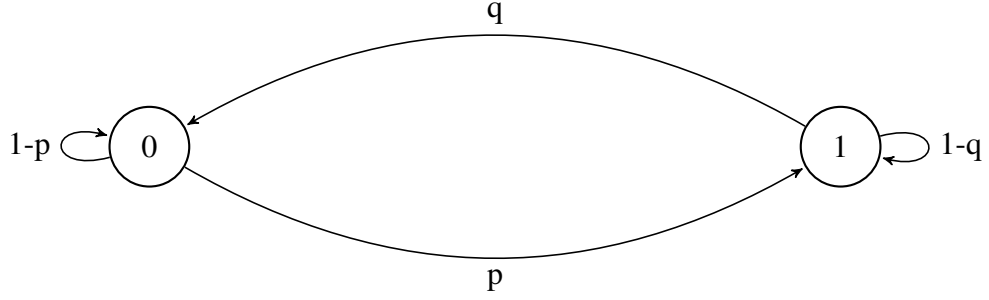
Figure 2.5. Markov chain model of a ligand receptor

receptor is ignored. In contrast, here, we use a modified version of the model in [135] in which the binding and unbinding of molecules are modeled with a Markov Chain (MC) to better capture the performance of receptors. The bound molecules occupy the binding site for a random amount of time. During this interval, the receptor remains occupied and no other molecule is able to bind to the receptor. The MC model for such a receptor is shown in Fig. 2.5. In this figure, state 0 corresponds to an empty receptor, i.e., $X_i = 0$, whereas state 1 corresponds to the receptor with a trapped molecule, i.e., $X_i = 1$. Here, p is the concentration-dependent binding probability and q is a fixed probability that a trapped molecule is released at each time interval. As before, we are interested in the steady-state behavior of the receive. The steady-state probability distributions for the above MC are given by

$$\begin{cases} \pi_0 &= \mathbf{P}(X = 0) = \frac{q}{p+q} \\ \pi_1 &= \mathbf{P}(X = 1) = \frac{p}{p+q} \end{cases}.$$

Since the diffusion channel is low-pass [35], the variations in the channel are slow relative to the mixing time of the MC, which is the time that takes for the MC to reach the steady state. In other words, the transition time to reach the steady state is quite small compared with the time intervals that information is transmitted via the diffusion channel. Therefore, we may assume that the MC reaches the steady state before the concentration level at the receiver switches from high to low or vice versa.

Let $\hat{\Pi}_1$ be the estimator for π_1 and denote by Π_1 the random variable representing π_1. Again, we have: $\hat{\Pi}_1 = \frac{1}{N} \sum_{i=1}^{N} X_i$. We use the method in the previous section to obtain the

optimal distribution for Π_1 to maximize the mutual information described in below:

$$C = \max_{f_{\Pi_1}(\pi_1)} I(\hat{\Pi}_1; \Pi_1) = \max_{f_{\Pi_1}(\pi_1)} [H(\hat{\Pi}_1) - H(\hat{\Pi}_1|\Pi_1)] \tag{2.8}$$

However, the difference is that π_1 is limited to $[0, \frac{1}{1+q}]$ as p varies in the range $[0, 1]$. Consequently, Π_1 cannot take an Arcsine distribution as in the ideal receptor case.

One approach for finding the distribution of Π_1 is to use Lagrange multiplier to maximize (2.8) with the constraint $\int_0^{1/(1+q)} f_{\Pi_1}(\pi_1) = 1$. Since the Lagrange method is intractable, instead, we obtain the capacity-achieving distribution for Π_1 numerically by the Blahut-Arimoto algorithm [136] for several values of q. The result is shown in Fig. 6(a). We observe that the distribution of Π_1 is asymmetric and its range decreases by increasing the parameter q.

From the distribution of Π_1, we can determine the optimal distribution for P; which in turn will determine the required distribution of the transmitter output. The distribution for P is shown in Fig. 6(b). We observe that the distribution of P does not depend considerably on the value of q. Since the transformation from p to π_1 is one-to-one and deterministic, we can calculate the capacity of the ligand receptor receiver by computing the mutual information between Π_1 and $\hat{\Pi}_1$. The numerical results for different number of receptors and q are shown in Fig. 2.4. We observe that the capacity increases by decreasing q. This can be explained by the fact that the range of π_1 increases when q decreases and hence, the mutual information is increased. Note that $q = 0$ corresponds to the ideal receiver for which the MC model would be meaningless.

2.2 Conclusion

In this chapter, we studied the ligand reception for a general bio-agent in MC. The functionality model is inspired by the Quorum Sensing in bacteria. We presented two models accounting for the concentration-estimation noise by the ligand receptors. In the ideal case, we showed that the Arcsine distribution is optimal and the corresponding capacity increases logarithmically with the number of receptors. In order to obtain a more practical model,
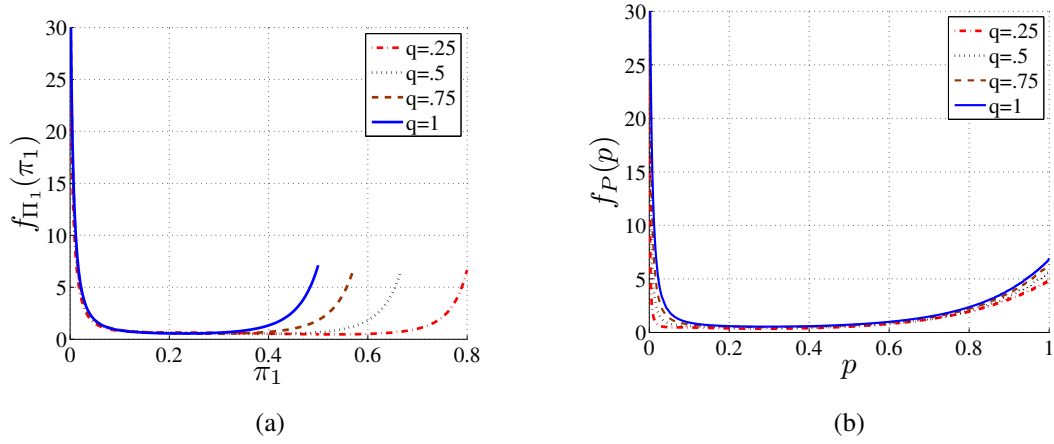
Figure 2.6. The capacity achieving distribution (a) π_1 **and (b)** p **for different values of** q.

we modeled the molecular unbinding with a Markov Chain and obtained the capacity numerically in the steady state. In both cases, we showed that the transmitter should mostly produce concentrations which are either low or high.

CHAPTER 3

ON/OFF SIGNALING FOR DIFFUSION CHANNEL

Analysis of the previous chapter suggests that the capacity-achieving distribution for a molecular receiver with ligand receptors is highly polarized, i.e., taking values close to 0 and 1 with high probability. Hence, binary on/off signaling would behave close to the optimal distribution. Having learned this, we study the diffusion channel capacity for the case where the transmitter uses binary level pulses [35].

In our model, the transmitter either releases molecules with a constant rate over a time period or remains silent. The emitted molecules are transferred through the medium by the diffusion process and reach the receiver. The low-pass frequency response of the diffusion channel restricts the rate of the information exchange; the receiver does not observe the high frequency elements which in turn means that the rapid changes in concentration of molecules at the receiver are absent. Molecules tend to linger in the medium after each transmission and some amount of time is needed for the molecules to diffuse away and channel to be reset. Unlike the previous section, here, we assume a noiseless receiver that compares the concentration of the received molecules with a specific threshold and decides whether the concentration in the environment is low or high.

3.1 Background

Assuming a molecule-production rate $r(x, t)$ inside the channel, the Fick's second law of diffusion [30] gives the concentration of molecules $c(x, t)$ at position x and time t as follows:

$$\frac{\partial c(x, t)}{\partial t} = D\nabla^2 c(x, t) + r(x, t). \tag{3.1}$$

Here, x is the distance of any point in the environment from the source and D is the diffusion coefficient of the medium. The impulse response of (3.1) is the Green's function
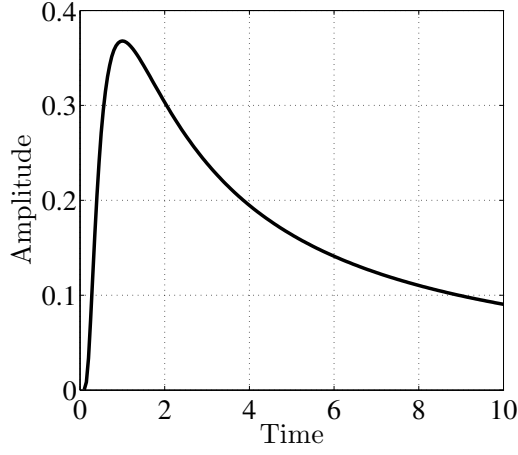
Figure 3.1. Impulse Response of the Diffusion Channel.

$g_d(x, t)$, shown in Fig. 3.1 whose expression is as follows for a 2-D medium:

$$g_d(x, t) = \frac{1}{4\pi Dt} \exp\left(-\frac{|x|^2}{4Dt}\right).$$ (3.2)

Since the diffusion equation is linear, the solution to (3.1) for an arbitrary input $r(x, t)$, denoted by $c^*(x, t)$, can be obtained by $c^*(x, t) = g_d(x, t) \otimes r(x, t)$ where $\otimes$ denotes a multi-dimensional convolution operation on x and t. In our setup, we assume that there is only one transmitter emitting molecules. Therefore, $r(x, t) = F(t)\delta(x)$, where $F(t)$ is the input signal. Hence, we will have

$$c^*(x, t) = \int_0^\infty F(\tau) \frac{1}{4\pi D(t - \tau)} \exp\left(-\frac{x^2}{4D(t - \tau)}\right) d\tau.$$ (3.3)

This response is valid for open free media in which the only boundary conditions are at the transmitter. Note that in our model, we do not consider the delay due to the travel time of molecules between the transmitter and the receiver. That is we assume molecules reach the receivers instantly. This assumption, however, does not affect our analysis of the capacity as it only shifts the time that molecules are arrived at the receiver.

3.2 Diffusion Channel Model

We consider a discrete-time model for the communication in which an arbitrary string of binary information is given to the transmitter. This string is to be transferred to the receiver

23
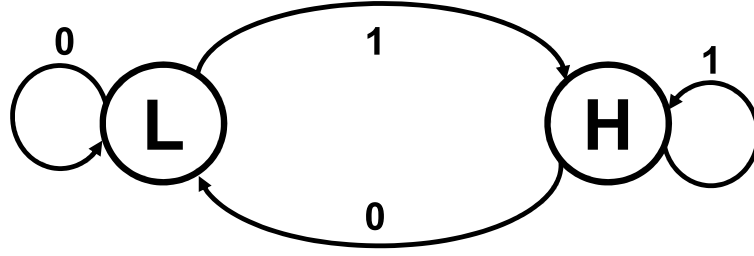
Figure 3.2. Markovian model to capture the channel memory

at distance *r* from the transmitter. The transmitter encodes the information bits into proper concentration of molecules and releases them for specific durations.

The main difference here with a typical paradigm of communication is the memory which exists in the diffusion channel and influences the communication dramatically. The concentration of molecules cannot change momentarily and unlike the typical binary symmetric channel, previously sent symbols affect the new ones. Hence, the transmitter might need to wait a specific amount of time to send a new bit. Note that we do not assume existence of negative rates nor any noise in the environment.

Based on the previous discussion, we observe that each bit depends only on the current state of the channel which is set by the last transmitted bit and it is independent of the other previously transmitted bits. Therefore, a Markov chain can be used to model the communication in the diffusion channel. In such a model, the channel state is "H" if the last transmitted bit was "1", and it is "L" otherwise. Hence, there are two states in the channel, as shown in Fig. 3.2. In the "L" state, it can either stay in this state by sending "0" or go to the "H" state by sending "1". In the high state, however, for sending the bit "1" again, it is inefficient to wait for the channel to reset to the "L" state. Instead, the transmitter can send "1" which is shorter in time duration and needs less molecules or equivalently less energy. To send "0" when channel is at the "H" state, it suffices that the transmitter waits a specific amount of time such that the channel clears itself from the molecules; returning to the "L" state.

The above discussion implies that depending on the channel state, duration of the bit

"0" is different. Likewise, the duration for which the transmitter emits molecules for the bit "1" depends on the channel state. Therefore, we can think of four different symbols sent by the transmitter, namely, s_0 ="00", s_1 ="01'", s_2 ="10'", and s_3 ="11'". The first bit in each symbol indicates the previous bit which was already sent (and hence the channel state), and the second bit is the one to be transmitted next. Assuming a binary symmetric source, all these four symbols are equiprobable. However, a different transmission time is associated with each, as explained.

In order to calculate the channel capacity, i.e., the maximum information rate with which the information can be reliably sent, we effectively need to obtain the number of combinations that the above symbols can be put together. Since our model involves symbols with various time duration, we adapt the method by Shannon in [137] to compute the capacity of a discrete noiseless channel as

$$C = \lim_{T \to \infty} \frac{\log N(T)}{T}, \tag{3.4}$$

where $N(T)$ is the number of allowed blocks of duration T. Let $T_{ij}^{(s)}$ be the duration of s-th symbol which is allowable in state i and leads to state j. Then $N_j(T)$, the number of blocks of length T ending in state j is given by

$$N_j(T) = \sum_{i,s} N_i(T - T_{ij}^{(s)}). \tag{3.5}$$

The asymptotic solution for these difference equations would be in the form $N_j = A_j W^T$ where A_j is a constant [137]. By substituting this form in (3.5), the possible number of blocks would be equal to $\sum_j A_j W^T$ where W can be found as follows. We define a matrix $M = [\sum_s W^{-T_{ij}^{(s)}} - \delta_{ij}]$; W would the largest real root of the determinant equation $|M| = 0$ [137], i.e.,

$$|M| = \left| \sum_s W^{-T_{ij}^{(s)}} - \delta_{ij} \right| = 0. \tag{3.6}$$

Here, $\delta_{ij} = 1$ if $i = j$ and is zero otherwise. Hence, following (3.4), the channel capacity C is obtained as

$$C = \lim_{T \to \infty} \frac{\log \left(\sum_j A_j W^T \right)}{T} = \lim_{T \to \infty} \left(\frac{\log W^T}{T} + \frac{\log \sum_j A_j}{T} \right) = \log W. \tag{3.7}$$

Rewriting (3.6) for the diffusion channel described above results in

$$\begin{vmatrix} W^{-T_{00}} - 1 & W^{-T_{01}} \\ W^{-T_{10}} & W^{-T_{11}} - 1 \end{vmatrix} = 0. \tag{3.8}$$

Here, T_s where $s \in \{00, 01, 10, 11\}$ is the duration of the symbols. This leads to

$$W^{-(T_{01}+T_{10})} + W^{-T_{00}} + W^{-T_{11}} - W^{-(T_{00}+T_{11})} = 1. \tag{3.9}$$

By solving (3.9) with respect to T_s for $s \in 00, 01, 10, 11$, we obtain the capacity of the channel in bits per second. In the next section, we solve for T_s for the diffusion channel.

3.3 Channel Capacity Analysis

Consider the scenario in which for symbol s, the transmitter sends a pulse-shaped rate of molecules with amplitude F_s to the receiver for duration T_s. It is clear that F_s is zero for symbols $s_1 = 00$ and $s_2 = 10$ because the transmitter does not need to emit any molecules. Instead, it must wait specific amounts of time. We assume F_{01} (for s_1) to be equal to F, the maximum rate that the transmitter can produce. For $s_3 = 11$, there is no need for the transmitter to send as many molecules as for s_1. Hence, we assume $F_{11} = \alpha F$. Thus a fraction $0 < \alpha < 1$ of the maximum rate is allocated to s_3. We denote by $c_s(r, t)$ the response at the receiver, i.e. $x = r$, at time t due to transmission of symbol s. Using (3.3), we have

$$c_s^*(r, t) = \int_0^{T_s} F_s(\tau) \frac{1}{4\pi D(t - \tau)} \exp\left(-\frac{r^2}{4D(t - \tau)}\right) d\tau. \tag{3.10}$$

Note that ,the diffusion equations of the channel do not set any limits on T_{00}. Instead, it depends on the receiver sensitivity, the distance r between the transmitter and receiver and the diffusion coefficient D. Specifically, T_{00} can be considered as the time sensitivity of the receiver with which it can sense the medium periodically. Hence, T_{00} is the fundamental time of the channel and the other T_s for $s \in \{01, 10, 11\}$ can be considered as multiples of T_{00}. In the following, we derive equations for T_s for $s \in \{01, 10, 11\}$ corresponding to different symbols.

Assume that the channel is in the low state. The transmitter may send bit "0", i.e $s_0 = 00$, or change the channel state to high, i.e. $s_1 = 01$. In the former case, the transmitter must wait for an interval of T_{00} but in the latter, it must emit molecules into the channel. Hence, for the $s_1 = 01$, we will have (for $0 \leq t \leq T_{01}$)

$$c^*(r, t) = c_{01}(r, t). \tag{3.11}$$

On the other hand, when the channel is in the high state, we have to take into the account the effect of the existing molecules in the channel, i.e. the channel memory. We can replace the molecules in the channel by the source that produces this concentration before the transmission of the current symbol and is zero afterwards.Hence, we can capture the channel memory by incorporating the effect of the symbol s_1 on the next symbol. In the case that the transmitter sends the bit "0" afterwards, i.e. $s_2 = 10$, it must wait for the channel to become low. Hence, we have (for $0 \leq t \leq T_{10}$)

$$c^*(r, t) = c_{01}(r, t + T_{01}) + c_{10}(r, t) = c_{01}(r, t + T_{01}). \tag{3.12}$$

where the first term captures the memory effect. The second term $c_{10}(r, t)$ is equal to zero which implies that the transmitter does send any molecules but must wait an appropriate amount of time. Finally in the case that the transmitter sends the bit "1" again, i.e. $s_3 = 11$, we have (for $0 \leq t \leq T_{11}$)

$$c^*(r, t) = c_{01}(r, t + T_{01}) + c_{11}(r, t). \tag{3.13}$$

Here the first term in (3.13) corresponds to the channel memory and the second term is due to the emission of molecules for the current symbol.

In the absence of noise, any intended concentration can reach the receiver without any interference from the medium. Therefore, the only limiting factor for capacity is the channel memory. Let S denote the concentration sensitivity of the receiver. This implies that the receiver cannot differentiate between the levels of concentration that differ by less than

S. We map the low concentration on S and high concentration on $2S$. We want the concentration at the receiver to be equal to one of these values at the end of each interval $t = T_s$. Using (3.11), (3.12), and (3.13), we have

$$c_{01}(r, T_{01}) = 2S,$$
$$c_{01}(r, T_{01} + T_{10}) = S, \qquad \qquad (3.14)$$
$$c_{01}(r, T_{01} + T_{11}) + c_{11}(r, T_{11}) = 2S$$

Note that in these equations the time delay between the transmitter and the receiver is not considered. We can write the solution for (3.14) based on the function $\text{Ei}(x)$ defined as [138]

$$\text{Ei(x)} = \int_x^\infty \frac{\exp(-y)}{y} \, dy. \qquad (3.15)$$

Then expressions in (3.14) can be written as

$$\text{Ei}\left(\frac{r^2}{4DT_{01}}\right) = \frac{8\pi DS}{F},$$
$$\text{Ei}\left(\frac{r^2}{4D(T_{01}+T_{10})}\right) - \text{Ei}\left(\frac{r^2}{4DT_{10}}\right) = \frac{4\pi DS}{F}, \qquad (3.16)$$
$$\text{Ei}\left(\frac{r^2}{4D(T_{01}+T_{11})}\right) - (1-\alpha)\text{Ei}\left(\frac{r^2}{4DT_{11}}\right) = \frac{8\pi DS}{F}.$$

Since finding closed form formula for (3.16) is intractable, in the following we solve for (3.16) numerically to obtain T_{01}, T_{10}, and T_{11} in terms of F. The parameter F indicates the maximum power used by the transmitter which affects the capacity. We solve (3.16) based on the normalized input rate $\tilde{F} = \frac{F}{4\pi DS}$ and obtain T_s for $s \in \{01, 10, 11\}$ as multiples of $\frac{R^2}{4D}$. As discussed before, T_{00} depends on r and D. Therefore, we may assume $T_{00} = \frac{kR^2}{D}$ where k is a constant. We arbitrarily choose $k = 1$, although our analysis holds for any values of k.

It can be shown that T_{11} is smaller, by orders of magnitude, than both T_{01} and T_{10}. Intuitively, this is due to the fact that producing a high state needs much more molecules than maintaining it. Hence, for simplicity, we assume T_{11} to be equal to T_{00}, and perform our numerical analysis only on T_{01} and T_{10}. The numerical results for $\tilde{T}_{01} = \frac{T_{01}}{T_{00}}$ and $\tilde{T}_{10} = \frac{T_{10}}{T_{00}}$ versus the normalized maximum rate of the molecule production $\tilde{F}$ are shown in Fig. 3(a) and 3(b), respectively.

28
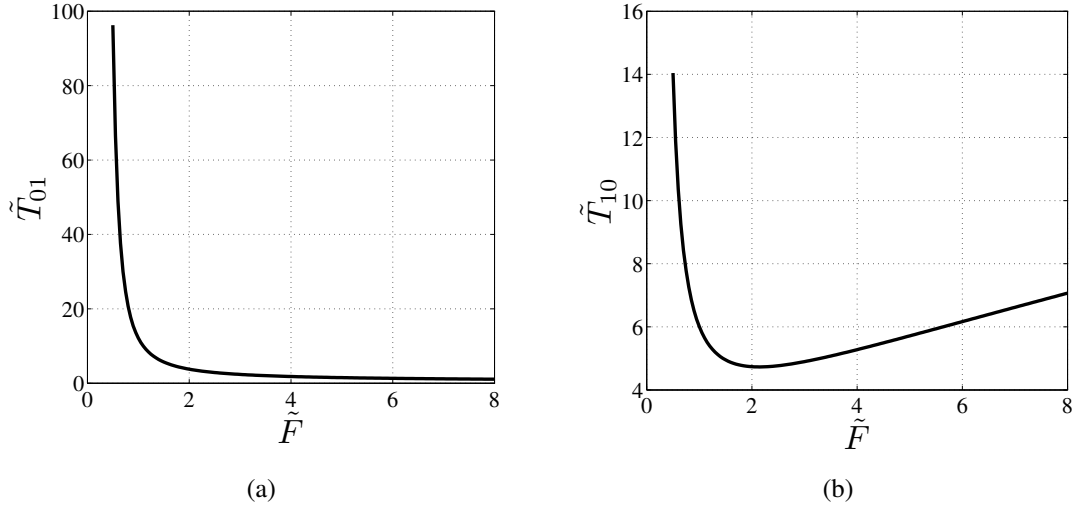
Figure 3.3. Diffusion channel transition time versus maximum rate of production.

We observe that the transition time from low to high $\tilde{T}_{01}$ is monotonically decreasing with respect to $\tilde{F}$, and approaches to infinity when $\tilde{F}$ is close to zero. In Fig. 3(b), the normalized transition time from high to low state $\tilde{T}_{10}$ is presented. It has a minimum around $\tilde{F} = 2$. This behavior can be explained by the shape of the channel impulse response shown in Fig. 3.1. As we see in this plot, the impulse response increases to a maximum and then falls. To obtain the response to the transmitter, a pulsed-shape signal in time has to be convolved with the impulse response. By increasing the input rate (or equivalently decrease $\tilde{T}_{01}$), at some point the threshold $2S$ is reached before the impulse response peaks. Hence, in order to send the symbol "10", the transmitter has to wait until the pulse is slided to the right side of the peak and hence, $\tilde{T}_{10}$ would be longer for a higher input rate.

Hence, although larger $\tilde{F}$ results in smaller $\tilde{T}_{01}$, it makes $\tilde{T}_{10}$ to grow larger, and hence has a negative effect on the capacity. Hence, the optimum value for the production rate can be found by considering the trade-off between $\tilde{T}_{01}$ and $\tilde{T}_{10}$.

Using (3.9) and the assumption that $T_{11} = T_{00}$, the capacity of the channel in "bits per an interval of T_{00}" can then be obtained by solving for W in the following equation and using it in $C = \log W$.

$$W^{\tilde{T}_{01}+\tilde{T}_{10}} - 2W^{\tilde{T}_{01}+\tilde{T}_{10}-1} + W^{\tilde{T}_{01}+\tilde{T}_{10}-2} = 1, \tag{3.17}$$

29
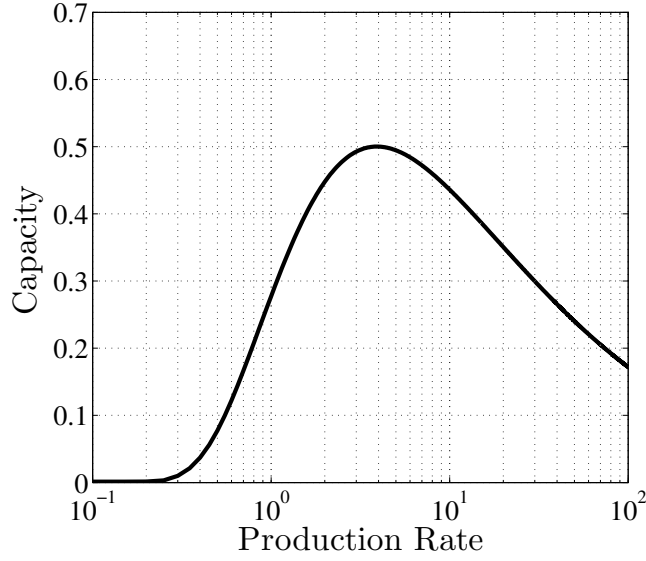
Figure 3.4. Diffusion channel capacity vs production rate.

We note that the maximum capacity is achieved when $\tilde{T}_{01} + \tilde{T}_{10}$ is minimized. The plot of the resulting capacity is shown in Fig. 3.4 with respect to $\tilde{F}$.

As shown in the figure, the maximum capacity is approximately 0.5 (bit/T_{00}) which is achieved when choosing $\tilde{F} = 3.9$ (units) and corresponds to the minimum value of $\tilde{T}_{01} + \tilde{T}_{10}$ which is approximately 7 (time units). The left tail of the graph converges to zero which corresponds to the no production rate. The right tail of the graph converges to zero as well but at a slower pace. In this case, symbols "00", "11", and "01" can be transmitted assuming the channel is in the proper state. However, since $\tilde{T}_{10}$ becomes very large, the transition between the channel states takes a long time, leading to zero capacity.

3.4 Conclusion

In this chapter, we obtained the diffusion-channel capacity for a binary noiseless signaling. We showed that the channel state affects the next bit to be sent and modeled the channel memory with a two-state Markov chain. This resulted in four symbols that the transmitter needs to choose from in order to send the binary inputs. We showed that beyond a threshold, increasing the power level would decrease the capacity.

CHAPTER 4

TWO-NODE MOLECULAR COMMUNICATION

In this chapter, we analyze molecular communication between nodes containing a population of bio entities. Reliable communication is not possible between individual unreliable primitive agents. Hence, we consider using their collective response to form reliable bio nodes [15, 62]. Note that, unlike the previous section, we are not concerned with the channel memory and focus on the transmitter/receiver noise. We will show that this can be achieved by using long pulses for transmission or through various interference-canceling techniques [38].

We study the communication between two nodes where information is encoded in the concentration of molecules by the transmitter [64, 65]. The molecules produced by the bacteria in the transmitter node propagate through the diffusion channel. Then, the concentration of molecules is sensed by the bacteria population in the receiver node which would decode the information and produce a corresponding output such as light, fluorescent, or another type of molecules. We study the uncertainty in the communication caused by all three components of communication, i.e., transmission, propagation and reception and investigate the theoretical limits over the information transfer rate in the presence of such uncertainties. Finally, we consider *M*-ary signaling schemes and study their achievable rates and corresponding error probabilities

4.1 Bio-entity Functionality Model and Node Design

The communication between bio entities (e.g. synthetic bacteria) entails huge amount of randomness and, hence, is highly unreliable. This is observed in various experiments [139] and will become more clear later through our results. Hence, one fundamental challenge is how to form reliable communication out of unreliable bio entities (e.g. bacteria). To

address this issue, rather than having molecular communication between individual bio entities, we propose an architecture in which a cluster of biological entities (i.e. a cluster of bacteria) communicates with another. We will refer to this cluster of biological entities trapped in a chamber as a *node*. The basic building blocks of the communication system are these clusters of bio entities which are able to transfer information from one point to another. Throughout this chapter, these bio entities are considered to be genetically modified bacteria [17, 18] which can sense specific types of molecules and respond accordingly. Although the principles of molecular communication is expected to hold for the bio entities, we particularly choose bacteria due to the prevalence of models and experimental results in the literature and also because of the relative ease in modifying them.

We consider molecular communication between two nodes each containing *n* engineered bacteria as depicted in Fig. 1.1. Here, we explain the signal transduction inside the synthetic E.coli bacteria which follow the DNA-RNA-Protein chain. Upon stimulation, e.g., heat, nutrition etc, the bacteria in the transmitter node transcribe the LuxI gene from the DNA and the messenger-RNA (mRNA) is sent to the ribosome to be translated. Ribosomal RNA (rRNA) associates with a set of proteins to form ribosomes. These complex structures catalyze the assembly of amino acids into protein chains. The ribosome reads the mRNA triplet codons (e.g., AUG) and matches the codon in the mRNA to the anti-codon on the transfer-RNA (tRNA). Each tRNA bears the appropriate amino acid residue to be added to the chain being synthesized. Upon translation, the molecular signals Acyl Homoserine-Lactone (AHL) diffuse through the cell membrane. The production rate of the AHL molecules depends on the intensity of the initial stimulation. As such the transmitter information can be encoded in the alternation of the concentration of AHL molecules. The molecules diffuse through the channel and reach the receiver. Upon arrival, AHL molecules bind to the LuxR protein, which itself is translated from the LuxR gene, and form a complex molecule which in turn transcribe the GFP gene. The GFP gene is translated at the
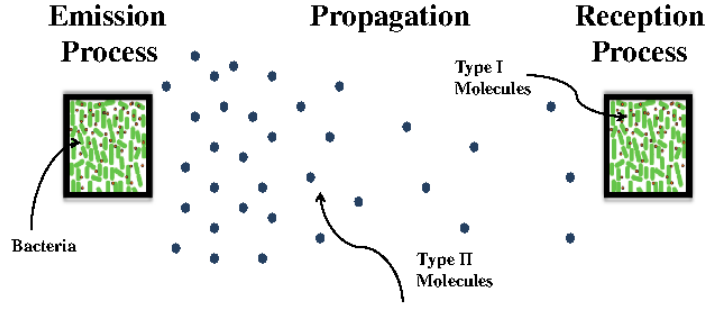
Figure 4.1. The molecular communication setup consisting of the transmitter, channel and the receiver

receiver ribosome and the GFP output is produced. The intensity of the output (i.e., fluorescence) depends on the input AHL molecules. As such, the input concentration can be decoded from the GFP output. Note that the genes responsible for the GFP production can be added via a plasmid to the bacteria.

The simplified schematic for the communication between two nodes is depicted in Fig. 4.1. Note that throughout our analysis, we assume that the number of bacteria inside a chamber remains constant. The bacteria inside the chambers grow and divide. To maintain the population size constant, the new bacteria can be washed away from the chambers as explained in [10]. Each bacterium is assumed to be able to sense and produce two different types of AHL molecules, namely type I and II [2].

Let assume the transmitter node has some information in the form of concentration A_0 that would like to convey to the receiver node. The bacteria inside the transmitter node can be stimulated through its chamber with different levels of concentration of type I molecules in order to produce various concentrations of type II molecules which are to be propagated through the channel. The transmitter output as shown in the following has a probabilistic nature such that higher levels of molecular stimulant would, on average, result in higher levels of the output. The probabilistic nature of the molecule production introduces the first component of the uncertainty in the communication. The specifics of the transmitter

---

[2]The labeling of the molecular types is chosen for the convenience of the presentation. Please refer to [140] for the technical labeling of these molecular signals.

33

node will be discussed in the next section. The emitted molecules would then diffuse through the channel to the receiver at the distance r from the transmitter. The induced molecular concentration at the receiver node depends on r. We assume that the transmitter node has an estimate r_0 for r which maybe slightly different. That introduces the second component of the uncertainty in the communication from the transmitter to the receiver which will be explained in Section 4.3. At the receiver, as explained in Section 4.4, each bacterium senses the concentration of type II molecules through the corresponding type II receptors. The reception of molecules again has a probabilistic nature which introduces the third component of the communication uncertainty. Upon the reception of molecules, a chain of reactions is triggered resulting in the production of GFP by bacteria. The GFP output of the receiver node is used to decode the signal (i.e., the concentration A_0).

We obtain the maximum information that the GFP output of the receiver node can give about the input concentration produced by the transmitter node. As such, we consider the models for the transmitter, the channel, and the receiver and analyze the uncertainty in each component which is aggregated with the noise from previous components. The capacity of the communication will be obtained by considering all these three components together.

Note that in order to perform its functionality as a transmitter or a receiver, each synthetic bacterium must be able to sense either type I or type II molecules, respectively. Each bacterium might be equipped in general with two distinct receptor types: one for each molecule types. However, depending on the functionality, as a transmitter or receptor, only one type of receptors is enabled. We assume N ligand receptors for each type of molecules. The bacteria response to these two stimulants (i.e., molecular types) is different, i.e., producing type II molecules upon the reception of type I but producing GFP in response to type II molecules. The functionality model for the reception of these two molecule types is assumed to be the same, i.e., the process of reception is governed by the same set of equations with possibly different coefficients.

The response of various strands of bacteria to different levels of inter-cellular AHL

molecule concentrations has been studied in the biological literature which account for the chain of chemical reactions inside the bacterium due to the AHL molecular stimulus. In [4], a model consisting of a chain of linear differential equations is introduced and validated experimentally to account for the production of luminescence or fluorescence in response to the presence of AHL molecules in the medium. These equations capture the average dynamic behavior of bacteria in the steady state. They account for three main phases in the process as described above

1. Binding of AHL to LuxR

2. transcription of GFP genes

3. GFP translation

The differential equation accounting for probability p of binding of molecules to the cell receptors is given by [4]:

$$\dot{p} = -\kappa p + A\gamma(1 - p),\qquad(4.1)$$

where A is the concentration of molecules surrounding the bacterium, γ is the input gain and κ is the dissociation rate of trapped molecules in the cell receptors. Here, $\dot{p}$ is the derivative of p with respect to time. In this model, each cell receptor is activated (via a trapped molecule) with a probability that depends on the concentration of molecules in the medium surrounding the cell. According to (4.1), this probability starts growing from the moment a constant concentration A is applied until it takes its final steady-state value p^*, given by

$$p^* = \frac{A\gamma}{A\gamma + \kappa}.\qquad(4.2)$$

Note that p^* increases monotonically with respect to A and approaches to 1 for very high concentrations. The production of complex molecules, the transcription of genes and the production of GFP are modeled similarly as [4]:

35

$$\begin{cases} \dot{S}_1 & = & (b_0 p + a_0) - b_1 S_1 \\ \dot{S}_2 & = & a_1 S_1 - b_2 S_2 \end{cases}.$$ (4.3)

where S_1 and S_2 are two post-transcription messengers and b_i and a_i are some constants [4]. In the steady state, the final product S_2 is obtained as

$$S_2^* = \frac{a_1(b_0 p^* + a_0)}{b_1 b_2}$$ (4.4)

Note that S_2^*, i.e., the intensity of GFP, has an initial value even when $p^* = 0$ and increases linearly when p^* increases. In the following, we use the above results to model the behavior of different components of the molecular communication system.

4.2 The Transmitter Model

As discussed in the previous section, to generate the desired type II concentration A_0 at the receiver, the bacteria residing in the transmitter node must be stimulated with type I molecules with the appropriate concentration A_s. We assume that the noise in the transmitter output (i.e., the aggregated type II concentration A_0 at the receiver due to all n bacteria residing in the transmitter node) is originated from the discrepancy in the individual behavior of the bacteria in the transmitter node. In other words, even though the average behavior of bacteria can be described by the set of deterministic differential equations in the previous section, the individual behavior of bacteria features randomness.

Two factors contribute to the uncertainty of the molecular concentration output of the transmitter node. One is the probabilistic nature of the number of activated receptors within a single bacterium in response to the type I stimulus. We model this by assuming each receptor being active as a Bernoulli random variable that is 1 with probability p^* defined in (4.2). The other factor is the randomness in p^* itself from one bacterium to another within the node; due to the variation of the constant parameters (i.e., γ and κ) in (4.2) among the population of bacteria. Note that the other parameters, in addition to γ and κ, in the model can be considered as random variables as well but the form of the obtained model would

remain the same. Hence, for simplicity of modeling the discrepancy of bacteria behavior in a node, we only consider the above parameters to contain randomness. We model this variation with an iid additive noise ϵ_γ in the input gain γ and ϵ_κ in the dissociation rate κ. Hence, the entrapment probability p_s upon the reception of the stimulant concentration A_s by the bacteria at the transmitter would be given by

$$p_s = \frac{A_s(\gamma + \epsilon_\gamma)}{A_s(\gamma + \epsilon_\gamma) + (\kappa + \epsilon_\kappa)}, \tag{4.5}$$

where ϵ_γ and ϵ_κ are zero-mean Normal noises with variances σ_γ^2 and σ_κ^2, respectively. The variance of these noises is assumed to be sufficiently small such that we can ignore the second and higher orders of $(\frac{\epsilon_\gamma}{\gamma})$ and $(\frac{\epsilon_\kappa}{\kappa})$ in the Taylor expansion of (4.5). We assume the same p_s for all the receptors belonging to the same bacterium, but it varies from one bacterium to another inside a node, as we described in (4.5). We define the noiseless entrapment probability at the transmitter as

$$p_s^* = \frac{A_s\gamma}{A_s\gamma + \kappa}. \tag{4.6}$$

Hence, by approximating (4.5) as described above, we have

$$p_s \simeq p_s^* + p_s^*(1 - p_s^*)\frac{\epsilon_\gamma}{\gamma} - p_s^*(1 - p_s^*)\frac{\epsilon_\kappa}{\kappa}. \tag{4.7}$$

The total number of activated receptors of ith bacterium, X_i, is a Binomial random variable with parameters $(N, p_{s,i})$ where $p_{s,i}$ is the realization of p_s for the ith bacterium. Recall that N is the number of ligand receptors per bacterium for a given molecule type. We denote X as the total number of activated receptors of all the bacteria in the transmitter node. Hence, $X = \sum_{i=1}^{n} X_i$. Using the conditional expectation, we have

$$E(X_i) = E(E(X_i|p_{s,i})) = E(Np_{s,i}) = Np_s^*,$$

where the last equality is due to the fact that the ϵ_γ and ϵ_κ have zero means. Hence, we have

$$E(X) = nNp_s^* = nN\frac{A_s\gamma}{A_s\gamma + \kappa}. \tag{4.8}$$

By using the conditional variance, we have

$$
\begin{aligned}
Var(X_i) &= E(Var(X_i|p_{s,i})) + Var(E(X_i|p_{s,i})) \\
&= E(Np_{s,i}(1 - p_{s,i})) + Var(Np_{s,i}) \\
&= Np_s^*(1 - p_s^*) + (N^2 - N)p_s^{*2}(1 - p_s^*)^2(\frac{\sigma_\gamma^2}{\gamma^2} + \frac{\sigma_\kappa^2}{\kappa^2}).
\end{aligned}
$$

The first term in (7.5) is due to the general uncertainty in a Binomial random variable (i.e., the probabilistic nature of the ligand reception) and the second term is due to the noise in the parameter p_s. Assuming independency among the behavior of different bacteria, the variance of the total number of activated receptors at the transmitter node is obtained as

$$
Var(X) = nNp_s^*(1 - p_s^*) + n(N^2 - N)p_s^{*2}(1 - p_s^*)^2(\frac{\sigma_\gamma^2}{\gamma^2} + \frac{\sigma_\kappa^2}{\kappa^2}).
$$

Since the number of receptors N per bacterium is usually large enough, the second term is dominating. Hence, we can approximate the variance by

$$
Var(X) \simeq nN^2 p_s^{*2}(1 - p_s^*)^2(\frac{\sigma_\gamma^2}{\gamma^2} + \frac{\sigma_\kappa^2}{\kappa^2}). \tag{4.9}
$$

As observed in (4.4), the average output of bacteria has an initial value corresponding to $p^* = 0$ and increases linearly with the average number of activated receptors. We assume that this offset value is the same for all the bacteria in a population and independent of the input concentration. Hence, the measured output is considered to be the GFP production due to the presence of AHL molecules, which depends linearly on the number of activated receptors X. Therefor, the total type II molecular output of the transmitter node is equal to αX where α is associated with a single activated receptor. Using (4.4), we note that $\alpha N = \frac{a_1 b_0}{b_1 b_2}$. To the rest of this chaper, we consider αX as the output of the transmitter node.

In order to make the analysis tractable, we use Central Limit Theorem (CLT) to approximate X, which is a Binomial random variable with known mean and variance, as a Normal random variable. In other words, since the number of receptors N is large, we can use CLT to approximate X_i by $\mathcal{N}(Np_s^*, Var(X_i))$ where $Var(X_i)$ is given in (7.5). Hence, X would be

38

the sum of n Normal variables given by

$$X = nNp_s^* + \epsilon_X, \qquad (4.10)$$

where p_s^* is given in (4.6) and ϵ_X has a Normal distribution $\mathcal{N}(0, Var(X))$ where $Var(X)$ is given by (4.9). The emitted molecules are propagated through the diffusion channel and reach the receiver. In the next section, we introduce the diffusion channel and study its effect in the communication.

4.3   Diffusion Channel

We characterized the temporal and spatial variations of molecules in the channel in the previous chapter. Here, in contrast, we are interested in the steady-state behavior of the channel. Assume that the channel is stimulated with a constant molecule rate β for the duration t_0. In other words, the channel input rate is a constant concentration of β molecules per unit of volume for $0 \leq t \leq t_0$. From (3.3), the concentration of molecules $A(r, t)$ at position r at time t is given by:

$$A(r,t) = \int_0^t \beta \frac{1}{(4\pi D\tau)^{\frac{3}{2}}} \exp\left(-\frac{r^2}{4D\tau}\right) d\tau = \frac{\beta}{4\pi Dr} \mathrm{erfc} \frac{r}{(4Dt)^{\frac{1}{2}}} \quad 0 \leq t < t_0 \qquad (4.11)$$

where $\mathrm{erfc}(x)$ is the error function complement(i.e.,1-erf(x)). Note that the error function erf(x) is defined by the integral

$$erf(x) = \frac{2}{\sqrt{\pi}} \int_0^x e^{-u^2} du.$$

Note that for $t_0 < t$ the concentration of molecules can be obtained from

$$A(r,t) = \frac{\beta}{4\pi Dr} (\mathrm{erfc}(\frac{r}{(4Dt)^{\frac{1}{2}}}) - \mathrm{erfc}(\frac{r}{(4D(t-t_0))^{\frac{1}{2}}})) \qquad (4.12)$$

Since $\mathrm{erfc} \frac{r}{(4Dt)^{\frac{3}{2}}}$ approaches 1 for large values of t, the pulse duration t_0 must be long enough to allow the channel output concentration in (4.11) to approach its steady-state value given by

$$A^*(r) = \frac{\beta}{4\pi Dr} \qquad (4.13)$$

This response is valid for open free medium in which the only boundary conditions are at the transmitter. If the dimension R of the receiver node is comparable to the distance r between the nodes, a factor $(1 - \frac{R}{r})$ should be multiplied to the expression in (4.13). Here, we assume that the distance between the transmitter and receiver nodes is significantly larger than the size of the nodes. Hence, we ignore the effect of this term on the steady-state response.

As discussed in the previous section, each activated receptor contributes an amount of α to the output rate. Since the diffusion channel is linear, the total response at the receiver will be the superposition of individual responses. Hence, $\beta = \alpha X$ and the steady-state concentration A_r at the receiver is given by

$$A_r = \frac{\alpha X}{4\pi D r}, \tag{4.14}$$

where r is the distance between the transmitter and the receiver nodes. The response in (4.14) is the average response of Brownian motion of the individual molecules without any other interferences [141]. Here, we consider another source of uncertainty which potentially arises in molecular communication due to uncertainty on the distance r of the two nodes. We denote by r_0 the transmitter estimate for r, which maybe slightly different from r. Hence, we have

$$A_r = \frac{\alpha X}{4\pi D(r_0 + \epsilon_r)} \simeq \frac{\alpha X}{4\pi D r_0}(1 - \frac{\epsilon_r}{r_0}), \tag{4.15}$$

where ϵ_r is a zero-mean Normal random variable with variance σ_r^2 which is assumed to be much smaller than r_0^2. Therefore, we only considered the first order term $\frac{\epsilon_r}{r_0}$ in (4.15). By using (4.8), we obtain

$$E(A_r) = \frac{\alpha n N}{4\pi D r_0} \frac{A_s \gamma}{A_s \gamma + \kappa}. \tag{4.16}$$

Hence, the required stimulating concentration A_s for type I molecules at the transmitter can be obtained by equating the expected concentration of molecules at the receiver (4.16) to A_0. As described in the previous section, A_0 is the desired concentration of type II

molecules to be transferred from the transmitter to the receiver node. Hence, we have

$$A_s = \frac{\kappa A_0}{\gamma(\frac{\alpha n N}{4\pi D r_0} - A_0)}.$$

From (4.10) and using the fact that $A_0 = \frac{\alpha n N p_s^*}{4\pi D r_0}$, we can write (4.15) as

$$A_r = (A_0 + \frac{\alpha}{4\pi D r_0}\epsilon_X)(1 - \frac{\epsilon_r}{r_0}) \simeq A_0 + A_0\epsilon_t - \frac{A_0}{r_0}\epsilon_r, \qquad (4.17)$$

where we have ignored the second-order noise terms and ϵ_t is a zero-mean Normal random variable with variance given by

$$\sigma_t^2 = \frac{(1 - p_s^*)^2}{n}(\frac{\sigma_\gamma^2}{\gamma^2} + \frac{\sigma_\kappa^2}{\kappa^2}). \qquad (4.18)$$

The first term in (4.17) can be viewed as the signal to be decoded by the receiver node. The second and third terms are signal-dependent additive Gaussian noises due to the randomness at the transmitter and the channel uncertainty, respectively. We refer to these two noises as the transmitter and the channel noise perceived at the receiver in the molecular communication, respectively.

4.4   Receiver Model

The concentration A_r derived in (4.17) is sensed by the bacteria in the receiver node. The sensing process of type II molecules is similar to that of the type I molecules we analyzed for the transmitter, but through different receptors. Hence, it follows the same chain of differential equations as in Section 4.2. The difference is that the input concentration is noisy itself which introduces an additional uncertainty to the output of the receiver node; which is in the form of GFP. This output is used to decode the information sent by the transmitter. Note that we assumed an ideal GFP detection system. However, in practice, the GFP detection system may introduce an additional uncertainty to the overall communication system. One may refer to [142] where the GFP sensors are studied in details.

Here, we incorporate the effect of both noises introduced in the previous section in addition to the uncertainty contributed by the reception process itself. Again, assume the

noises ϵ_γ and ϵ_κ with variances σ_γ^2 and σ_κ^2 account for the dependencies of gain γ and the parameter κ among the bacteria at the receiver node, respectively. In other words, the variations in the behavior of bacteria at the receiver node are incorporated by ϵ_γ and ϵ_κ. Hence, the entrapment probability of type II molecules by a receptor at the receiver can be written as

$$p_r = \frac{(A_0 + A_0\epsilon_t - \frac{A_0}{r_0}\epsilon_r)(\gamma + \epsilon_\gamma)}{(A_0 + A_0\epsilon_t - \frac{A_0}{r_0}\epsilon_r)(\gamma + \epsilon_\gamma) + (\kappa + \epsilon_\kappa)}. \tag{4.19}$$

Note that the input concentration noises ϵ_t and ϵ_r affect all the receiver bacteria in the same manner but ϵ_γ and ϵ_κ which account for the reception process of bacteria, are independent for different bacteria. By approximating (4.19) and again keeping only the first-order terms of the noises, we obtain

$$p_r \simeq p_0 + p_0(1 - p_0)(\frac{\epsilon_\gamma}{\gamma} - \frac{\epsilon_\kappa}{\kappa} - \frac{\epsilon_r}{r_0} + \epsilon_t), \tag{4.20}$$

where we defined $p_0 \triangleq \frac{A_0\gamma}{A_0\gamma+\kappa}$. The first term in the right hand side of (4.20) is the ideal channel input. The noise terms in (4.20) capture the uncertainty in all three components of communication, i.e., the molecule production at the transmitter, the diffusion in the channel, and the reception of molecules at the receiver. Note that ϵ_γ, ϵ_κ and ϵ_r have constant variances σ_γ^2, σ_κ^2 and σ_r^2, respectively but the variance of ϵ_t given by (4.18) is signal dependent. Since the number of bacteria n in a node is large, the variance in (4.18) is negligible relative to the other noise terms in (4.20). In other words, the noise of the transmitter is effectively filtered in the reception process as it was expected due to the low-pass nature of bacterial communicaton as discussed in [4].

We denote by Y_i the number of activated receptors of the ith bacterium in the receiver node at steady state. Then, $Y = \sum_{i=1}^{n} Y_i$ would give the total number of activated receptors of all n bacteria in the node. Note that Y is the sum of binomial random variables with parameters $(N, P_{r,i})$. Here, $p_{r,i}$ is the realization of p_r for the ith bacterium. With a discussion similar to the transmitter in Sec. 4.2, the GFP output of the receiver depends linearly on Y. Here, we consider Y itself to be the output of the receiver. The expected value of Y can be

obtained as

$$E(Y) = Nnp_0. \tag{4.21}$$

Computing the variance of the output will be more involved. Since ϵ_r is the same for all the bacteria of a node, Y_i's are independent given the value of ϵ_r. Hence,

$$Var(\sum_{i=1}^{n} Y_i|\epsilon_r) = \sum_{i=1}^{n} Var(Y_i|\epsilon_r) \simeq nN^2(\frac{\sigma_\gamma^2}{\gamma^2} + \frac{\sigma_\kappa^2}{\kappa^2})(p_0 - p_0(1-p_0)\frac{\epsilon_r}{r_0})^2(1 - (p_0 - p_0(1-p_0)\frac{\epsilon_r}{r_0}))^2, \tag{4.22}$$

where the last equality is resulted by using $p_0 - p_0(1 - p_0)\frac{\epsilon_r}{r_0}$ as p_0 in (7.5) and neglecting N relative to N^2. By keeping only the terms with the first order of ϵ_r and the assumption that $E(\epsilon_r) = 0$, we obtain

$$E(Var(Y|\epsilon_r)) = nN^2(\frac{\sigma_\gamma^2}{\gamma^2} + \frac{\sigma_\kappa^2}{\kappa^2})p_0^2(1 - p_0)^2. \tag{4.23}$$

On the other hand, we have

$$Var\left(E(\sum_{i=1}^{n} Y_i|\epsilon_r)\right) = Var\left(\sum_{i=1}^{n} N(p_0 - p_0(1-p_0)\frac{\epsilon_r}{r_0})\right) = nN^2 p_0^2(1 - p_0)^2\frac{\sigma_r^2}{r_0^2}. \tag{4.24}$$

From (4.23) and (4.24) and using the conditional variance, we obtain

$$Var(Y) = nN^2 p_0^2(1 - p_0)^2(\frac{\sigma_\gamma^2}{\gamma^2} + \frac{\sigma_\kappa^2}{\kappa^2} + \frac{\sigma_r^2}{r_0^2}). \tag{4.25}$$

The analysis of the noisy Binomial random variable Y is cumbersome. Hence, with the same argument as for the transmitter, we approximate Y with a Normal random variable with the expected value and variance given by (4.21) and (4.25), respectively. Hence, the output of the receiver node would be in the form

$$Y = nNp_0 + \epsilon_Y, \tag{4.26}$$

where ϵ_Y is a zero- mean normally distributed random variable with the mean and signal-dependent variance given by (4.21) and (4.25). Note that, the first term in (4.26) is the signal and the second term is the additive noise due to both the channel and the reception process. In the next section, we obtain the communication capacity from the model derived above.

4.5 Communication Capacity Analysis

As described in the previous section, the noise due to the transmitter is neglected in ϵ_Y relative to the other two noises. In addition, if we assume that the uncertainty in the position of the receiver is negligible (i.e., $\frac{\sigma_r^2}{r_0}$ is small due to sufficiently large r_0), then ϵ_Y is only due to the randomness in the reception of the molecules by the receiver. Note that throughout the discussion, we assumed that the number of bacteria n remains constant inside the chambers. The effect of variations of the number of bacteria would result in an additional variance term in the final output. However, it can be shown that this term is negligible compared to the other terms in the variance.

In order to calculate the capacity per channel use from the transmitter to the receiver, we should obtain the optimized distribution of A_0 which maximizes $I(A_0; Y)$; the mutual information between the input and the output. Since p_0 is deterministically obtained from A_0 through (4.2), we can consider p_0 as the channel input and maximize the information that Y gives about p_0:

$$\max_{f_{p_0}(p_0)} I(p_0; Y) = H(Y) - H(Y|p_0). \tag{4.27}$$

The optimal distribution on p_0 would in turn give the optimized distribution of A_0. To proceed, we observe that, in practice, A_0 cannot take any arbitrary value due to the limitation in the molecule production of bacteria. Hence, we assume a maximum output concentration that is equal to A_{max}. This corresponds to probability $p_{max} = \frac{A_{max}\gamma}{A_{max}\gamma + \kappa}$ via (4.2). This maximum probability is due to the maximum concentration range with which the transmitter can emit the molecules into the medium. By using a higher range, the transmitter can increase the maximum concentration of molecules at the vicinity of the receiver node and increase p_{max}. Therefore, we obtain the optimized distribution for p_0 over the interval $[0 \ \ p_{max}]$ and calculate the capacity with respect to p_{max} or equivalently A_{max}.

The noise term in (4.26) is complicated since the noise power depends on the signal
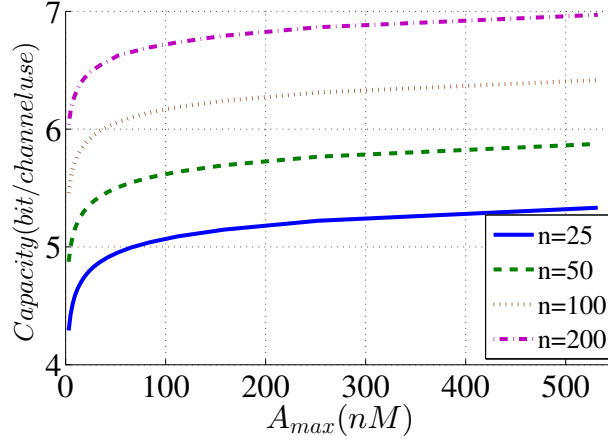
Figure 4.2. Capacity versus maximum concentration of molecules at the receiver for different numbers of bacteria in a node.

itself as it can be seen in (4.25). Hence, we resort to use the numerical method of Blahut-Arimoto algorithm (BA) to obtain the optimal distribution for p_0 and its corresponding capacity. Equation (4.25) implies that the noise power is at its maximum at $p_0 = \frac{1}{2}$ and goes to zero when p_0 approaches to either zero or one. Hence, we expect that the distribution of p_0 should take values closer to 0 and p_{max} with a higher probability. The results from the numerical algorithm confirms this fact and the distribution has local maximums at 0 and p_{max}.

We define $\sigma_0^2 \triangleq \frac{\sigma_\gamma^2}{\gamma^2} + \frac{\sigma_\kappa^2}{\kappa^2} + \frac{\sigma_r^2}{r_0^2}$. Results for the capacity (in bits per sample) with respect to A_{max}, the maximum concentration of molecules which results in p_{max}, for different numbers of bacteria in the nodes is shown in Fig. 4.2. The unit of measurement used for the concentration of molecules is nano-Moles per litre (nM). In this setup, we assume $N = 50$, $\sigma_0^2 = 0.1$ and also use the values $\kappa = 0.1$, and $\gamma = 0.0004$ from [4]. As we observe from the plot, the capacity increases when we increase A_{max} which results in higher p_{max} or increase the number of bacteria n. The ratio of the expected value of the output to its standard variance which is a measure of the decoding precision can be obtained using (4.21) and (4.25) as

$$\frac{E(Y)}{\sqrt{Var(Y)}} = \frac{\sqrt{n}}{(1 - p_0)\sigma_0}. \tag{4.28}$$

45
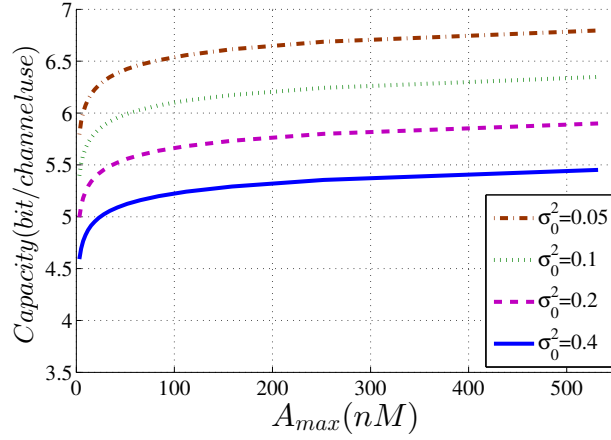
Figure 4.3. Capacity versus maximum concentration of molecules at the receiver for different levels of noise.

As we observe in (4.30), the ratio of the expected value and the standard deviation of the output increases as $\sqrt{n}$ and, hence, the capacity of the bacteria increases by using more bacteria in a node. Note that the maximum achievable capacity is limited even if the transmitter used infinite A_{max} to make $p_{max} = 1$. The capacity for different values of σ_0^2 is shown in Fig. 4.3. The results are shown for $n = 100$ and $N = 50$. Note also that, in practice, N and in particular n can be very large. However due to the exponential growth of the time complexity of the numerical method with respect to N and n, we only provided the capacity for relatively small values of N and n.

4.5.1 Information rate per time

Thus far, we obtained the capacity per sample in the molecular communication system. In order to compute the information exchange rate per unit of time, we now study a Return-to-Zero communication scenario. In other words, the transmitter sends the information, waits until the information is received by the receiver, and finally the channel becomes empty and ready for the transmission of the next sample. In order to obtain the information rate per unit of time, we should consider both the delay imposed by the channel as well as the delay due to the the reception process. In particular, we obtain the time it takes for the concentration of molecules to reach the steady state at the receiver, the time it takes for the
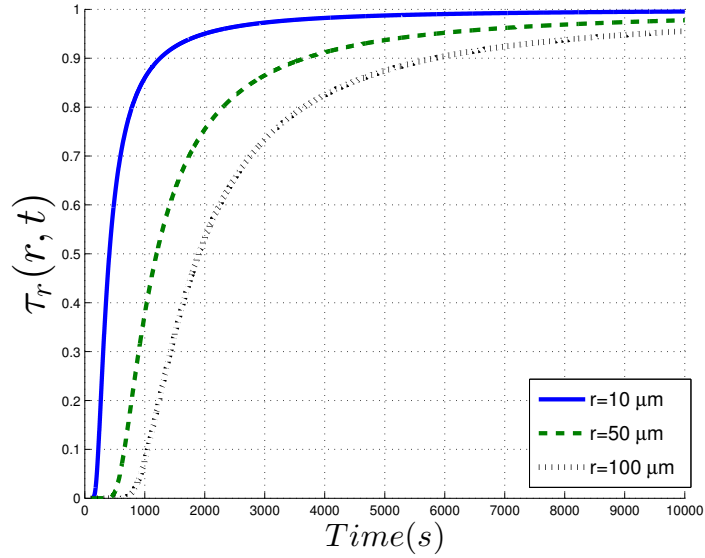
Figure 4.4. Rise time of the diffusion channel.

receiver bacteria to decode the concentration of molecules, and the time for the channel to become ready for transmission of the next sample.

In order to account for the delay due to the channel, we need to obtain both the rise time T_r and fall time T_f of the diffusion process of the channel. Note that the time for the channel to reach the steady-state response depends on the diffusion coefficient D and the distance r. In particular, using (4.11) and (4.13), we obtain the ratio of the transient to the final steady-state response as

$$\tau_r(r,t) = \frac{A(r,t)}{A^*(r)} = \text{erfc}\frac{r}{(4Dt)^{\frac{1}{2}}} \tag{4.29}$$

In Fig. 4.4, we have plotted this ratio vs time for different distances between the transmitter and the receiver. In this plot, D is assumed to be equal to $10^{-5} \frac{cm^2}{sec}$ which is a typical value for diffusion in water. The steady-state can be defined as the time that τ_r surpasses a specific threshold (e.g., $\tau_r = 0.9$).

On the other hand, in order to account for the fall time T_f of the channel, we define by τ_f the ratio between the falling concentration of molecules and its maximum value at the steady state. Using (4.12) and (4.13)), we have:

$$\tau_f(r,t) = \frac{A(r,t)}{A^*(r)} = \text{erfc}(\frac{r}{(4Dt)^{\frac{1}{2}}}) - \text{erfc}(\frac{r}{(4D(t-t_0))^{\frac{1}{2}}}) \tag{4.30}$$

47
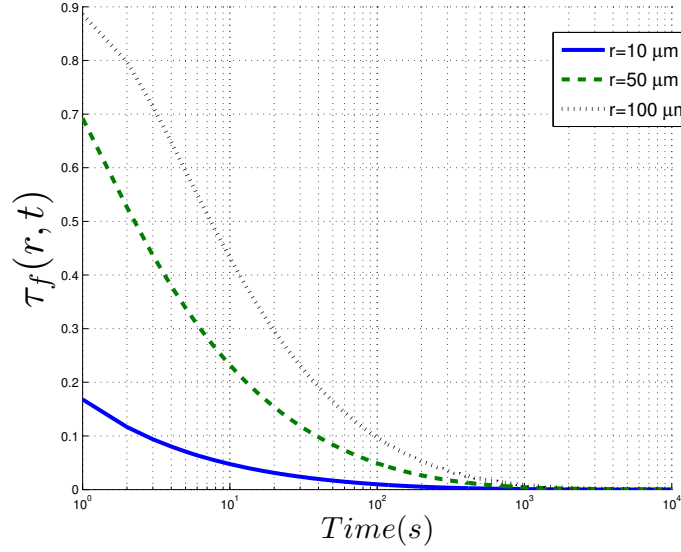
Figure 4.5. Fall time of the diffusion channel.

We assume the fall time of the channel to be the time that τ_r falls below a specific threshold (e.g., $\tau_r = 0.1$). We have plotted this ratio vs time for different distances in Fig. 4.5. The aggregation of the rise time and fall time gives the total delay imposed by the channel in the communication from the transmitter to the receiver. As we see in the plots, both the rise time and the fall time are in the order of tens of minutes and increase with the distance r.

The second component in the communication delay is the time it takes for the receiver bacteria to receive and decode the concentration of molecules. Note that the concentration of molecules at the receiver should remain constant until decoded by the receiver. Here, we use the set of differential equations introduced in Section 4.1. Moreover, we use the estimated parameters given in [4] to obtain the value of the reception delay. As described in Section 4.1, the total delay is due to the three processes that occur consecutively: entrapment of molecules, production of the proteins and transcription of genes, and production of the GFP. Using (1), the time constant for the entrapment of molecules is obtained as $T_1 = \frac{1}{A\gamma + \kappa}$. For a typical value of concentration of molecules (e.g., A=100nM), we have

bits per hour	$r = 10\mu$	$r = 50\mu$	$r = 100\mu$
$n = 50$	1.7	1.4	1.2
$n = 100$	1.9	1.6	1.3
$n = 200$	2.1	1.8	1.4

Table 4.1. The information rate per hour

$T_1 \simeq 5$ *min*. The time constant for the production of protein and transcription of genes, obtained from the first equation in (3), is equal to $T_2 = \frac{1}{b_1} \simeq 1$ *hr* . Finally, the time constant for production of fluorescent is obtained from the second equation in (3) and is equal to $T_3 = \frac{1}{b_2} \simeq 10$ *min*. Due to the exponential behavior of the differential equations in (3), we consider three times of these time-constants as the time required to reach the steady-state response. Hence, the overall delay is approximated as $T_R \simeq 3$ *hr*. Note that the production of proteins and transcription of genes are the dominating factors in the response delay and they are independent of the concentration of molecules A. Hence, we can assume that the above analysis holds true for all the values of A in the range.

Based on the discussion above, the total time it takes for the molecules to propagate through the channel and decoded by the receiver can be obtained by accumulating the delays discussed above. In other words, the total delay is given by $T_T = T_r + T_R + T_f$ and is in the order of a few hours. This is the time the transmitter should wait before sending the next sample. Hence, the information rate per unit of time can be obtain by dividing the rate per channel shown in Fig. 4.2 by the total delay T_T. Moreover, note that the stimulation time t_0 introduced in Section 4.3 would be equal to $T_r + T_R$. The information rate per hour is shown in Table 1 for different values of n in Fig 4.2, and variations of r in Fig. 4.4 and 4.5. We assumed $\sigma_0^2 = 0.1$ and $A_{max} = 400nM$.

As we see in the table, low information rates (1-2 bits per hour) can be achieved in the diffusion-based molecular communication by trading the rate for reliability.

4.6 *M*-ary Modulation in DbMC

The analysis in the previous section was based on the assumption that any continuous values of the concentration less than A_{max} can be produced and received by the nodes. With that assumption, we obtained the maximum amount of information that can be communicated per channel use. In this section, we consider a practical signaling method (i.e., *M*-ary modulation) and study the information exchange rate and the corresponding achievable error rate. We use only a finite discrete number of levels of molecular concentrations A_0 for communication which results in discrete levels of p_0. The range of the input is determined by p_{max}. Two factors influence the signaling performance: the number of levels of molecular concentration and the choices for the values of those levels.

We consider the scenario in which m symbols to be chosen with uniform spacing from the interval $[0 \quad p_{max}]$. Therefor, the ith symbol level would correspond to $p_{max}\frac{i}{m-1}, 0 \le i \le m-1$. We show by $p_{e,i}$ the probability of error in the detection of ith symbol. Hence, the total probability of error is given by

$$p_e = \sum_{i=0}^{m-1} w_i p_{e,i}, \tag{4.31}$$

where the weights w_i associated with the m symbols must be obtained.

We consider a hard-decision scenario in decoding the symbols. In other words, the receiver chooses the closest symbol to the received one. Hence, the error occurs when the detected symbol passes the half way from the previous or the next symbol. As observed in (4.25), the variance of the noise, and hence $p_{e,i}$ depends on the chosen symbol i. Therefore, we have

$$p_{e,i} = 1 - Pr(\frac{-p_{max}}{2(m-1)} \le \epsilon_{Yi} \le \frac{p_{max}}{2(m-1)}). \tag{4.32}$$

Here, ϵ_{Yi} comes from $\mathcal{N}(0, \sigma_i^2)$ where σ_i^2 can be computed by replacing p_0 with $\frac{i}{m-1}p_{max}$ in (4.25). As discussed in the previous section, variance of the noise is the smallest when the input is closets to 0 or 1. Hence, it is intuitive to choose larger weights for the inputs
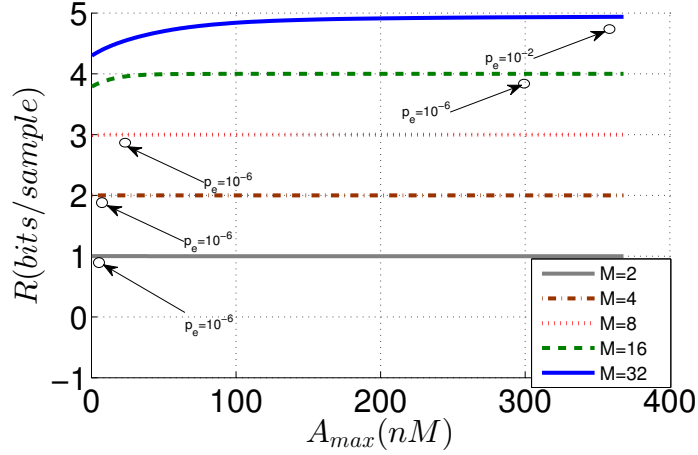
Figure 4.6. The information rate versus the maximum concentration of molecules at the receiver for different M-ary schemes.

closer to these two points. In our scheme, we use the weights from the optimal distribution calculated by the Blahut-Arimoto algorithm. In Fig. 4.6, we have shown the rate of information for different M-ary modulations versus A_{max}, the maximum concentration of molecules at the receiver. In this setup, again we have chosen $N = 50$ and $\sigma_1^2 = 0.1$. In addition, the number of bacteria in a node is chosen to be $n = 100$. As shown by the plot, reliable communication (i.e., $p_e = 10^{-6}$) is feasible for $M = 2, 4, 8, 16$ and the required range is shown as well. For larger number of symbols, reliable communication is not possible as for the case of $M = 32$. It was obtained that the least error rate (by maximizing A_{max}) would be 10^{-2} for $M = 32$. This is in contrast with traditional communication in which the reliability of M-ary schemes can be increased arbitrarily by using more power. Instead, in molecular communication, smaller error rates can be achieved by increasing the number of bacteria n.

Finally, in Fig. 4.7, we have shown the probability of error versus A_{max} for different values of M. Note that error for $M = 2$ and 4 is negligible and is not shown in the plot. As we observe in the plot, the probability of error decreases with increasing the range of input (i.e., A_{max}) but it is not possible to make the error arbitrarily small for large M. In the next section, we present the experimental results validating the observations made above.
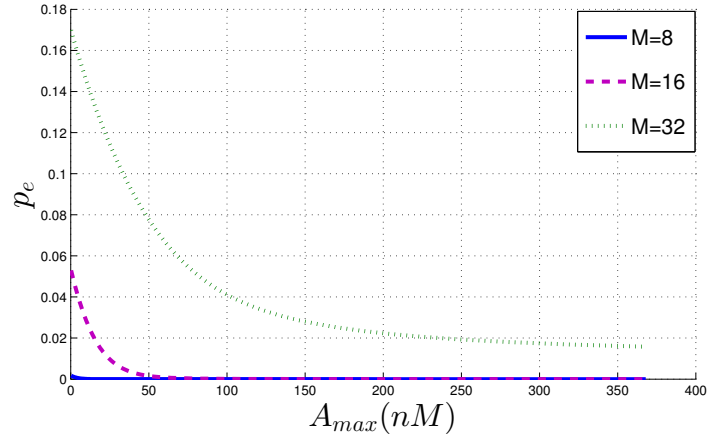
Figure 4.7. The probability of error versus the maximum concentration of molecules at the receiver for different M-ary schemes.

4.7 Experimental Results

The results in this section have been procured in collaboration with the Precision Biosystem Lab (PBL) run by Dr. Forest at the mechanical engineering department of Georgia Institute of Technology. In all experiments, a genetically engineered strain DH5 E. coli bacteria is used. Explanation of methods and functionality of the bacteria and the microfluidic device fabrication and specifications can be seen in [139, 143], but will be briefly reviewed here. In this system, the stimulus is autoinducer N-acyl homoserine lactone (AHL) and the bacterial response is the expression of green fluorescent protein (GFP). The design consists of a main channel with in direct fluidic contact with adjacent chambers that house the bacteria for the duration of the experiment as seen in Fig. 4.8. After initial loading of the chip, the bacteria were allowed to populate the chambers for 24 hrs to reach chamber capacity. During this time the bacteria were supplied with a constant flow of Lysogeny Broth (LB) at 100 μl/hr. Once the bacteria had filled the chamber flow rate was increased to 360 μl/hr. One syringe was used for LB (at 350 μl/hr), while the second (10 μl/hr) was used to deliver varying concentrations of AHL. An AHL pulse is the duration and concentration over which this AHL was delivered to the bacteria chamber. Pulse durations of 50 min that have been previously optimized [139] were used. Fluorescent images were captured once every 10
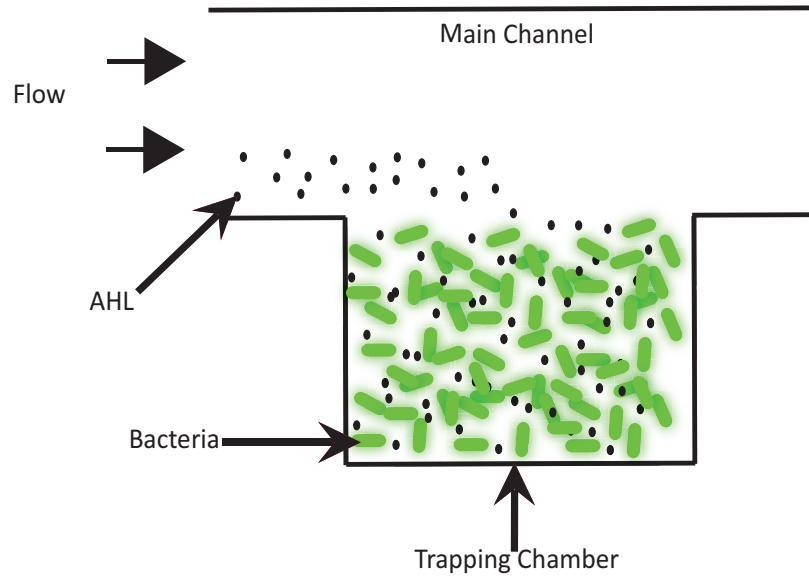
Figure 4.8. The experimental setup consists of microfluidic channels in a direct contact with trapping chambers housing bacteria.

min and post-processed using MATLAB. The intensity of the pixels within the bacteria chamber was averaged and the background fluorescence was subtracted, yielding relative fluorescence (arbitrary units, or AU).

Table. 4.2 summarizes the data related to the amplitude of the relative fluorescence response of the bacterial populations in the microfluidic chambers to AHL stimuli of varying concentrations at constant 50 min duration. The AHL concentrations used for the experiments ranged from 15 μM to 30 μM corresponding to the dynamic range of the bacteria response. As we can see in the table, the average output amplitude increases monotonically with the input molecular signal. However, the growth of the output tends to saturate as we increase the input concentration. Moreover, the output variance shrinks where the input takes values from its dynamic range extreme points. These observations are aligned with the model we obtained in this chapter. Note that, unlike the theoretical model, the variance does not approach zero at its extreme points. The biological noise due to the output production, spatial heterogeneity of molecules inside the chambers, and measurement noise are among the reasons for this discrepancy.

Table 4.2. The experimental data for M-ary modulation

AHL concentration (μM)	Average peak fluorescence	Standard deviation	Sample size
30	25.86	1.32	7
25	22.04	1.94	5
22.5	13.60	2.17	5
20	11.52	1.36	7
15	5.03	0.87	4

4.8 Conclusion

In this chapter, we studied two-node communication between nodes in MC and showed how reliable communication can be formed out of collective behavior of unreliable agents. We showed that the transmitter noise effect diminishes due to the low-pass property of the reception process. We studied the information capacity and investigated the effect of model parameters such as number of bacteria per node, noise level and maximum molecule production levels. We observed that the capacity increases with the number of bacteria in the nodes.

Further, we considered M-ary schemes and analyzed the achievable rates and their error probabilities. We observed that, unlike conventional wireless communication, for a fixed number of bacteria per node, reliable communication is not possible for large M, even with arbitrarily increasing the range of the molecular input. Instead, reliable communication can be achieved by increasing the effective number of bacteria in the nodes. Finally, we presented the experimental results for M-ary signaling which validate the conclusions derived from our models.

CHAPTER 5

RELAYING IN MOLECULAR COMMUNICATION

In the previous chapter, we discussed how the molecular communication reliability can be improved via using a population of primitive agents as bio nodes. We also showed that unlike conventional forms of communication, it is not possible to reduce the probability of error arbitrarily by using more power. In [90], it has been shown that the signal-to-noise attenuation in molecular communication is higher than the conventional wireless communication. Therefore, communication to long distances remains a challenge especially whenever other types of molecules are present at the medium.

One method to increase the communication range is by increasing the number of bacteria per node, i.e., a higher density of the population in a chamber node. However, due to introduction of spatial diversity of molecular concentration by using larger chambers and the restrictions on food availability and waste disposal at the node, a limited number of bacteria should be used inside a node. Instead, here, we resort to relaying to mitigate this problem and achieve more reliable communication between two nodes at large distances.

We consider two relaying scenarios. First, we study a theoretical case in which the transmitter is able to emit continuous concentration of molecules. In such a case, we introduce the sense-and-forward relaying in the molecular communication context [93]. Second, we introduce the decode-and-forward relaying in M-ary signaling [94]. In each of the two scenarios, we study two variations in which the relay node would transmit the information message either by a different or the same type of molecules as the original signal from the sender node. We show how relaying in the molecular communication can improve the capacity or probability of error, by either increasing the effective range of the molecular input or forming molecular diversity at the destination.

5.1 Molecular Sense-and-Forward Relaying

The schematic for a relay setup is shown in Fig. 5.1. In this setup, the relay node forms another path to the destination node to help it in decoding the information. Here, we assume a theoretical case in which the nodes are able to produce any continuous concentration of molecules in their maximum range. Moreover, no decoding occurs at the relay node and the same concentration (or a constant multiple of it) is relayed to the destination. In the setup shown in Fig. 5.1, the direct distances from the transmitter to the destination, from the transmitter to the relay and from the relay to the destination are assumed r_1, r_2 and r_3, respectively.

In the previous chapter, we obtained the output expression for the two-node communication as

$$Y = nNP_0 + \epsilon_Y, \tag{5.1}$$

where Y is the node output, n is the number of bacteria inside the nodes and N is the number of receptors on each bacteria. Moreover, P_0 is the molecular binding probability that depends on the concentration of input signal. Hence, P_0 can be considered as the transmitted symbol to be decoded. Further, ϵ_Y is a signal-dependent zero-mean Gaussian noise with variance

$$Var(\epsilon_Y) = nN^2 p_0^2 (1 - p_0)^2 \left(\frac{\sigma_\gamma^2}{\gamma^2} + \frac{\sigma_\kappa^2}{\kappa^2} + \frac{\sigma_r^2}{r_0^2} \right). \tag{5.2}$$
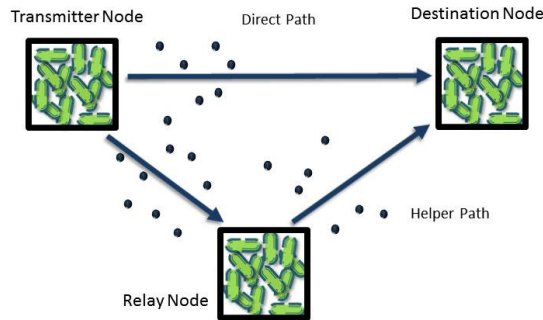
Figure 5.1. Communication via molecular relaying

Hence, the normalized GFP output at the receiver node can be written as:

$$Y = P_0 + \epsilon, \qquad (5.3)$$

where ϵ is a signal-dependent zero-mean Gaussian noise with variance $P_0^2(1 - P_0)^2 \frac{\sigma_0^2}{n}$ and

$$\sigma_0^2 = \frac{\sigma_\gamma^2}{\gamma_0^2} + \frac{\sigma_\kappa^2}{\kappa_0^2}. \qquad (5.4)$$

Assume that the transmitter produces the concentration A_{TD}, and correspondingly the probability P_{TD}, at the destination node. Hence, using (5.3), the output Y_{TD} at the destination due to the direct transmission would be

$$Y_{\mathrm{TD}} = P_{\mathrm{TD}} + \epsilon_{\mathrm{TD}} \qquad (5.5)$$

where ϵ_{TD} is a zero-mean Gaussian noise with signal-dependent variance as in (5.3). Note that the diffusion channel has a broadcast nature. Therefore, the output molecular concentration of the transmitter node travels to both the destination and relay nodes. Since the steady-state concentration of molecules depends inversely on the distance as shown in (4.13), the average concentration of molecules received at the relay would be $A_{\mathrm{TR}} = \frac{A_{\mathrm{TD}} r_1}{r_2}$. In response to the molecular concentration A_{TR}, similar to the destination node, the relay would produce Y_{TR} as

$$Y_{\mathrm{TR}} = P_{\mathrm{TR}} + \epsilon_{\mathrm{TR}} \qquad (5.6)$$

where $P_{\mathrm{TR}} = \frac{A_{\mathrm{TR}} \gamma_0}{A_{\mathrm{TR}} \gamma_0 + \kappa_0}$ and ϵ_{TR} is a signal-dependent zero-mean Gaussian noise whose variance is similar to the noise variance in (5.3), i.e., $Var(Y_{\mathrm{TR}}) = P_{\mathrm{TR}}^2(1 - P_{\mathrm{TR}})^2 \frac{\sigma_0^2}{n}$.

Being stimulated by the type I molecules from the transmitter, the output of the relay node's bacteria which depends on P_{TR}, is assumed to be designed to induce the concentration $A_{\mathrm{RD}} = \beta A_{\mathrm{TR}}$ of molecules at the destination. Note that such a functionality would be programmed into the plasmid of the synthetic bacteria at the design stage. Here, β is a constant amplification factor due to the chemical processes. We refer to this relaying scenario as the sense (the concentration A_{TR}) and forward relaying. Whether the molecules used for

this relaying are the same as the transmitter node's molecules (i.e., type I) or another type of molecules (namely type II), the problem is divided into two cases. In the following, we study and compare the two cases. Note that we assume that the necessary relative distances are known to the corresponding nodes.

5.1.1 Same-type Sense-and-Forward Relaying

Here, the relay is assumed to produce type I molecules in response to its input from the transmitter node. We assume that the nodes have the same maximum rate $A_{\max}$ of type I molecule production, and $\beta = \frac{r_2}{r_3}$. Therefore, the total steady-state concentration of molecules A_D at the destination is equal to the aggregate of all molecules received from both the transmitter node and the relay. That is:

$$A_D = A_{TD} + A_{TD}\frac{r_1}{r_3} + \epsilon_r \tag{5.7}$$

where ϵ_r is a zero-mean noise due to the reception process at the relay node (i.e., a function of ϵ_{TR} and the distance r_3).

Since no decoding is done by the relay, the noise incurred by the relay node is dominated by the reception process at the receiver; as in the case of the transmitter noise in the previous chapter. As such, the concentration of molecules A_D, sensed by the destination, produces the output (in form of GFP) Y_D as

$$Y_D = P_D + \epsilon_D \tag{5.8}$$

where $P_D = \frac{A_{TD}(1+\frac{r_1}{r_3})\gamma_0}{A_{TD}(1+\frac{r_1}{r_3})\gamma_0+\kappa_0}$ and ϵ_D is the resulting signal dependent zero-mean Gaussian noise with variance $P_D^2(1-P_D)^2\frac{\sigma_0^2}{n}$. Using (5.8), the capacity of the system involving relay can be computed by maximizing $I(P_D; Y_D) = I(A_{TD}; Y_D) = I(P_{TD}; Y_D)$.

In the previous chapter, we showed that one major factor in the capacity of molecular communication is the range of concentration of molecules $[0\ A_{\max}]$ that the transmitter can induce at the receiver. As we see in (5.8), the relaying in this case results in increasing $A_{\max}$ to $A_{\max}(1 + \frac{r_1}{r_3})$. Note that $A_{\max}$ is itself inversely proportional to r_1. Moreover, in order
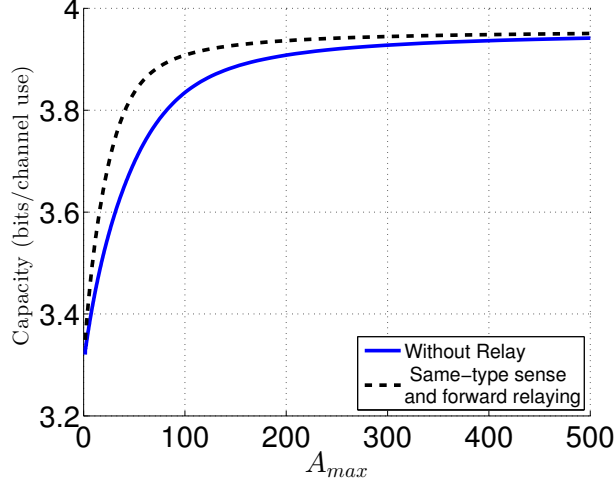
Figure 5.2. Capacity improvement in sense-and-forward relaying with a single molecule type.

to neglect the relay noise, r_3 should be large enough (compared with r_2). In Fig. 5.2, we have shown the capacity improvement, resulted from relaying, for different values of $A_{\max}$. Here, we assumed $n = 50$, $\sigma_0^2 = 0.1$, and $r_1 = r_2 = r_3$.[1] As shown in the plot, the advantage of relaying decreases for large $A_{\max}$.

5.1.2 Hetero-type Sense-and-Forward Relaying

In this scenario, in response to receiving type I molecules from the transmitter, the relay outputs another type of molecules, namely type II. Hence, there will be two types of molecules at the destination which would result in two different receiver node outputs, e.g., GFP and YFP, the Green and Yellow Fluorescent Proteins. Here, we neglect the interference between the two different types of molecules at the destination and assume they act independently.

We assume that the reception is the same for the both types of molecules but each type has its own separate receptors in the bacteria. Hence, the two outputs can be written as

$$
\begin{cases}
Y_{\text{TD}} = P_{\text{TD}} + \epsilon_{\text{TD}} \\
Y_{\text{RD}} = P_{\text{RD}} + \epsilon_{\text{RD}}
\end{cases}
\tag{5.9}
$$

---

[1]Since the computations are prohibitive for large n, we used a small value for n.

59
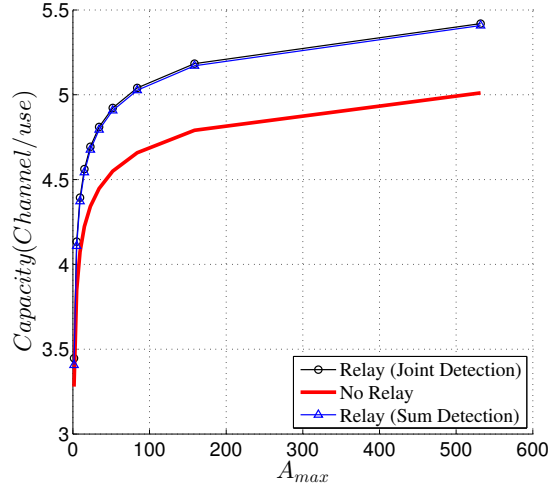
Figure 5.3. The capacity improvement by using two types of molecules in sense-and-forward relaying

where $P_{RD} = \frac{\beta A_{TD} \frac{r_1}{r_2} \gamma_0}{\beta A_{TD} \frac{r_1}{r_2} \gamma_0 + \kappa_0}$. In addition, ϵ_{TD} and ϵ_{RD} are zero-mean noises with variances $P_{TD}^2 (1 - P_{TD})^2 \frac{\sigma_0^2}{n}$ and $P_{RD}^2 (1 - P_{RD})^2 \frac{\sigma_0^2}{n}$, respectively. Here, we have assumed that the number of bacterium's receptors for the both types are equal.

In order to make the analysis tractable, we assume that the amplification factor β in the production of type II molecules is $\beta = \frac{r_2}{r_1}$. Hence, we have $P_{TD} = P_{RD}$. The goal is to maximize the mutual information between the input P_{TD} and the outputs Y_{TD} and Y_{RD}:

$$C = \max_{f(P_{TD})} I(P_{TD}; Y_{TD}, Y_{RD}). \tag{5.10}$$

The equations in (5.9) resembles the Single-Input/Multiple Output (SIMO) configuration in classical communication. With constant-variance noises, the sum of the two outputs Y_{TD} and Y_{RD}, i.e., performing Maximum Ratio Combining, would have been the sufficient statistics for decoding P_{TD}:

$$\hat{Y} = 2P_{TD} + \hat{\epsilon} \tag{5.11}$$

where $\hat{\epsilon}$ is a zero-mean Gaussian noise with variance $2P_{TD}^2 (1 - P_{TD})^2 \frac{\sigma_0^2}{n}$. In our case, however, since the noise powers are signal dependent and only conditionally Gaussian, $\hat{Y}$ is not the sufficient statistics for decoding P_{TD}. As such, some information would be lost if we use only $\hat{Y}$. We note that the output Y_{TD} and Y_{RD} are independent given P_{TD}, i.e.,

$P(Y_{\text{TD}}, Y_{\text{RD}}|P_0) = P(Y_{\text{TD}}|P_0)P(Y_{\text{RD}}|P_0)$. Hence, we may use the numerical Blahut Arimoto algorithm for the joint outputs to maximize the joint mutual information in (5.10).

In Fig. 5.3, we have shown the numerical results for the maximum mutual information $I(P_{\text{TD}}; Y_{\text{TD}}, Y_{\text{RD}})$ as well as $I(P_{\text{TD}}; \hat{Y})$. The case without relaying is shown for comparison as well. The results are shown for $\sigma_0^2 = 0.1$ and $n = 100$. As we see in the plots, the difference between using the sum $\hat{Y}$ instead of both Y_{TD} and Y_{RD} to decode P_{TD} is almost negligible. In other words, the improvement due to using two different outputs (e.g., GFP and YFP) instead of using only one output in response to both type I and type II molecules is negligible. Finally, comparing Fig. 5.3 with Fig. 5.2, we note that unlike the same-type relaying, the capacity improvement by hetero-type relaying persists for even large molecular ranges A_{max}.

5.2   Decode-and-Forward Relaying in Molecular M-ary Signaling

In the previous section, we discussed the cases that the relay forwards a continuous concentration of molecules that it senses. Here, we study the improvement in probability of error for a practical scenario in which the transmitter uses the M-ary signaling discussed in Section 4.6. In particular, as shown in the theoretical and experimental results, for a fixed number of bacteria in the nodes n, reliable communication is not possible for values of M larger than a threshold. Here, we employ relay to mitigate this problem.

The schematic for the relay setup is the same as the one in Fig. 5.1. We assume that nodes are able to produce as well as decode M levels of concentration of molecules. The transmitter broadcasts the information symbol through type I molecules to both the relay and the destination nodes. The received symbol by the relay node is decoded and forwarded on the helper path which arrives at the destination node alongside with the symbol from the direct path.

The ith symbol corresponds to $p_i = \frac{i}{M-1}p_{\text{max}}$ for $i = 0, 1..., M-1$. In the setup shown in Fig. 5.1, the direct distances from the transmitter to the destination, from the transmitter to

the relay and from the relay to the destination are assumed r_1, r_2 and r_3, respectively. Note that since the distances may not be equal, each symbol would correspond to a different concentration of molecules at the nodes. Hence, in order to obtain the proper symbols, nodes must know the distances and scale the concentration of molecules accordingly. Here, without loss of generality, we assume that $r_1 = r_2 = r_3$. Using (5.3), the normalized output Y at the relay due to the transmission of the symbol p_T where $P_T \in \{p_0, p_2, \ldots, p_{M-1}\}$, would be equal to

$$Y = P_T + P_T(1 - P_T)\epsilon \tag{5.12}$$

where ϵ is a zero-mean Gaussian noise with the variance $\frac{\sigma_0^2}{n}$.

5.2.1 Hetero-type Decode-and-Forward Relaying

Here, we consider a scenario in which the relay uses a different molecule than the transmitter node. In other words, upon the reception of the type I molecules from the transmitter, the relay forwards the decoded symbol P_R by using type II molecules (i.e., hetero-type relaying). Note that due to noisy decoding at the relay, P_R is not necessarily equal to P_T. The two types of molecules arriving from both the direct path and from the relay are then used at the destination to decode the transmitted symbol.

The two types of molecules at the destination would result in two different outputs such as GFP and YFP, i.e., the Green and Yellow Fluorescent Proteins. We neglect the subtle interference between the two different types of molecules at the destination and assume that they act independently. We assume that the reception is the same for the two types of molecules but may differs in the noise attribute σ_0^2. We denote by Y_D and Y_R the normalized outputs due to the direct and relay paths, respectively. Hence, we have

$$\begin{cases} Y_D &= P_T + P_T(1 - P_T)\epsilon_D \\ Y_R &= P_R + P_R(1 - P_R)\epsilon_R \end{cases} \tag{5.13}$$

where ϵ_D and ϵ_R are zero-mean noises with variances $\frac{\sigma_D^2}{n}$ and $\frac{\sigma_R^2}{n}$, respectively. Moreover, σ_D^2 and σ_R^2 correspond to the noises in the reception of type I and II molecules, respectively.
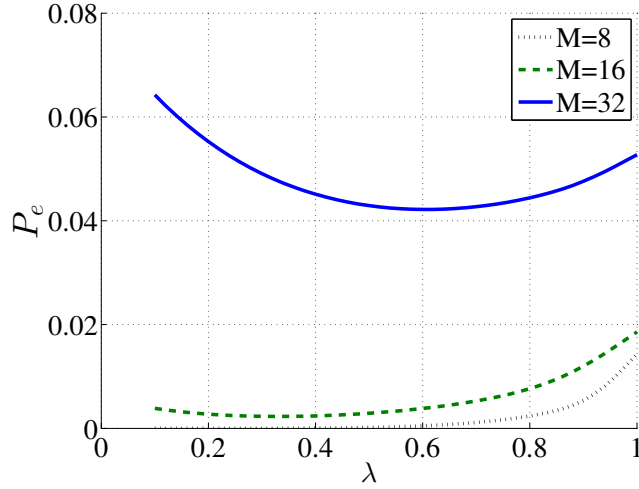
Figure 5.4. Average probability of error vs λ for different M-ary schemes.

Note that P_R would be different from P_T in case the decoding at the relay node is erroneous.

We consider a linear combination of the outputs $\hat{Y} = w_D Y_D + w_R Y_R$ in order to decode the transmitted symbol. In a collocated multiantenna setup [144], Maximum Ratio Combining (MRC) employs the optimal weights $w_i = \frac{h_i}{\bar{n}_i^2}$, where h_i is the attenuation of the ith channel and $\bar{n}_i^2$ is the average power of the corresponding channel noise. Likewise, adapting MRC in our setup, the optimal weights would be given by $w_R = \frac{1}{\sigma_R^2}$ and $w_D = \frac{1}{\sigma_D^2}$. However, since the relaying node may have a decoding error, the performance of MRC would be sub-optimal for our setup.

Different approaches have been proposed in classical wireless communication literature to find the optimal weights in a decode-and-forward relaying scenario. In [145], the two consecutive source-relay and relay-destination channels are replaced with an equivalent Gaussian channel. In [146], authors have introduced a generalized form of λ-MRC in which w_D is fixed to its MRC value and w_R is considered to be λ times its MRC value, where $0 \leq \lambda \leq 1$. Here we use a similar method as the one in λ-MRC. Without loss of generality, we assume $\sigma_R^2 = \sigma_D^2 = \sigma_0^2$. Further, we fix $w_D = \frac{1}{\sigma_0^2}$ and assume $w_R = \frac{\lambda}{\sigma_0^2}$ where $0 \leq \lambda \leq 1$. Hence, by combining the outputs in (5.13), we have

$$\hat{Y} = P_{\mathrm{T}} + \lambda P_{\mathrm{R}} + \epsilon_Y, \tag{5.14}$$

where ϵ_Y is a zero-mean Gaussian noise with the variance $\frac{\sigma_0^2}{n}(P_{\mathrm{T}}^2(1 - P_{\mathrm{T}})^2 + \lambda^2 P_{\mathrm{R}}^2(1 - P_{\mathrm{R}})^2)$.

We obtain the optimal value of λ that minimizes the M-ary average probability of error in (4.31). Further, we assume that only transitions to the adjacent symbols would cause error at the relay node. In other words, if the ith symbol is sent, P_{R} would be in $\{p_{i-1}, p_i, p_{i+1}\}$. In Fig. 5.4, we have plotted P_e vs λ for different values of M. The results are shown for $n = 100$, $p_{\max} = 0.95$ and $\sigma_0^2 = 0.6$ corresponding to a highly-noisy situation. Fig. 5.4 shows the existence of an optimal λ. The rationale for this behavior is that increasing λ, on the one hand, extends the maximum range of the output and hence, improving the reliability. On the other hand, increasing λ would increase the influence of the more noisy symbol from the relay node, which in turn would decrease the reliability.

In Fig. 5.5, we have plotted the probability of error with and without using the relay with the optimal choice of λ for $M = 8$ and $M = 16$. Furthermore, $r_1 = r_2 = r_3$, $n = 100$ and $\sigma_0^2 = 0.6$. As we can see in the plots, the advantage of relaying diminishes for large values of $A_{\max}$ for $M = 8$ where the probability of error approaches zero, but prevails for $M = 16$ where achieving an arbitrary probability of error is impossible without relaying. In other words, depending on the signaling, the relative advantage of hetero-type relaying can be either achieving a lower asymptotic probability of error or achieving the asymptotic value with a lower range of the molecular input (i.e., power).

5.2.2 Same-type Decode and Forward relaying in M-ary signaling

In this section, we study the scenario in which the relay node decodes the incoming information symbol from the transmitter and forwards it via the same type of molecules to the destination. We compare the performance of such a relaying scenario with the hetero-type relaying scenario discussed in the previous section. It is important to note that we assume the production of the same type of molecules by the relay does not affect the relay input

(a) M=8   (b) M=16
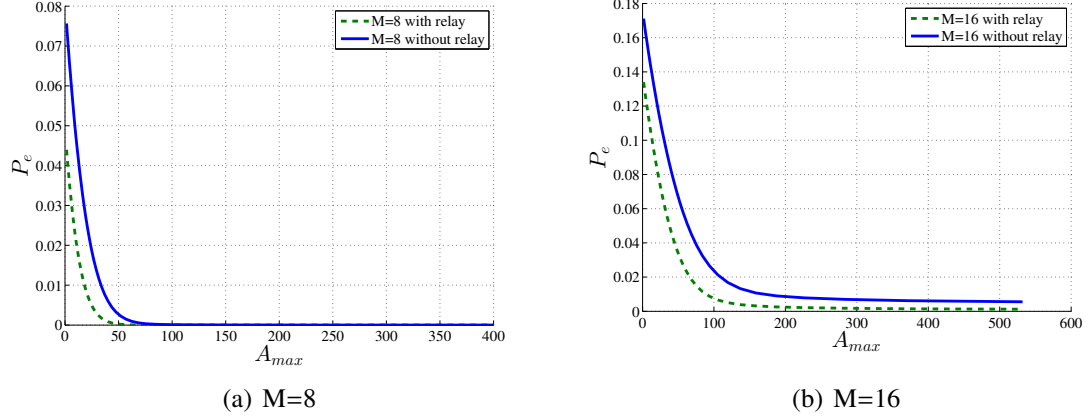
Figure 5.5. The average probability of error with and without using relaying vs maximum concentration of molecules.

coming from the transmitter. The relay output production contains a huge amount of delay and the relay node can be designed such that the production of molecules would shut off the reception of molecules by the relay node. The arriving molecules from both the relay and direct paths would form the concentration of molecules at the destination. Since the relay employs the same type of molecules as at the transmitter node and also the diffusion is linear [31], the concentration of molecules at the destination would be the superposition of the individual concentrations of molecules induced by the transmitter and the relay nodes.

For $0 \leq i \leq M - 1$, let A_i and B_i be the concentrations of molecules induced by the transmitter at the destination node and the relay node, respectively. Likewise, let C_i be the concentration induced by the relay at the destination node. As discussed in the previous section, by the broadcast nature of the diffusion channel, producing the concentration A_i at the destination corresponds to the production of the concentration $B_i = A_i \frac{r_1}{r_2}$ at the relay. Assume each concentration symbol A_i designed optimally in the range $[0 \ A_{\max}]$ for the destination node is mapped linearly to the concentration symbol B_i in $[0 \ \frac{r_1}{r_2} A_{\max}]$ at the relay node. Hence, the distribution of the B_i concentration symbol at the relay input would be optimal as well.

Assume the concentration symbol $B_j, (0 \leq j \leq M - 1)$, is decoded at the relay. In response, the relay induces the concentration symbol C_j in the range of $[0 \ \frac{r_1}{r_3} A_{\max}]$ at the

65
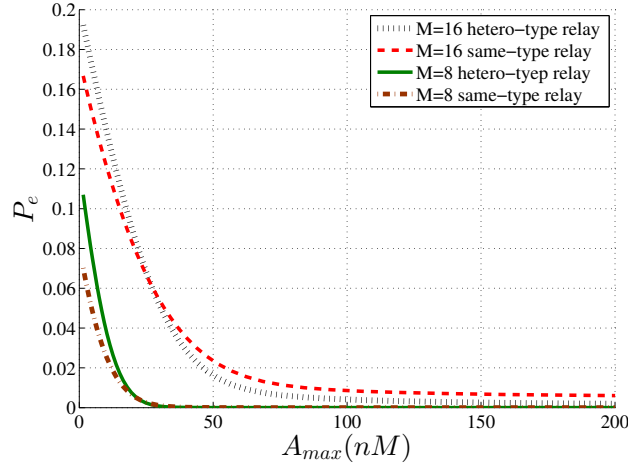
Figure 5.6. Comparison between relaying using one and two types of molecules.

destination. Then the aggregated concentration of molecules from both the direct and relay paths would be $A_i + C_j$ which is in the range $[0 \ A_{\max}(1 + \frac{r_1}{r_3})]$. The output Y_D at the destination is given by

$$Y_D = \frac{(A_i + C_j)\gamma_0}{(A_i + C_j)\gamma_0 + \kappa_0} + \epsilon_D, \tag{5.15}$$

where ϵ_D is a signal-dependent noise as in the previous section. We assume the destination uses maximum a posteriori (MAP) detection to decode the concentration symbol A_i. Hence, we have

$$P(A_i|Y_D) \propto P(Y_D|A_i)P(A_i) = \sum_{j=0}^{M-1} P(Y_D|A_i, C_j)P(C_j|A_i)P(A_i), \tag{5.16}$$

In (5.16), $P(Y_D|A_i, C_j) = P(Y_D|A_i + C_j) = P(\epsilon_D|A_i + C_j)$ where ϵ is the conditionally Gaussian noise in (5.15). Moreover, since the mapping from B_j to C_j and from A_i to B_i are one-to-one, $P(C_j|A_i) = P(B_j|B_i)$ and we have

$$P(B_j|B_i) = P(j = arg\max_k P(B_k|Y_R)) \tag{5.17}$$

where Y_R is the output at the relay with a conditionally Gaussian distribution $\mathbf{N}(p_i, p_i^2(1 - p_i)^2 \frac{\sigma_0^2}{n})$ in which $p_i = \frac{B_i\gamma}{B_i\gamma + \kappa}$.

We have plotted the probability of error for the same-type relaying scenario in Fig. 5.6 and compared it with the hetero-type relaying discussed in the previous section for $M = 8$

and $M = 16$. We have used the parameters $n = 100$ and $\sigma_0^2 = 0.6$, and $r_1 = r_2 = r_3$, as in the previous section. As we see in the plot, the same-type relaying outperforms the hetero-type scenario for very low molecular input ranges but underperforms it otherwise. Moreover, by comparing this plot with Fig. 5.5, we observe that same-type relaying loses its effectiveness for large A_{max}. This is in contrast with hetero-type relaying which is advantageous even for large A_{max}. This is due to the fact that hetero-type relaying not only results in the extension of the range of the molecular concentration but also introduces molecular diversity at the destination.

5.3   Conclusion

In this chapter, we studied the relaying problem in the context of molecular communication to enhance the reliability. We considered both the case that the relay node simply senses and forwards the received continuous concentration of molecules and the practical case that relay decodes the received M-ary symbol and forwards it to the destination node. In the first case, we showed that if the relay uses the same type of molecules as the transmitter, relaying effectively results in expanding the range of the concentration of molecules at the destination, and hence, increases the capacity. This effect is more significant for the low range of concentrations. On the other hand, by using a different type of molecules, relaying nearly corresponds to increasing the effective number of bacteria in the nodes which increases the capacity for low and high molecular ranges alike.

For decode-and-forward relaying with M-ary scheme, the relay node decodes the incoming symbol from the transmitter and forwards it to the destination using the same or different type of molecules as the transmitter. In the hetero-type case, we showed as to how the optimal combining of the outputs results in improving the reliability of the communication. We also compared the results with the same-type relaying scenario. We showed that except for the mid-range values of maximum concentration of molecules, the hetero-type relaying outperforms the same-type relaying.

CHAPTER 6

ERROR-DETECTION SCHEMES IN MOLECULAR COMMUNICATION

In the previous chapters, we discussed how the MC reliability can be improved via the node design and also by the use of relay nodes. In certain sensitive applications such as biochemical sensing, (nearly) perfect error detection may be required while loss of some symbols can be tolerated. Hence, in this chapter, we develop suitable error-detecting coding schemes which meet the molecular communication specific constraints in terms of reliability and complexity, and take into account the communication channel properties [100].

We show the trade-off between the code rate and probability of error in such detection codes. Using the constant-weight codewords can achieve a perfect error detection capability at the cost of losing the rate significantly. However, in most of the applications, a small probability of error can be tolerated by the system without significantly harming the functionality. As such, we will study how the rate can be optimized with constraining the probability of error [107].

6.1   Error in binary Diffusion-based Molecular Communication

In this chapter, we focus on a binary molecular communication setting in which the transmitter emits a certain molecular concentration level for a duration T in order to send symbol "1" and shuts off for sending symbol "0". The duration T must be long enough to give the receiver sufficient time to sense the concentration of molecules. It must also provide enough time for the channel to reset from high to low. The optimal values of T was discussed in Chapter 4. Here, we assume that T is sufficiently large that the receiver output can reach the steady state and there would be no inter-symbol interference (ISI). The independent decoding of the successive symbols can be further justified through the use of variant strategies to cancel the ISI in the channel. In [39], the authors have introduced the use of enzyms

to expedite the channel reseting process. Alternative use of multiple molecule types (depending on the channel memory intensity) to transmit successive symbols independently has also been discussed in [40].

Let $A_0^{(i)}$ and $p_0^{(i)}$ be the values of A_0 and p_0 for transmitting bit i, where $i = 0, 1$. As we can see in (4.25), the variance and hence, the probability of error is zero for sending $A_0^{(0)} = 0$ (i.e., $p_0^{(0)} = 0$) which corresponds to the transmitter being shut off for sending the symbol "0". For the transmission of symbol "1", one may assume a very large $A_0^{(1)}$ in (4.2) that would approximately result in $p_0^{(1)} = 1$. However, inducing high entrapment probabilities are impractical, especially for longer communication distances, due to energy constraints. Based on (4.25), by choosing p_0 for sending bit "1", the probability of error (i.e., decoding symbol "1" as "0") can be written as:

$$p_e = \int_{-\infty}^{p_{th}} \frac{1}{\sqrt{2\pi p_0^{(1)2}(1 - p_0^{(1)})^2 \frac{\sigma_0^2}{m}}} \exp\left(-\frac{(p - p_0^{(1)})^2}{2p_0^{(1)2}(1 - p_0^{(1)})^2 \frac{\sigma_0^2}{m}}\right) dp \qquad (6.1)$$

where p_{th} corresponds to the minimum concentration of molecules that bacteria are able to sense. Numerical analysis of (6.1) shows that p_e is monotonically decreasing for $p_0^{(1)}$ greater than p_{th}. In other words, in order to minimize the probability of error in transmission of the symbol "1", the transmitter should use the highest concentration of molecules that it can induce at the receiver. On the other hand, factors such as the limited rate of molecule production, energy constraints, and the need for longer shut-off time (to avoid inter-symbol interference) prevent the transmitter from using high concentrations of molecules [35].

Furthermore, in the absence of other transmitters in the vicinity, the molecules cannot be produced in either the channel or the receiver and can only be lost. As such, unlike the bit "1", the bit "0" can be transmitted almost without any error. Hence, based on the above discussion, we model the above two-node molecular communication with a z-channel, depicted in Fig. 6.1, in which the bit "0" is transmitted with no error while the bit "1" entails a non-zero probability of error p_e as derived in (6.1). Note that the proposed error-detection codes are envisioned for sensing purposes which require high-accuracy but
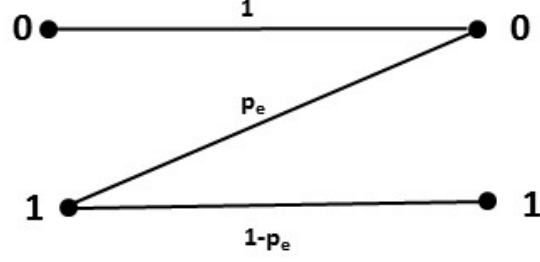
Figure 6.1. The z-channel model

communication is sparse. Hence, one needs to worry only about the ISI between bits of the same codeword. Moreover, this assumption could only increase the theoretical bounds obtained in the following sections whereas the actual decoding proposed in Section 6.4 is done biologically over the code block length.

6.1.1 The Error Detection Model

We consider a binary completely asymmetric channel (i.e., z-channel) with the transition probability of p_e from the bit "1" to "0". Clearly, by the z-channel definition, there is no error in transmitting the bit "0". Our objective is to find the optimal codewords for an error-detection scheme in this z-channel. We denote by **S** the codeword set where **S** $\subseteq \{0, 1\}^n$, and the codewords by $X^n \in$ **S** where X^n are length n binary vectors. In order to capture the transition between the codewords in the aforementioned z- channel, we define a codeword transition matrix **P** where

$$\mathbf{P}_{i,j} = Prob(X_i^n \rightarrow X_j^n). \tag{6.2}$$

As an example, the general transition matrix is as follows for $n = 2$ (illustrated for the hypothetical case of **S** $= \{0, 1\}^2$):

$$
\begin{array}{c c c c c}
 & (0,0) & (0,1) & (1,0) & (1,1) \\
\begin{array}{c} (0,0) \\ (0,1) \\ (1,0) \\ (1,1) \end{array} &
\left[\begin{array}{c} 1 \\ p_e \\ p_e \\ p_e^2 \end{array} \right. &
\begin{array}{c} 0 \\ 1 - p_e \\ 0 \\ p_e(1 - p_e) \end{array} &
\begin{array}{c} 0 \\ 0 \\ 1 - p_e \\ p_e(1 - p_e) \end{array} &
\left. \begin{array}{c} 0 \\ 0 \\ 0 \\ (1 - p_e)^2 \end{array} \right]
\end{array}
$$

70

At the receiver side, any vector that is not in **S** is erroneous and hence, discarded. Thus, we treat all such received vectors as an erasure symbol E. Hence, the received set would be $\{S'\} = \{S\} \cup E$. The average probability of error in such a setting can be written as

$$P_{\text{avg}} = \sum_{i=1}^{K} p_i \sum_{j:X_j^n < X_i^n} \mathbf{P}_{i,j,} \tag{6.3}$$

where p_i is the probability of sending X_i^n and K is the number of codewords. Note that $X_j^n < X_i^n$ if and only if $i \neq j$ and for every "1" in X_j^n, the corresponding position in X_i^n is "1" as well. The new transition matrix, by considering the E symbol, can be obtained by reducing the general transition matrix and removing the rows corresponding to the vectors $X_i \notin \mathbf{S}$ and adding the corresponding column to the E column. For example, the reduced transition matrix resulting from removing the vector $(0,0)$ from $\mathbf{S} = \{0,1\}^2$ would be:

$$
\begin{array}{c}
\begin{array}{cccc}
(0,1) & (1,0) & (1,1) & E
\end{array} \\
\begin{array}{c}
(0,1) \\
(1,0) \\
(1,1)
\end{array}
\left(
\begin{array}{cccc}
1 - p_e & 0 & 0 & p_e \\
0 & 1 - p_e & 0 & p_e \\
p_e(1 - p_e) & p_e(1 - p_e) & (1 - p_e)^2 & p_e^2
\end{array}
\right)
\end{array}
$$

The performance of such a detection scheme can be measured in terms of probability of error and the code rate. Our goal is to find the detection code set **S** (and equivalently the set **S'**) that is optimal in the sense that a given probability of error is satisfied and the code rate (or information rate) of the detection scheme is maximized. Hence, the end-to-end model to transmit and receive the codewords is captured by the codeword transition matrix $P(Y^n|X^n)$ where the input symbols are the codewords $X^n \in \mathbf{S}$, the outputs are the received words $Y^n \in \mathbf{S'}$, and the bit-wise transition probabilities follow a z-channel model. Depending on the assumptions and the encoding/decoding complexity, we deploy two different theoretical measures to capture the optimality of the coding scheme.

In the first case, we consider an encoder that can generate the codewords with any arbitrary relative frequency. Moreover, we do not assume any source coding at the transmitter which means the input symbols may have different probability of occurrence. This is especially of interest for the bio-sensing applications where the low concentration regime is usually more probable to occur. Moreover, since it is not possible to achieve zero probability of error with the simple error-detecting receiver described above, in the erasure channel with error model $H(Y^n|X^n) \neq 0$. Now the question of interest is to find the upper-bound on the rate of the error-detection code over the z-channel subject to a detection-error probability constraint. This question is equivalent to finding an upper-bound on the information delivery over the erasure channel with error, subject to an inter-symbol error constraint. From now on, we refer to this model as the erasure channel. In order to establish a theoretical upper limit to the rate of the error-detection scheme, we define the error-detection capacity as follows:

$$c'(p_T) \triangleq \max_{p(x)} H(X) - H(X|Y) \text{ provided that } P_{\text{avg}} < p_T, \quad (6.4)$$

where X is a transmitted symbol and Y is a received symbol. Moreover, p_T is the constraint on the detection-error probability and $p(x)$ is the probability distribution over the set of input symbols in the erasure channel model. Moreover, we consider the rate of the error-detection code to be the amount of information that a transmitted codeword yield on average at the receiver. This corresponds to $r = I(X;Y)$ over the erasure channel, which is a function of the input codeword distribution. Hence, the maximum rate of any error-detection code subject to a detection-error probability constraint can be written as:

$$r'(p_T) = \max\{r : P_{\text{avg}} < p_T\}. \quad (6.5)$$

Note that by definition, $r'(p_t) \leq c'(p_T)$. In other words, $c'(p_T)$ is the theoretical limit for the rate of any error-detection scheme in the z-channel given the detection-error constraint p_T and the model described above. Hence, in order to find the optimal codeword set for the z-channel, given the probability of detection-error constraint, one needs to find the

Table 6.1. The effect of removing a vector from $\mathbf{S} = \{0, 1\}^2$

	$(0, 0)$	$(0, 1)$	$(1, 0)$	$(1, 1)$
R ($bits/codeword$)	1.2076	1.2118	1.2118	1.2592
P_{avg}	0.0436	0.0615	0.0615	0.0647

optimal codeword subset and the corresponding optimizing distribution that maximizes the detection capacity in (6.4).

In the second case, we consider an encoder that generates the codewords equiprobably and the decoder performs single codeword decoding by discarding any received codewords outside the codebook (i.e., ignoring the erasure symbols). Note that, unlike the previous theoretically optimal case, here the information about the input by observing the erasure output, which is non-zero when different codewords have different probability of transforming into the erasure symbol, is lost. Hence, in order to find the optimal subset, given the error probability constraint, one needs to maximize $R = \frac{\log N}{n}$ where N is the number of codewords.

6.2 Optimal error-detection codes via Maximizing the Mutual Information

In this section, we study the first case discussed in the previous section. In order to obtain the optimal distribution and hence, the maximum information rate for each choice of $\mathbf{S}$, we use the Blahut-Arimoto (BA) algorithm [147] on the corresponding codeword transition matrix. As a toy example, for $n = 2$ and $\mathbf{S} = \{0, 1\}^2$, the maximum rate and the corresponding average probability of error are obtained as $R = 1.525$ bits/codeword and $P_{\text{avg}} = 0.089$. The resulting average probability of error P_{avg} and optimal rate R achieved by removing only one vector from the general transition matrix, are shown in Table 6.1. Here, the vector shown in the column is removed from $\mathbf{S} = \{0, 1\}^2$. As we observe in this Table, there exists a trade-off between the rate and the probability of error. We also observe that perturbing the error constraint may result in a completely different subset of codewords. In other words,

different constraints on P_{avg} may result in different orders that the vectors are removed.

It can be shown that finding the optimal codewords in the above general scenario is an NP-hard problem. In order to solve the problem for a more specific case, we model it on a directed graph. We have shown the codeword transition graph for $n = 3$ in Fig. 6.2. In such a directed graph, each potential codeword is represented by a vertex and the vectors are arranged from the highest (hamming) weight to the lowest such that vectors with the same weights are on the same level (i.e., drawn on the same horizontal level). The edges of the codeword graph represent the transition of a vector to another with only a single bit error. A vector can be transformed to another by the channel error if and only if there exists a directed path between input and the output vectors. Due to the asymmetric nature of the channel, the transformations can only happen from a codeword to the ones with lower weights located on lower levels of the graph. The probability of such transformation p_t is equal to:

$$p_t = p_e^h (1 - p_e)^{w-h} \tag{6.6}$$

where w is the transmitted vector weight and h is the number of hops in the directed path to the received vector.

We can also observe that the transformation probability is unique regardless of the path. The reason is that at each hop, the vector weight decreases by 1. Since traversing to above or across nodes are not possible, the number of hops is always equal to the difference in vector weights and independent of the chosen path. Based on the above description, the problem of finding the optimal code would reduce to finding the optimal subset of vertices of the above graph that satisfies the error probability constraint.

6.2.1 Dynamic-programming based Algorithm to Find the Optimal Code

In order to provide an algorithm rather than the brute-force search to find the optimal codewords, we make two simplifying assumptions to the optimality definition we had:
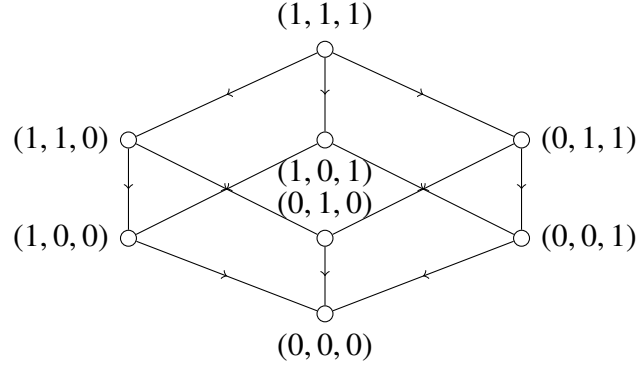
Figure 6.2. The codeword graph for n=3; the collection of all potential codewords

1. We relax the average probability of the detection error constraint and instead use an upper limit on the maximum probability of the detection error. The advantage of this modification is that we will be able to set a minimum distance h^* between each pair of chosen codewords and hence, can decide whether a subset is a viable code set before running the BA algorithm.

2. We confine ourselves to small enough p_e such that the transition probability between two codewords of the distance more than h^* would be negligible. This assumption, as shown later, makes choosing the optimal codewords of two subsets with distance more than h^* independent of each other. In the case that p_e does not satisfy this condition, h^* needs to be increased beyond the level set by the maximum error probability constraint.

In the first phase of the algorithm, we need to obtain the minimum edge distance of the codewords to satisfy the maximum error probability constraint. Edge distance of two codewords is the directed distance between their corresponding vertices on the codeword graph.

Lemma 2. *In order to comply with the maximum error probability p_{max}, the codewords must be at least in the distance h^* from each other where h^* is the minimum integer that satisfies* $\max_w \binom{w}{h}\left(\frac{p_e}{1-p_e}\right)^h (1 - p_e)^w \leq p_{max}$ *for* $0 \leq w \leq n$.

75

Proof. Consider the codeword c_w with the weight w. Since the weight of the vectors at the distance h from c_w is $w - h$, there are $\binom{w}{h}$ vectors at distance h that c_w can be transformed to. Using (6.6), to satisfy the error constraint, we need $\max_w \binom{w}{h} \left(\frac{p_e}{1-p_e} \right)^h (1 - p_e)^w \leq p_{\max}$ where $0 \leq w \leq n$. Note that for the small values of p_e, $w = n$ maximizes the above criterion. □

In the second phase of the algorithm, we employ dynamic programming [148] to find the optimal code given the minimum edge distance h^*. First, we observe the following:

Lemma 3. *If one vector with weight w is chosen as a codeword, all the vectors with the same weight must be selected.*

Proof. First, we observe that since all the vectors with the same weight are on the same level in the codeword graph, the minimum edge distance remains intact by exhausting all the codewords in that level. Hence, the maximum probability of error constraint would still hold. Secondly, adding more codewords to the existing subset of codewords can only increase the information rate of the detection scheme. The reason is that the optimal distribution for the original subset can be achieved by setting the channel input distribution corresponding to the new codewords to zero. Hence, the rate of the old codeword set is always sub-optimal to the one obtained by the new set. □

Hence, the problem of finding the optimal code reduces to finding the optimal codeword weights. Note that this alone reduces the number of viable sets, i.e., number of BA algorithm runs, from $O(2^{(2^n)})$ to $O(2^n)$. Now, we resort to dynamic programming to obtain the optimal weights with $O(n)$ runs of the BA algorithm. We assume C_k to be the set of weight-k vectors, S_k to be the optimal codeword set using only the weights lower than or equal to k, and R_k^* to be the corresponding optimal rate. Moreover, we denote by $R(\Pi)$ the rate of the set Π. Our objective is to obtain S_n and R_n^*. The algorithm works as follows:

- Initialize S_0 by C_0 and S_k by the empty set for $k < 0$.

- Initialize R_k^* to zero for $k \leq 0$.

- for $k = 1, 2, 3, \ldots, n$, do:

$R_k^* = \max(R(C_k \cup S_{k-h^*}), R(C_k \cup S_{k-h^*-1}), R_{k-1}^*, R_{k-2}^* \ldots, R_{k-h^*+1}^*)$.

Update S_k according to the set that achieves the maximum in the above term. In other words, set S_k to either $C_k \cup S_{k-h^*}$, or $C_k \cup S_{k-h^*-1}$, or $S_{k-1}, \ldots$, or S_{k-h^*+1}, accordingly.

The above algorithm ensures that the minimum edge distance between the codewords is always held at h^* and builds upon the solutions to the smaller sets in order to obtain the optimal solution of the larger ones. Note that at the maximization step, the average probability of error can be calculated since the optimal distribution of the codewords is already obtained by the BA algorithm at that step. Hence, one could discard the choices that yield average probability of error greater than a threshold with no additional cost. In order to obtain R_n^* and S_n, in each iteration, we need two runs of the BA algorithm and $O(h^*)$ comparisons which is negligible compared with the BA algorithm cost. Hence, we have reduced the total number of BA algorithm runs from $O(2^n)$ to $O(n)$. It is worth noting that the overall performance of the above algorithm is not linear in n as the BA algorithm itself has quadratic complexity with respect to number of symbols and hence, exponential with respect to n. Before we prove the correctness of the above algorithm, we need the following lemma.

Lemma 4. *Assume the codeword subsets S_1 and T_1 are the optimal subsets of the sets S and T, respectively, which satisfy the maximum error detection probability constraint. If there exists no transition probability between the codewords of the sets S and T, $S_1 \cup T_1$ would be the optimal codewords for $S \cup T$ under the same constraints.*

Proof. First, notice that since there is no transition probability between the codewords of S_1 and T_1, the overall transition matrix is in the form of $C = \begin{bmatrix} T_1 & 0 \\ \hline 0 & S_1 \end{bmatrix}$. Hence, this transition matrix can be viewed as two independent parallel channels with overall rate of $R(S_1 \cup T_1) = R(S_1) + R(T_1)$. Now imagine there were subsets $S_2 \subset S$ and $T_2 \subset T$ which $S_2 \cup T_2$ would give the optimal rate for the set $S \cup T$, i.e., $R(S_1 \cup T_1) < R(S_2 \cup T_2)$. Since the

transition matrix of $S_2 \cup T_2$ has a similar form as above, we would have $R(S_1) + R(T_1) < R(S_2) + R(T_2)$ which would mean that either $R(S_1) < R(S_2)$ or $R(T_1) < R(T_2)$, or both. Suppose the first case was true. Since $S_2 \cup T_2$ is assumed to satisfy the maximum error probability, each one of the individual sets must satisfy the constraint individually. Hence, there would exist a subset $S_2 \subset S$ that achieves a higher rate than the optimal subset S_1 under the same constraint, which is a contradiction. □

Theorem 5. *The proposed dynamic algorithm ensures finding the optimal code under the maximum error probability constraint.*

Proof. In order to show the correctness of the algorithm, we need to show that given the optimal answer for the sub-problems $1, 2, \ldots, k-1$, the algorithm gives the optimal answer for the kth problem. First, assume the weight-k vectors C_k are not included in S_k. Since the minimum edge distance of the codewords must be h^*, R_k^* would be $\max(R_{k-1}^*, R_{k-2}^*, \ldots, R_{k-h^*+1}^*)$ and S_k would be the corresponding subset. Note that $R_{k-h^*}^*$ cannot be the optimal answer as adding C_k to S_{k-h^*} would increase the optimal rate while we assumed C_k is not included in S_k. Now consider the case where C_k is indeed in the optimal codeword set S_k. We consider two sub-cases:

First, consider the case that C_{k-h^*} is not included in S_{k-h^*}, i.e., $S_{k-h^*} = S_{k-h^*-1}$. Here, the set $S_{k-h^*} \cup C_k$ would be the optimal set because the minimum edge distance between C_k and S_{k-h^*} is greater than h^* and since we ignore the transition between two codewords of edge distance more than h^*, using Lemma 4, choosing C_k does not impact the optimality of S_{k-h^*}.

Next, consider the case that C_{k-h^*} is actually included in S_{k-h^*}, and hence, picking C_k could possibly impact the optimality of S_{k-h^*} for the smaller problem. This could possibly result in evicting C_{k-h^*} from the optimal set. If so, the rest of the codewords are in distance at least $h^* + 1$ from C_k, and hence, S_{k-h^*-1} would be the optimal subset for the smaller problem. If C_{k-h^*} is not evicted from the optimal set, since other codewords in S_{k-h^*} are not
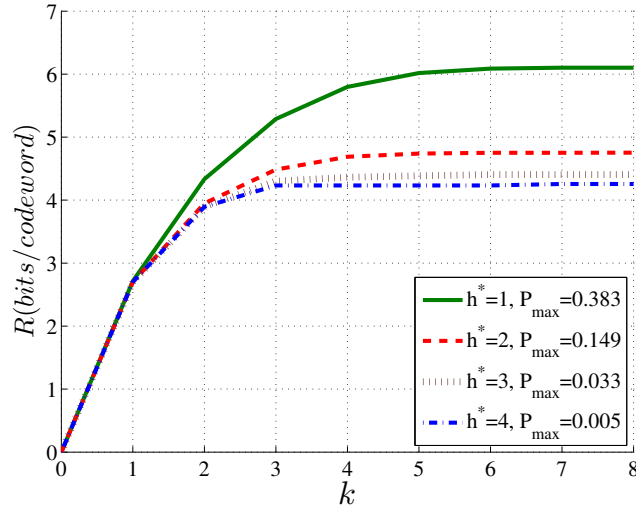
Figure 6.3. Optimal rates at each step of the algorithm

impacted by the presence of C_k (as their distance is more than h^*), S_{k-h^*} remains optimal. Hence, we need to consider $R(C_k \cup S_{k-h^*})$ and $R(C_k \cup S_{k-h^*-1})$ in the maximization step of the algorithm for the case that C_k is included in the optimal set as well as $R^*_{k-1}, R^*_{k-2}, \ldots, R^*_{k-h^*+1}$ for the case that C_k is not included. $\square$
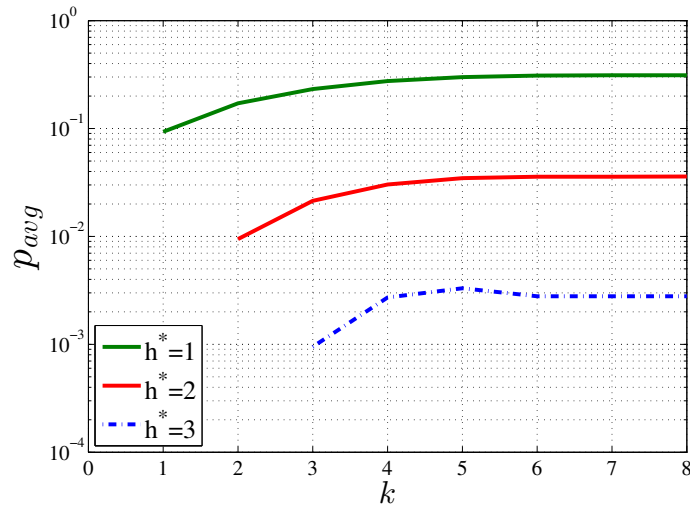
Figure 6.4. Optimal codewords' average probability of error at each step

In Fig. 6.3, we have shown the optimal rate at each step of the algorithm for $n = 8$, $p_e = 0.1$, different values of h^*, and the corresponding maximum error probability. Note that $h^* = 1$ corresponds to the case that all the vectors can be used. We can observe the
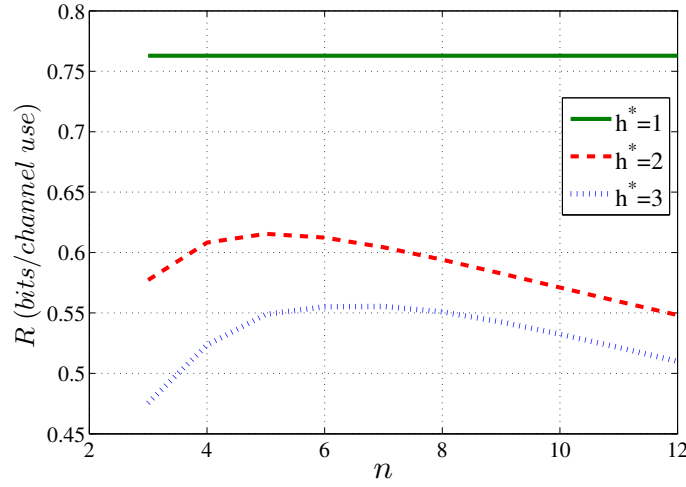
Figure 6.5. Optimal rate for different block lengths

amount of forgone rate in order to achieve lower maximum error probabilities. Further, the incremental value of the higher-weight vectors diminishes at each step. On the other hand, in order to show the negative effect of high-weight codewords, we have plotted the average probability of error for the optimal codewords at each step of the algorithm in Fig. 6.4. As we can see in this plot, the average probability of error continues to increase even when there is no significant improvement in the rate by including more high-weight vectors in the code set. This suggests stopping the algorithm when the rate improvement is negligible by increasing k. In Fig. 6.5, we have shown the behavior of optimal rate per channel use versus the block length n for different values of h^* and $p_e = 0.1$. As we see in the plot, for $h^* = 1$, where we can employ all the vectors, the rate is independent of n. In contrast, for higher values of h^* (where the erasure symbol exists), there exists an optimal code length beyond which the code rate decreases and eventually approaches zero.

6.3   Optimal error-detection codes via Maximizing the Code Rate

In this section, we consider the second case discussed in Section 6.1 which finds the optimal error-detection codewords with more practical assumptions than in the previous section. We achieve this goal through maximizing the codeword rate $R = \frac{\log N}{n}$, where N is the

number of codewords in $\mathbf{S} = \{0, 1\}^2$. We also assume the average probability of error defined in (6.3) is limited to P_T. Since we assume equiprobable codewords (i.e., the channel input), the average probability of error can be written as

$$P_{avg} = \frac{1}{n} \sum_{i=1}^{n} \sum_{j=1, j \neq i}^{n} \mathbf{P}(i, j), \tag{6.7}$$

where $\mathbf{P}$ is the transition matrix in (6.2). Hence, our objective is to find the optimal submatrix of $\mathbf{P}$, by removing the minimum number of rows and the corresponding columns, that would result in maximum R and meet the error probability criterion. Note that each column, upon its removal, should be added to the last column corresponding to the erasure symbol.

The above problem resembles the bi-clustering problem which has been studied extensively in the gene expression context. In such applications, the objective is to find the sub-clusters of a two-dimensional matrix which meet specified patterns on the rows and/or columns [149]. As the general problem in biclustering is NP-hard, greedy algorithms are among the most common methods to find the near-optimal clusters. Here, we deploy the two-phased δ-biclustering algorithm introduced in [150]. In the first phase of the algorithm, rows (and their corresponding columns) are greedily removed until the specified criterion is met. In the second phase, the algorithm greedily adds back the removed rows (and columns) which would still hold the criterion. Here is the outline of the algorithm to find the maximum number of codewords that satisfy the $P_{avg} < P_T$ requirement:

- while $P_{avg} > P_T$:

  - Remove the row (and the corresponding column) that would result in maximum reduction in P_{avg}

- while $P_{avg} <= P_T$:

  - Add back the row (and the corresponding column) that would result in minimum increment to P_{avg}
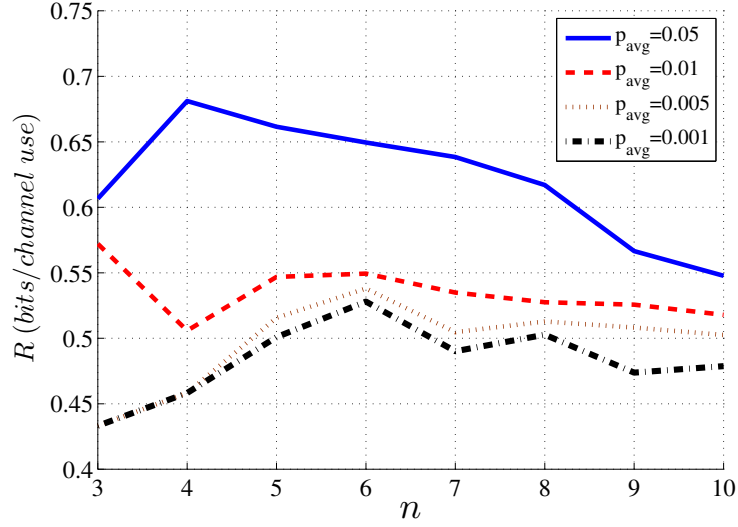
Figure 6.6. Code rate versus block length for various values of average probability of error

In Fig. 6.6, we have plotted the transmission rate $R = \frac{\log N}{n} * (1 - P_E)$ versus the codeword length n for different values of P_{avg} and $p_e = 0.1$. Here, P_E is the average probability of erasure which corresponds to the case where the codewords are discarded by the receiver. As we can see in the plot, due to the greedy nature of the algorithm, the curves behave irregularly with respect to n, especially for larger values of P_{avg}. By lowering P_{avg}, the curves converge; as extremely small error probabilities are only possible by choosing a single weight corresponding to zero error probability.

6.4 Coding Schemes for Perfect Error Detection in Molecular Communication

In this section, we study and analyze the constant-weight codes for molecular communication. Constant-weight codes, notably the four out of eight codes, have been commonly used for error detection in completely asymmetric channels in the context of conventional communication systems [151]. Note that throughout this section, the code weight refers to the hamming weight. In such channels, the fixed weight of the codewords results in a perfect error detection mechanism as the codeword weights can only decrease by error and hence, any number of errors in a codeword can be detected. Berger in [152] introduced

a new class of perfect error-detection codes for completely asymmetric channels. In such codes, known as Berger codes, the number of zeros in each codeword is sent along with the codeword to the receiver as a binary number. Since errors can only reduce the number of "1" bits in a transmitted codeword, the number of zeros in the received codeword can only increase whereas the accompanying binary number can only decrease in value due to an error. Hence, in case any number of errors happen, the number of zeros in the received codeword would not match the received binary number which results in a perfect error detection.

These codes are sub-family of the general optimal codes discussed in Section 6.2, but they constrain the maximum probability of error to be zero. This coding scheme is suitable for the low complexity requirements of the molecular communication especially for the communication systems that need perfect error detection. As discussed in the previous section, the binary molecular communication can be approximated with a completely asymmetric channel in which the symbol "0" can be transmitted impeccably while there is a non-zero probability of error p_e in transmitting "1".

In addition, unlike the common case in molecular communication literature, we do not assume the existence of an additional mechanism to synchronize the transmitter and the receiver [153], and instead, we seek to provide synchronization using the proposed code. Moreover, since sending the symbol "0" and sending nothing are indistinguishable, the receiver cannot differentiate between codewords such as (0,0,1,1) and (0,1,1,0). To mitigate this problem and also synchronization, each codeword should begin with "1" to signal the beginning of a codeword. Note that we assume that the least significant digit is sent first. As such, no two codewords are the same by placing any number of "0" to their end or beginning.

One of the main constraints in designing a coding scheme for molecular communication is the low complexity requirements in encoding and decoding. Our objective is to

implement perfect error-detection schemes for the above molecular communication by employing constant weight codes, and to compare the rate loss compared with the theoretical limits from sections 6.2 and 6.3. Note that since the conversion of the symbol "0" into "1" is impossible, error among the codewords of the same weight cannot happen. At the receiver side, weight of the codewords is examined and in case of a mismatch with a preset weight, the codeword is discarded.

Here, we explain how the decoding at the receiver works. The arriving symbols are decoded one by one for the duration of the codeword length which is known to the receiver. The output of the receiver agents (e.g., bacteria) is only produced when symbol "1" is detected and it is in the form of Green Fluorescent Protein (GFP) [154]. Equipped with a circuitry, the receiver chamber should have the capability of detecting the aggregate output produced by the agents during the entire codeword. In order to check the codeword weights, the chamber circuitry accepts a codeword only if the aggregated level of the output surpasses a threshold. This threshold can be programmed beforehand and should be higher than the level obtained where the codeword weight is less than the preset weight. This way, any erroneous codeword can be detected and discarded when the output is below the threshold.

In order to analyze the general length n family of codes described here, we denote by w the constant weight of such codes and by p_e the probability of error for transmitting the symbol "1". Hence, the probability that error is occurred in a codeword, which results in being rejected by the receiver, is equal to $P_c = 1 - (1 - p_e)^w$. As the number of information bits in such a codeword is $\log_2 \binom{n}{w}$, the average rate (bits per channel use) for such a code would be

$$R = \frac{(1 - p_e)^w}{n} \log_2 \binom{n}{w}. \tag{6.8}$$

The code rate versus weight is shown in Fig. 6.7 for $n = 8$ and for different values of p_e. As we observe in the plot, and shown to be true for other values of n, optimal w
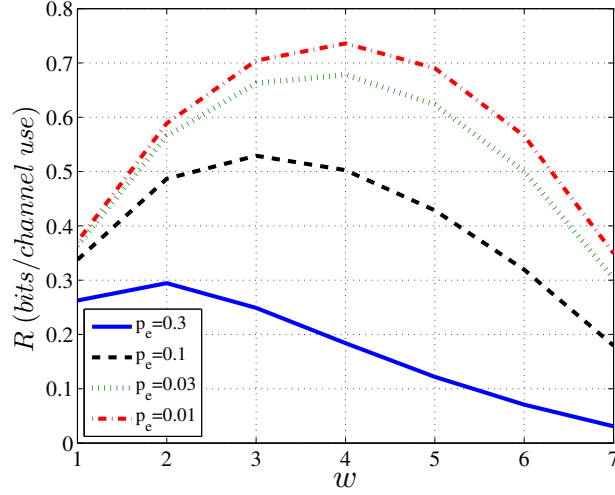
Figure 6.7. Code rates versus the codeword weight for different values of p_e
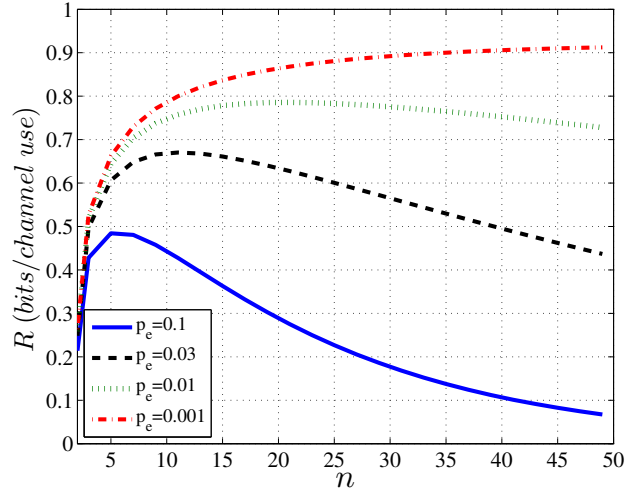
Figure 6.8. Optimal code rates versus the code length for different values of p_e

approaches to $\frac{n}{2}$ for small values of p_e. In Fig. 6.8, we have shown the effect of block size n for different channel probability of error when the optimal weight is chosen for each case. Since p_e is small, $w = \frac{n}{2}$ is chosen as the optimal weight. As we see in the plot, the optimal block size increases for a more reliable channel. Notice that the rate (in bits per channel use) eventually approaches to zero as the code length continues to increase (this effect is not shown on the plot for the curves corresponding to very low p_e). Moreover, we can observe the rate loss due to perfect error detection by comparing the curve in Fig. 6.7 for $p_e = 0.1$ with the plots in Fig. 6.5. We can see that imposing the perfect error detection

property results in about 30% loss in the code rate compared with the maximum theoretical limit obtained by imposing no constraints on probability of error (which results in the maximum rate for the top curve in Fig. 6.5). Moreover, by comparing the $p_e = 0.1$ curve with Fig. 6.6, we observe the convergence of the curves, at $n = 8$, below a certain error constraint.

In the above coding scheme, the only complexity imposed on the receiver node (i.e., the chamber circuitry) is the ability to read consecutive bio agents' output, aggregate and compare it with a threshold, and report the decoded output if it passes the threshold. In the next section, we show how can one extend the above coding scheme by the introduction of additional weights and molecular types without hurting the perfect error detection capability.

6.4.1 Extending the Constant-weight codes in Molecular Communication

As we observed in the previous section, imposing perfect error-detection constraint can hurt the code rate significantly. In order to increase the rate while keeping the perfect error detection capability, one needs to extend the introduced coding scheme. As shown in [154], the output of bacteria depends on both the type of the signal molecules and also on the level of the input signal. Hence, there seems to be two ways to extend the above coding scheme: 1- Using multiple constant-weight codeword families (with the optimal weight and block size) using different types of molecules that trigger different types of outputs at the receiver (e.g., Green and Yellow Fluorescent). 2- Using multiple constant-weight codeword families that each use different types of molecules but the same output at the receiver.

First consider the first scenario. Here, the decoding can be separately performed for each type of molecules and their corresponding outputs. As such, we would have parallel channels for different molecule types and each codeword family can use the optimal weight and block size obtained in the previous section without affecting the other codeword families. At the receiver side, each type of outputs should be compared to the corresponding

threshold by the detection circuit separately. This scenario would add decoding complexity in terms of the production of two different outputs by bacteria (e.g., Green and Yellow Fluorescent) and the corresponding sensing ability by the detection circuit.

Now consider the second scenario. Here, two different molecules are employed which trigger the same output but with different sensitivities. As such, we show how using different weights by each codeword family and only one threshold can result in a perfect error detection. As mentioned in Section 6.2.1, the problem with employing more than one weight is that the higher-weight codeword can be decoded as the lower-weight ones. For example, the constructed weight-three codewords for the coding scheme described in the previous section would be (0,1,1,1), (1,0,1,1), (1,1,0,1) and (1,1,1,0). Among other transitions, one can observe that (1,1,0,1) may be decodes as (0,1,0,1), a weight-two codeword. This problem can be mitigated by sending each weight with a different type of molecules. Take the case that we have two types of molecules, namely type I and type II. Note that these names are used generically and one can refer to [154] for more details. In this case, the weight-two codes can be sent with type I and weight-three codes with type II molecules. Further, assume that the bacteria are less sensitive to type II than type I molecules and hence, producing smaller output when triggered by the same concentration of molecules. We denote by Y_i^j the aggregated output resulting from a weight-i codeword of type j molecules. Hence, in the above example with two types of molecules (using type I and II to send $w = 2$ and $w = 3$ families), the range of the output threshold τ which results in perfect error detection between the two family codewords is obtained as

$$max(Y_1^I, Y_2^{II}) < \tau < min(Y_2^I, Y_3^{II}) \tag{6.9}$$

The right inequality in (6.9) ensures all the error-free codewords to pass the threshold test and the left inequality ensures that any output due to an erroneous codewords (from either family) would be below the threshold. Note that since we assumed the bacteria are less sensitive to type II molecules, we have $Y_2^{II} < Y_2^I$, and hence both inequalities in (6.9) are satisfiable. As such, the weight of the codes can be matched to the type of signal molecules

and the codeword is discarded in the case of a mismatch. The above inequality can also be generalized for more than two types of molecules. Note that for a general n and k types of molecules, the best k codeword weights should be chosen from Fig. 6.7. As such, the total rate would be the sum of the individual rates for each constant weight code family. For example, for the case that p_e is small and $k = 2$, $w = \frac{n}{2}, \frac{n}{2} + 1$ should be chosen. As a side note, the special case of $n = 1$ and $w = 1$ in the above coding scheme results in sending type I molecules and type II molecules to encode the binary information. This would be equivalent to Molecule Shift Keying (MSK) introduced in [83]).

6.5   Conclusion

In this chapter, we studied error-detection coding schemes for molecular communication channel that would achieve arbitrarily small probability of detection error. We focused on error detection instead of correction for two reasons: complexity of the error-correction schemes and the envisioned sensitive applications of molecular communication. We modeled the binary communication over a completely asymmetric channel and showed the trade-off between the rate and probability of error for such coding schemes. In order to obtain the theoretical limits, we introduced two optimality measures under different assumptions and proposed algorithms to find the optimal codewords for each case. We then studied constant-weight codewords, a sub-family of above codes, which meet the molecular communication specific needs in terms of both the perfect error detection and low complexity. We analyzed the optimal weight and length of such codes and compared the rate with the theoretical limit obtained earlier. We also showed how such codes can be extended by using multiple types of molecules and different detection thresholds.

CHAPTER 7

RATE DISTORTION AND OPTIMAL QUANTIZER IN MOLECULAR COMMUNICATION

So far, we have studied the fundamental problems in molecular communication such as the diffusion channel capacity, ligand-receptor capacity, and two-node communication. We also introduced methods such as relaying and error-control coding to mitigate the reliability issue in molecular communication. In this chapter and the following, we focus on the molecular sensing and study the relevant theoretical and practical problems.

In a molecular bio-sensor, signal distortion is a matter of paramount importance. In the world of biology, distortion and error are mitigated through redundancy (e.g., number of sensors). In this chapter, we study the rate-distortion problem in the context of molecular sensing via ligand receptors. We demonstrate the effect of receptor redundancy in distortion and obtain the optimal quantization that minimizes the distortion in the inference of the input signal. where the input distribution of molecules is known.

In a more practical case, either the distribution is completely unknown or there exists only some peripheral knowledge about it (e.g., the distribution family). Hence, we discuss the universal quantizer for a molecular sensor in the minimax sense. In such a quantizer, we minimize the distortion for the worst-case distribution in the environment. My colleague A. Abdi has mainly developed this section with my collaboration. The result will be briefly presented for the sake of completeness of discussion.

7.1 Optimal Quantizer in MC

There are two main sources of distortion in a molecular sensor with ligand receptors. The first is due to random discretization of a continuous signal (i.e., concentration of molecules) through the ligand receptors. As the concentration of molecules at the vicinity of receptors
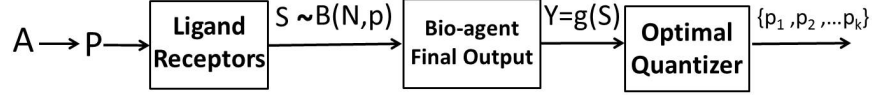
Figure 7.1. Quantizer in a molecular sensor

increases, the probability of ligand binding increases as well. Hence, the number of activated receptors is a random discrete indicator that can be used to infer the concentration of signal molecules. We model this source of distortion with a binomial random variable which represents the mapping from the continuous binding probability (or equivalently the corresponding concentration of molecules) onto a discrete level of activated receptors. The second source of the distortion is due to the limited number of output levels at a primitive molecular sensor node. As such, the node needs to map multiple levels of activated receptors to a single output representation value which can be viewed as quantization of the discrete binomial random variable from the previous stage.

We consider a node that comprises N ligand receptors that act independently to measure the steady-state concentration of molecules. We wish to measure the distortion imposed on the system by both the ligand reception process as well as the output representation with finite number of levels and ignore the distortion due to the latter stages of the output production. Hence, the measured distortion would be a lower bound for any node who uses ligand reception to sense the signal molecules.

Upon being stimulated by the concentration of molecules A^* in the steady state, as depicted in Fig. 7.1, a random S number of the receptors will be activated where $S \sim$ Binomial(N, p^*). From now on, we drop the superscript $*$ when referring to the steady-state values. The quantized value of p (i.e., the corresponding value of A in (4.2)) is inferred by observing the quantized value of S as the final output. Hence, the distortion on p has two sources: 1. Random and discrete nature of S in measuring p, and 2. Quantization error in representing S.

We formalize the problem as follows: Given the random variable corresponding to the

number of activated receptors $S \sim \text{Binomial}(N, p)$, where p is an instantiation of P with the density function $f_P(p)$, and k quantization levels at the output, the objective is to find an optimal (the notion of optimality will follow) mapping π from $N + 1$ levels of S to k levels of the node output. In other words, we need to find the optimal mutually exclusive sets S_i, $i \in \{1, \ldots, k\}$ and $S_i \subset \{0, 1, \ldots, N\}$, where $\bigcup_{i=1}^{k} S_i = \{0, 1, \ldots, N\}$. This would correspond to finding the optimal quantization intervals in a classical quantization problem [109]. Further, we need to find the optimal reconstruction points p_i, $i \in \{1, \ldots, k\}$, corresponding to each S_i. note that each A_i can then be computed from (4.2). Here, the optimality is defined as minimizing the modified distortion rate [109] for a noisy source. In other words, we minimize the conditional expectation $\mathbf{E}[d(P, \hat{p})|S = s]$ where $d()$ is a distance measure, which is assumed to be the squared error.

Following the footsteps of [155], we solve the above optimization problem, which can be shown to be convex, by simultaneously solving the following two problems: 1. For a given set of reconstruction points $p_1, \ldots, p_k$, find the best quantization sets $S_1, \ldots, S_k$, and 2. For a given set of S_i's, find the best corresponding reconstruction points p_i's. If we order the reconstruction points p_i in increasing order, Fine has shown that optimal S_i sets can be described as follows [155]:

$$S_i = \{s : \frac{p_i + p_{i-1}}{2} \leq \mathbf{E}[P|S = s] \leq \frac{p_i + p_{i+1}}{2}\}, \tag{7.1}$$

where $i \in \{1, \ldots, k\}$ and we define p_0 and p_{k+1} to be negative and positive infinity, respectively. Note that (7.1) resembles the first optimality criterion in a classical quantization problem [108] which declares each interval end point must be halfway between the reconstruction points immediately before and after that.

In the second step of the algorithm, we need to find the optimal reconstruction points for each S_i set. In other words, we need to minimize $\mathbf{E}[(P - p_i)^2|S \in S_i]$. It can be easily shown that the conditional mean of P minimizes this error. Hence, we have:

$$p_i = \mathbf{E}[P|S \in S_i], \quad i \in \{1, \ldots, k\}. \tag{7.2}$$

91

Rewriting (7.2) for our problem using the Bayes formula results in:

$$
\begin{aligned}
p_i &= \frac{\int_0^1 p\, \mathbf{P}(S \in S_i | p) f_P(p) dp}{\mathbf{P}(S \in S_i)} \\
&= \frac{\sum_{s \in S_i} \binom{N}{s} \int_0^1 p^{s+1}(1-p)^{N-s} f_P(p) dp}{\sum_{s \in S_i} \binom{N}{s} \int_0^1 p^s (1-p)^{N-s} f_P(p) dp},
\end{aligned}
\tag{7.3}
$$

where we have exchanged the order of summation and integration at the end. In the next section, we solve (7.1) and (7.3) simultaneously and compare the resulting distortion with both a simple uniform quantizer and the rate-distortion function.

7.2 Rate-Distortion in the Optimal Quantizer

We define the distortion $D(N, k)$ as the expected value of squared error over the input probability distribution. Hence, we have:

$$
\begin{aligned}
D(N, k) &= \mathbf{E}_P[(P - \hat{p})^2] = \mathbf{E}_S[\mathbf{E}_{P|S}[(P - \hat{p})^2 | S]] \\
&= \sum_{s=0}^{N} \int_0^1 (p - p_{\pi(s)})^2 \mathbf{P}(S = s | P = p) f_P(p) dp \\
&= \sum_{s=0}^{N} \binom{N}{s} \int_0^1 (p - p_{\pi(s)})^2 p^s (1-p)^{N-s} f_P(p) dp,
\end{aligned}
\tag{7.4}
$$

where $\pi(s)$ is the optimal mapping from $[0, \ldots, N]$ to $[1, \ldots, k]$ introduced in the previous section. Note that we have used the Law of total expectation and the Bayes rule to obtain (7.4).

In Fig. 7.2, we have shown the average distortion versus the number of quantization levels k for different values of N using the optimal technique described above. We have chosen $f_P(p)$ to be uniform in $[0, 1]$ but the following observations can be easily extended for any arbitrary distribution. As we observe in the plot, the effect of using larger quantization levels in reducing the overall distortion diminishes after a certain point. On the other hand, for small values of k, the distortion is approximately the same regardless of N. In particular, at $k = 1$ which corresponds to representing the input distribution with its expected value, the distortion is equal to the distribution variance, here $\frac{1}{12}$. These behavior can be
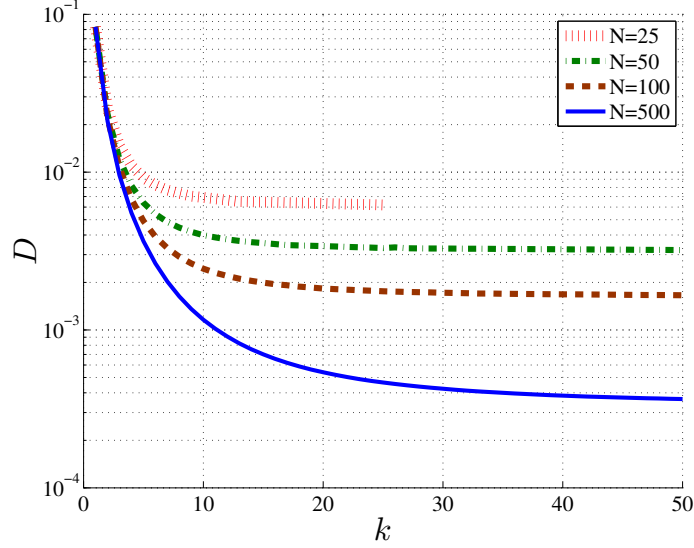
Figure 7.2. Distortion versus number of quantization levels for different values of N

explained by the observation that we made about the sources of the overall distortion in the previous section. The second source which stems from the size of the quantization levels and is independent of N, is the dominant term for small values of k but its effect diminishes in the form of $\frac{1}{k^2}$. The first source of the overall distortion which is due to the randomness in the observation of S, is enduring and the same for all the values of k. Hence, it becomes approximately the sole source of distortion for high values of k.

Here, we take a closer look at the first source of the overall distortion due to randomness in the observation of S. Given N and observing the value of $S = s$, from classical statistics, $\frac{s}{N}$ is the sufficient statistics for estimating the input p. For large values of k, this statistic can be represented with a near perfect precision. Hence the average asymptotic distortion D_∞ in inferring the value of p becomes the expected value of the variance of $\frac{S}{N}$. In other words:

$$D_\infty \cong \int_0^1 \frac{p(1-p)}{N} f_P(p)dp, \tag{7.5}$$

where we have used the fact that $\mathbf{Var}[\frac{S}{N}] = \frac{p(1-p)}{N}$. Here, we consider two input distributions $f_P(p)$. First is the uniform distribution discussed above which results in $D_\infty \cong \frac{1}{6N}$. The
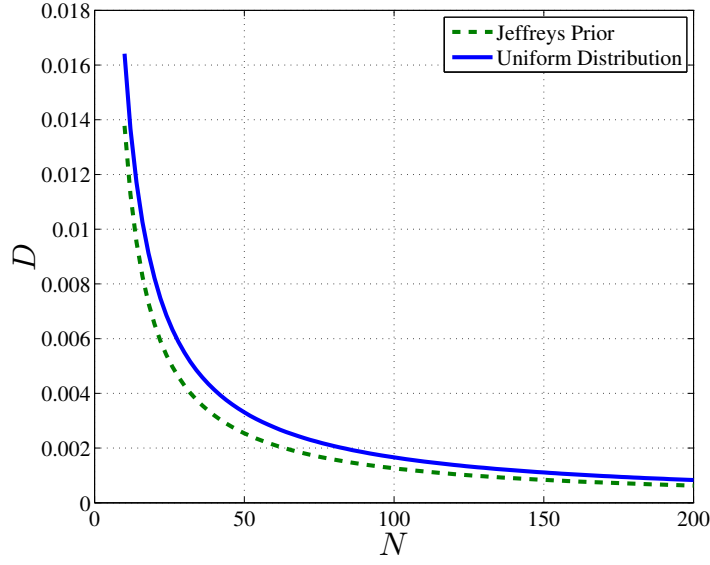
Figure 7.3. Asymptotic distortion of optimal random quantizer versus N

second distribution is the Jeffreys prior for a Binomial observation given by:

$$f_P(p) = \frac{1}{\pi \sqrt{p(1-p)}}, \quad 0 < p < 1. \tag{7.6}$$

In Chapter 2, we showed that the Jeffreys prior is the capacity-achieving distribution for the receiver model in which a continuous concentration of molecules is mapped to a Binomial observation. Calculating (7.5) for the distribution in (7.6) results in the asymptotic distortion $D_\infty \cong \frac{1}{8N}$. Moreover, based on (7.5), the worst case asymptotic distortion is resulted by the probability distribution having all its probability mass at $p = \frac{1}{2}$ which would result in $D_\infty \cong \frac{1}{4N}$. In Fig. 7.3, we have shown the asymptotic distortion of the optimal random quantizer for both the uniform distribution and the Jeffreys prior. We can observe perfect match of the two curves with the asymptotic distortion $D_\infty \cong \frac{1}{6N}$ and $D_\infty \cong \frac{1}{8N}$, respectively, as obtained above.

In order to show the advantage of using the optimal random quantizer, we compare its distortion performance with the performance of a uniform random quantizer where the binomial observations are uniformly assigned to the quantization levels and also, the reconstruction levels are uniformly picked in the interval [0, 1]. We have plotted the normalized
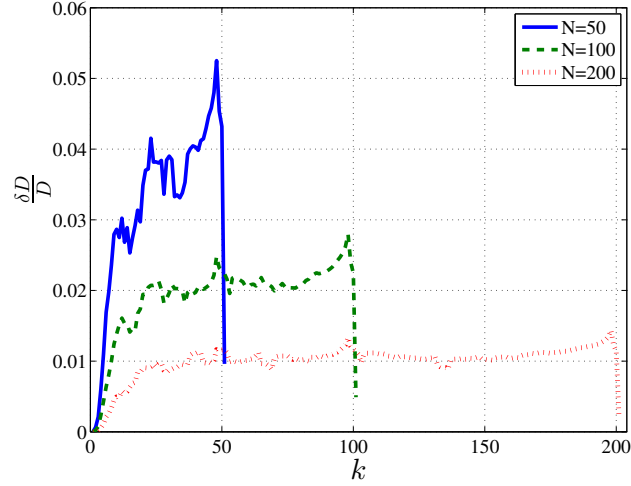
Figure 7.4. Comparison of the optimal versus uniform random quantization for the uniform distribution

difference between the distortion of the optimal and uniform random quantizers versus the number of quantization levels k for the uniform distribution in Fig. 7.4. As we can see in Fig. 7.4, the two techniques result in approximately the same distortion for small values of k where the quantization error is dominant. The relative advantage of the optimal random quantizer becomes more apparent in this case for larger values of k but falls sharply for $k = N + 1$. This latter case corresponds to the point where a one-to-one mapping from the receptor outputs and the reconstruction levels becomes possible and the optimal quantizer loses its advantage in picking the optimal mapping. We can also observe from the plot that the overall advantage of using the optimal quantizer diminishes for large values of N and k. This reinforces the observation in [110] that uniform quantization is asymptotically optimal.

In Fig. 7.5, we have made the same comparison for the case of the capacity-achieving distribution in (7.6). As we can observe in the plot, except for $k = 1$ which corresponds to representing the distribution with its expected value, the optimal quantizer outperforms its uniform counterpart considerably for small values of k. Moreover, unlike the uniform distribution case, the optimal quantizer advantage is even more accentuated for larger values of N. This phenomenon can be explained by the observation that for small k and large N,
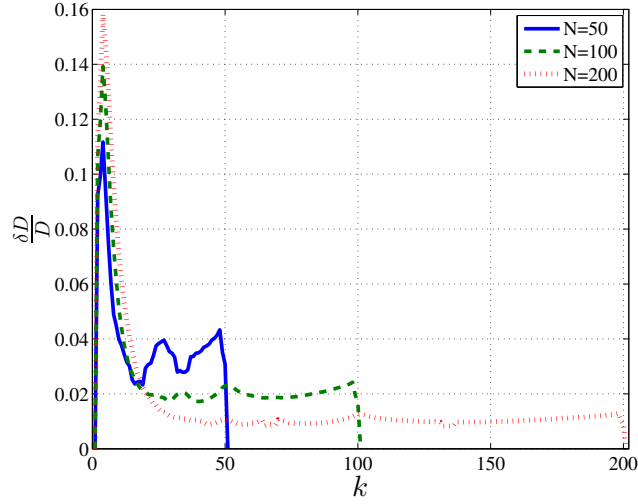
Figure 7.5. Comparison of the optimal versus uniform random quantization for the Jeffreys prior

the optimal distribution can fully take advantage of the asymmetric nature of the distribution in (7.6). Moreover, similar to the previous case, the uniform quantizer approaches its optimal counterpart for large values of N and k. Note that in both Fig. 7.4 and Fig. 7.5 , the curves have been smoothed to offset the illegibility due to their discrete nature.

We also compare the performance of the optimal random quantizer with the theoretical limit given by the distortion-rate function as defined by Shannon in [156]. Based on Shannon, $D(R)$ in estimating X by $\hat{X}$ is defined as:

$$D(R) = \min_{Q(\hat{X}|X):I(Q(\hat{X}|X))\leq R} d(Q(\hat{X}|X)), \tag{7.7}$$

where $Q(\hat{X}|X)$ is the conditional probability distribution over the reproduction alphabets given the source. Moreover, $d(Q(\hat{X}|X))$ and $I(Q(\hat{X}|X))$ are the average distortion and the average Shannon mutual information associated with $Q(\hat{X}|X)$, respectively, and are given by:

$$d(Q(\hat{X}|X)) = \sum_{x} \sum_{\hat{x}} p(x)Q(\hat{x}|x)d(x, \hat{x}),$$

where $p(x)$ is the input distribution and $d()$ is a distance measure (here the squared error) and

$$I(Q(\hat{X}|X)) = \sum_{x} \sum_{\hat{x}} p(x)Q(\hat{x}|x) \log \frac{Q(\hat{x}|x)}{\sum_{x} p(x)Q(\hat{x}|x)}$$

96
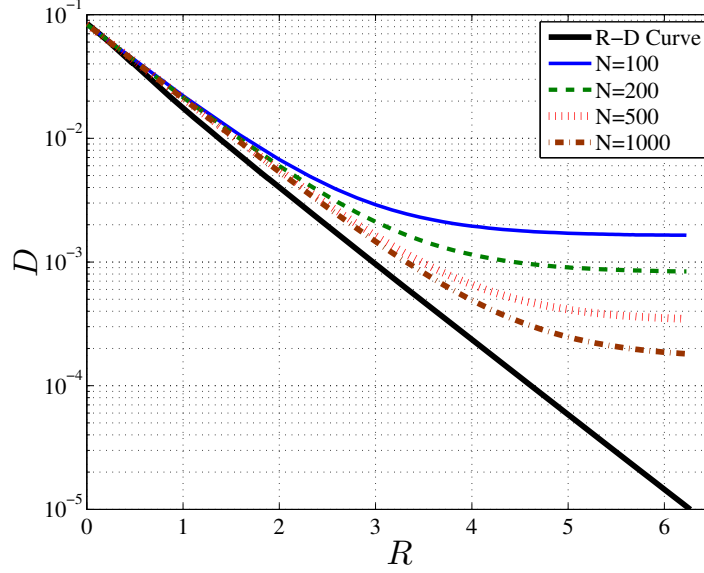
Figure 7.6. Comparison of the optimal random quantizer with distortion rate curve

Note that in the ligand receiver model, $Q(\hat{x}|x)$ has been fixed to be a Binomial distribution. Based on the definition above, $D(R)$ gives the lower bound on the distortion for any quantizing methods with the rate limited to R. In order to solve the constrained optimization in (7.7), we use the Blahut algorithm described in [157] which obtains the points on the rate-distortion curve (or equivalently, distortion-rate curve) iteratively. In Fig. 7.6, we have shown the distortion of the optimal random quantizer versus $R = \log(k)$ for different values of N and compared it with the Shannon distortion-rate curve. As we can see in the plot, the optimal random quantizer curves follow the theoretical limit closely for small R but fall short afterwards and approach their asymptotic distortion. Also, it is possible to get closer to the distortion-rate curve by using larger values of N but the curves will eventually diverge where the random observation error dwarfs the quantization error. This will also correspond to the best practical choice for the number of levels $k^*(N)$, i.e., the minimum k that satisfies $\frac{k^2}{N} > a$ where the left side is the relative variance of the two errors and a is a constant. Hence, $R^*(N) = \log k^*(N) = \frac{\log N}{2} + \frac{\log a}{2}$. Choosing $a = 10$, we observe a good match between $R^*(N)$ and the points of divergence in Fig. 7.6.

97

7.3 Minimax Universal Quantizer

The derivations in the previous sections assume the probability distribution of molecule concentration in the environment to be known. In practice, the performance of the sensor can be significantly deteriorated by the actual molecular distribution. Universal quantizers for unknown input distribution are discussed in [109]. A universal quantizer in the minimax sense (i.e., minimizing the distortion for the distribution that yields the maximum error) is introduced in [111]. Here, we study the design and performance of universal minimax quantizers for the ligand reception process. This section is developed in collaboration with my team member Afshin Abdi. While the analytic component is developed by Afshin, I provided the model and the setup of the problem. The results are briefly presented here for completeness of the molecular sensing discussion. More detailed presentation can be found at [158]

The objective in the minimax universal quantizer is to find a quantization Q, of k levels, such that it minimizes the worst case distortion, i.e.,

$$D_{\text{minimax}} = \min_Q \max_p D(p; \hat{p})$$

$$= \min_{\hat{p}, \pi(\cdot)} \max_p \sum_{s=0}^{N} \binom{N}{s} p^s (1-p)^{N-s} (p - \hat{p}_{\pi(s)})^2.$$

It is well known [159] that if there is no bound on the quantization levels, the optimum quantizer is given by $\hat{p}_s = \frac{s}{N + \sqrt{N}} + \frac{0.5}{1 + \sqrt{N}}$, which has $k = N + 1$ quantization levels. Furthermore, $D_{\text{minimax}} = \frac{1}{4(1 + \sqrt{N})^2} = O(\frac{1}{N})$.

However, when number of reconstruction points, $k < N$, is fixed a priori, finding optimum minimax quantizer is intractable and requires investigating almost all 'reasonable' quantization mappings, $\pi(.)$, as well as optimizing the reconstruction points, $\hat{p}$. In the following, we briefly present some bounds on the performance of the optimum minimax quantizer and propose an approximate solution [158].

Lemma 6. *Let $Q^* = \{\hat{p}_1, \ldots, \hat{p}_k\}$ be the optimum reconstruction points, sorted in an ascending order. Define $\eta = \max_{i;0 \leq i \leq k+1}(\hat{p}_{i+1} - \hat{p}_i)$, where $\hat{p}_0 = 0$ and $\hat{p}_{K+1} = 1$. Then,*

$D_{minimax} \geq \eta^2/4.$

Lemma 7. *Consider the class of quantizers with k levels, $k < N$. Then, the minimax distortion is bounded as [158]*

$$\frac{1}{4k^2} \leq D_{minimax} < \frac{2}{k}. \tag{7.8}$$

7.3.1 Performance of the Uniform Quantizer

Here, we present an upper bound for the maximum distortion of the uniform quantizer. The quantization points and regions are defined as $\hat{p}_i = (i-0.5)/k$ and $S_i = \{s : s/N \in [b_i, b_{i+1})\}$, for $i = 1, 2, \cdots, k$; where $b_i = (i-1)/k$ and $b_{k+1} = +\infty$. We show that the uniform quantizer converges to the minimax optimum quantizer at the rate of $O(\frac{1}{\sqrt{N}})$ and hence, for a fixed k, it is asymptotically optimal.

Lemma 8. *The maximum distortion of the uniform quantizer is bounded as [158]*

$$\max_p D_{uniform}(p) \leq \frac{1}{4k^2} + 1.75 \frac{k^4}{N^2} + \frac{2}{k\sqrt{2k-1}} \frac{1}{\sqrt{N}}. \tag{7.9}$$

Since, except in some special situations, it is almost impossible to analytically solve for the minimax quantizer, we adapt numerical approximate solution. To do so, we first quantize the possible values of p to $F = \{p_1, \ldots, p_J\}$, such that $\max_i |p_i - p_{i+1}| \leq \delta$. Note that since $\left|\frac{\partial D(p,\hat{p})}{\partial p}\right| \leq 2(N+1)$,

$$\max_p D(p, \hat{p}) \leq \max_{p \in F} D(p, \hat{p}) + 2(N+1)\delta \tag{7.10}$$

Hence, we can choose F such that the solution to the quantized minimax problem lies within given bound, ϵ, of the optimum quantizer, by setting $\delta = \epsilon/2(N+1)$.

We compared the performance of uniform quantizer with the (near) optimum minimax quantizer for $k = 8$ and different values of N in Fig. 7.7. Also, for a given uniform quantization regions, we optimized the reconstruction points, $\hat{p}_i$, to minimize the maximum distortion. As seen from figures, the performance of the uniform quantizer with optimized $\hat{p}_i$'s is close to the optimum minimax quantizer, mainly due to the fact that the quantization
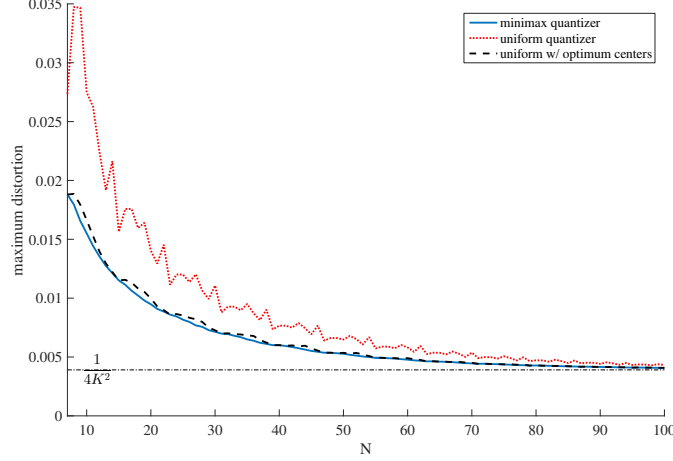
Figure 7.7. Maximum distortion of uniform and minimax quantizers with $k = 8$ **levels versus** N

regions (i.e., the mapping $\pi(.)$) of the optimum minimax quantizer are close to the uniform one.

7.4   Conclusion

In this chapter, we studied the rate-distortion theory in the context of molecular sensing and obtained the optimal quantizers for the receiver with ligand receptors. We identified two sources of distortion, namely the random ligand reception and the receiver output quantization. We proposed an optimal random quantization technique that minimizes the overall distortion through optimal mapping of the binomial output and finding the best corresponding reconstruction levels. We showed that the first source of distortion decreases inversely with the number of receptors while the second decreases as inverse squared of the number of quantization levels. As such, increasing the number of quantization levels (i.e., increasing the receiver output rate) after a certain point has negligible effect on improving the overall distortion where the random observation of the input becomes the dominant source of the distortion. We also compared the performance of the optimal quantizer with the theoretical limit given by the distortion-rate curve proposed by Shannon. We observed that it is possible to approach the distortion-rate curve in low rates by using large number of receptors but the curves always finally diverge as the optimal quantizer's distortion approaches its asymptotic value which is independent of the rate. We also studied the universal minimax

quantizer when the distribution of molecules are not known at the receptors. We derived lower and upper bounds on the distortion of the optimal minimax quantizer, and showed that as the number of receptors increases, the uniform quantizer approaches the optimum minimax quantizer.

CHAPTER 8

MICRO-RNA PROFILE DETECTION VIA FACTOR GRAPHS

Sensor cell arrays have long been a practical solution for detecting environment chemicals such as DNA molecules. In sensor cell arrays, redundancy in molecular sensing is achieved by using multiple types of sensors to measure a molecular signal. Micro-RNA (miRNA) molecules are small non-coding RNA molecules that have been shown to play a major role in the inter-cell communications inside the human body [6].

In this chapter, we study the problem of detecting irregular patterns of miRNA which are deemed to be related to various diseases such as cancer and heart failure [7]. In order to detect the miRNAs in the environment, we use a sensor cell array. Each sensor consists of one or multiple mRNA transcripts that can detect a subset of the environmental miRNAs. Interference is a major issue in miRNA sensing as multiple miRNAs can act on a single sensor and also, a single miRNA can act on multiple sensors. Here, we propose a framework to accommodate the pattern recognition problem without estimating the individual miRNA concentrations [133].

8.1 The case for Micro-RNA

Recently, RNA molecules have been employed as the key element in a variety of biosensors [12]. This is justified by RNA natural versatility, predictable base-pairing and its ability to interact with a variety of molecules such as nucleic acids and proteins. Moreover, RNA can be used in actuators to link biosensors to transcriptional outputs for diagnostic applications [160]. RNA parts are also highly composable and can be used as building blocks of more complicated biosensor structures. Finally, the rules for RNA folding are similar across different organisms which increases their portability from one organism to another [160].

On the other hand, miRNAs are a class of small non-coding RNA molecules that have

been recently identified as having various crucial regulatory functionalities in human body such as cell growth and development, and are associated with a wide variety of human diseases [7, 9, 161, 162]. miRNAs influence cell gene expression by silencing the protein translation of messenger-RNAs (mRNAs) inside the cell. There is a class of extracellular miRNAs, exRNA, that is observed to play a key role in cell-cell communication [6]. Cells communicate with neighboring cells to influence their behavior by changing the local environment [8]. miRNAs are packaged in microparticles (e.g., exosomes and microvesicles) alongside other molecules and change the gene expression of the receiver cells. Due to their remarkable stability and relative ease of detection, using circulating miRNAs in biological fluids as biomarkers are advantageous compared with current diagnostic methods [7].

There has been growing evidence that cancerous cells communicate to the healthy ones to spread the mutagenic information [163]. Irregular expression (i.e., higher or lower than normal levels) of several miRNAs have been linked to a number of diseases such as cancer and heart dysfunctionality [9, 164, 165]. Hence, one of the most promising methods of detecting cancer at the earliest stage could be to detect irregular patterns of multiple miRNAs which have been found to be related to certain types of cancer [9].

Recently, synthetic biologists designed a logic circuits that can detect a specific indicator pattern over a group of miRNAs which is associated with a certain type of cancer [9]. The sensing unit is coupled with an actuator that produces apoptosis-inducing protein when the cancerous cells are detected. In this thesis, we focus on a modular and generalized form of such sensor/acuator which would be promising for future non-invasive cancer detection that act with high selectivity and specificity.

Instead of aiming to measure all the gene expression levels (i.e., mRNA concentrations) as it is done in regular microarrays, we focus on sensing for the detection of specific indicator patterns in the miRNAs that are involved in certain types of cancer. In the following, we obtain a probabilistic model for the miRNA silencing and model the pattern detection

problem over a Factor Graph. We solve the inference problem directly without estimating the individual miRNA concentrations using Belief Propagation (BP). BP is an iterative message passing algorithm that has been shown to perform well in various contexts such as error control coding [166], computer vision [167], and recommender systems [168].

8.2 A Probabilistic Model for miRNA Silencing

To develop our framework, we derive a probabilistic model for a single miRNA silencing action on a single mRNA which will be extended later on for the sensor-cell array. A mathematical model is developed and experimentally verified in [169] to elucidate the average behavior of miRNA silencing system. We build upon it to capture the stochastic nature of this regularity system. The model in [169] explains the steady-state behavior of the expression level G_p of the output target gene (e.g., GFP) as a function of the input mature miRNA in the cell. With no miRNA present, the transcription/translation system can be described as

$$
\begin{cases}
\frac{dm(t)}{dt} & = k_{trs} - k_{deg}m(t) \\
\frac{dG_p(t)}{dt} & = k_{tln}m(t) - k_{pdeg}G_p(t)
\end{cases}
\tag{8.1}
$$

where coefficients k_{trs} and k_{deg} are the the transcription and degradation rates of the mRNA transcript, respectively, and $m(t)$ is the mRNA concentration. Moreover, coefficients k_{tln} and k_{pdeg} are the translation and degradation rates of the target gene protein, respectively. One can derive the steady-state quantities as

$$
m_m = \frac{k_{trs}}{k_{deg}}, \quad G_p = \frac{k_{tln}}{k_{pdeg}}m,
\tag{8.2}
$$

where m_m is the maximum mRNA level observed at the steady state with no miRNA-mediated degradation. Since G_p is linearly proportional to m, which has also been experimentally validated in [169], we work with m as the system output (and omit G_p in the discussion). In the presence of miRNA silencing, (8.1) is modified as

$$
\frac{dm(t)}{dt} = k_{trs} - k_{deg}m(t) - k_{cat}\mu\frac{m(t)}{m(t) + K},
\tag{8.3}
$$

where μ is the molar concentration of miRNA in the micro-environment of the transcripts, k_{cat} is the catalytic constant for miRNA degradation of the target gene transcript and K is the affinity constant (where usually $K \gg m + \mu$) [169]. Approximating $m + K$ by K in (8.3), the miRNA presence increases the mRNA degrading rate by $k_{cat}\frac{\mu m}{K}$, and hence decreasing the "effective" number of mRNA at the steady state. The reason for the mention of effective number is that miRNA regulates the protein translation by affecting the mRNA stability and/or its efficiency in protein translation. In this model, both of these possible effects are lumped into one term.

To reflect the stochasticity in miRNA pairing to the target mRNA, we treat the input *miRNA* as ligands binding with probability $\frac{\mu}{K}$ to the mRNA (as in target receptors) where each binding increases the transcript degradation by k_{cat}. Throughout the discussion, we assume μ to be in the low-concentration regime and hence, ignore the second-order (and higher) terms with respect to $\frac{\mu}{K}$. Assuming it is Binomially distributed, the bindings at the steady state would average at $m\frac{\mu}{K}$, as (8.3) shows, with variance $m\frac{\mu}{K}(1 - \frac{\mu}{K})$. Ignoring the second-order term in the variance and approximating the binomial random variable (rv) with a Gaussian rv (assuming m being large enough), the miRNA degradation effect k_μ would be equal to (with the abuse of the notation):

$$k_\mu = k_{cat}\left(\frac{\mu m}{K} + \epsilon(0, \frac{\mu m}{K})\right) \tag{8.4}$$

where $\epsilon(a, b)$ is a Normally-distributed rv with expected value of a and variance b. Considering the effect of k_μ as an additional term in (8.1) would yield the level of transcripts at the steady state m^* as:

$$m^* = \frac{k_{trs} - k_{cat}\epsilon(0, \frac{\mu m^*}{K})}{k_{deg} + k_{cat}\frac{\mu}{K}} \tag{8.5}$$

Assuming the worst case noise behavior, the normalized level of transcripts at the steady state would be

$$\frac{m^*}{m_m} = \frac{1 - A\epsilon(0, \frac{\mu}{Km_m})}{1 + \frac{A}{K}\mu}, \tag{8.6}$$

where $A = \frac{k_{cat}}{k_{deg}}$ is the miRNA efficacy in degrading mRNA. As explained earlier, in the

low-concentration regime, we can make a linear approximation by ignoring the second and higher-order terms of $\frac{\mu}{K}$ in the taylor series of (8.6). Considering $Y = 1 - \frac{m^*}{m_m}$ as the biosensor final output, we obtain:

$$Y = \frac{A}{K}\mu + A\epsilon(0, \frac{\mu}{Km_m}) \quad \text{for all } \mu \text{ such that } Y \in [0\ 1]. \tag{8.7}$$

In the next section, we extend this model to the silencing behavior of a group of miRNA and discuss the pattern detection problem.

8.3 Detection of Patterns in a Group of miRNAs

There has been growing evidence that cancerous cells communicate to the healthy ones to spread their mutagenic information [170]. Gene regulating miRNAs sent via micro-vesicles or ectosomes has been observed to play a key role in this inter-cell communication process [8]. Hence, one of the most promising methods of detecting cancer at the earliest stage could be to detect irregular patterns of multiple miRNAs which have been found to be related to certain types of cancer [9, 171]. This would give the opportunity to detect or potentially react when the destructive mutants have yet to spread throughout the tissue.

The irregular miRNA patterns can be in the form of concurrent constraints on the individual miRNAs (e.g., concentrations of miRNA$_1$ as "high" and miRNA$_2$ as "low") or on their collective concentration (e.g., $\mu_1 + \mu_2$ being "high") [9]. Instead of using single biomarkers, authors [9] made a circuitry by combining various biomarkers that could uniquely identify the cell of interest out of a limited number of candidates. This tedious task is not scalable and also may not be robust enough when exposed to the interference and noise in an actual setting where the sensor is being employed.

A schematic of the sensing mechanism, with some intermediate steps omitted, is depicted in Fig. 8.1. Loosely speaking, the miRNAs (from the cancerous cell) penetrate and interact with the synthetic cell array. The synthetic cell array consists of N biosensors each containing a population of synthesized cells (e.g., bacteria) containing one or several mRNA sensor circuitry. Examples of such a biosensor has been implemented in [9, 169].
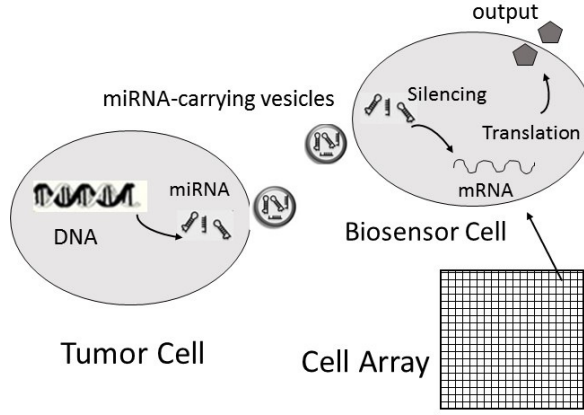
Figure 8.1. Illustration of miRNA silencing a biosensor (i.e., mRNA)

The silencing effect of miRNAs on their corresponding mRNA can be measured from the translated protein of each biosensor. It can be either directly measured (e.g., Green Fluorescent Protein output) or be connected to actuator circuitry in order to produce the appropriate response (e.g., apoptosis inducing proteins to kill tumor) [9, 169]. We assume there is set of M different potential miRNAs in the sensor micro-environment with independent prior probability distributions $f_{\mu_i}(\mu_i)$ $i \in 1, \ldots, M$. We are interested in detecting particular (cancer indicator) patterns over given subsets of the miRNAs using the cell array output.

Due to partial and imperfect pairing between a miRNA, with typical length of 20 nt (nucleotide), and a mRNA, with typical length of 200 nt, there could be multiple miRNAs in the sensor micro-environment silencing the same mRNA with different degrees of affinity and efficacy [7]. On the other hand, each miRNA can potentially silence multiple mRNA biosensors. We capture the pairing affinity, i.e., the average pairing likelihood between miRNA$_i$ and mRNA$_j$ transcript by a matrix $\mathbf{K}_{M \times N}$ where $K_{i,j}$ is inversely proportional to the pairing affinity between miRNA$_i$ and mRNA$_j$. Moreover, the efficacy of miRNA$_i$ in silencing mRNA$_j$ is captured by $\mathbf{A}_{M \times N}$ where $A_{i,j}$ is the ratio of mRNA$_j$'s degradation rate due to the silencing effect of miRNA$_i$, and the natural degradation rate of mRNA$_j$.

Our goal is to detect the patterns of interest in the environmental miRNAs by observing

their silencing behavior on the cell array biosensors with minimum error or distortion. The concentration-based probabilistic nature of miRNA silencing, interference-prone detection of the miRNA in the micro-environment of sensor cells together with nonlinearity of the cell output are among the challenges in the above problem. This calls for introducing both diversity and redundancy to the detection via multiple types of biosensors.

Here, we use the model in (8.7) and assume miRNAs influence their target mRNA transcripts independently and additively [9]. Hence, the output of the jth biosensor is given by

$$Y_j = \sum_{i=1}^{M} A_{i,j}\left(\frac{\mu_i}{K_{i,j}} + \epsilon\left(0, \frac{\mu_i}{K_{i,j}m_m^j}\right)\right) \tag{8.8}$$

Assuming M is large enough, we approximate the sum of conditionally Gaussian noises with $\mathcal{N}(0, \sigma_j^2)$ where $\sigma_j^2 = \sum_{i=1}^{M} \frac{A_{i,j}^2 \bar{\mu}_i}{K_{i,j}m_m^j}$. Here, $\bar{\mu}_i$ is the expected value of $f_{\mu_i}(\mu_i)$. Hence, we will have

$$\mathbf{Y} = \Theta\boldsymbol{\mu} + \boldsymbol{e}, \tag{8.9}$$

where $\mathbf{Y}$ is the $N \times 1$ biosensor output vector and Θ is a $N \times M$ matrix where $\Theta_{i,j} = \frac{A_{i,j}}{K_{i,j}}$ models the silencing effect of miRNA$_j$ on mRNA$_i$. Moreover, $\boldsymbol{\mu}$ is the $M \times 1$ concentration vector of all the potential miRNA in the sensors' micro-environment, and $\boldsymbol{e}$ is a signal-dependent $N \times 1$ noise vector.

In the next section, we introduce a general framework to solve the above detection problem.

8.4   Pattern Inference via Belief Propagation on Factor Graphs

In this section, we propose a graphical model framework to solve the miRNA pattern detection problem introduced in the previous section. As explained earlier, the input set $\boldsymbol{\mu}$ consists of the miRNAs in the patterns of interest and also the interfering ones. Note that this set is not necessarily sparse and the patterns of interest may impose both "high" or "low" constraints on each individual input. Here, we solve the pattern detection problem directly without estimating the individual miRNA concentrations using Belief Propagation
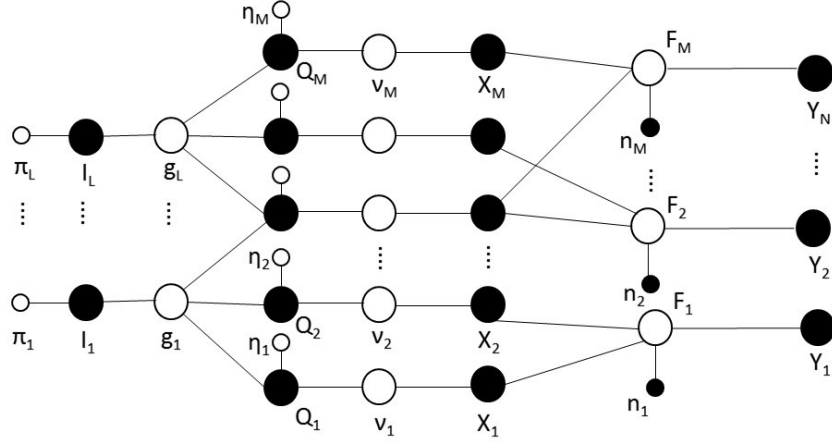
Figure 8.2. Decoding miRNA patterns on a factor graph

(BP) on a Factor Graph. Since, the exact values of the input miRNAs are not needed, fewer observation are required to achieve the same level of pattern-detection accuracy relative to the method that finds the concentrations first and then aim at detecting the patterns. Furthermore, the BP method provides a generic setup that would work with the linear or nonlinear miRNA silencing model. Note that though we solve the detection problem using the model in (8.9), the factor graph model can be readily extended for the nonlinear model in (8.6) or the one introduced in [9].

The factor graph, as depicted in Fig. 8.2, consists of edges that connect a variable node (shown in black) to a constraint node (white). Each variable node corresponds to the random variable that it represents. Every constraint node represents the dependencies enforced on its neighbors (i.e., the variable nodes it is connected to). Denote the ith pattern of interest on miRNAs by R_i which is over a known subset of the input miRNAs. BP is an iterative message passing algorithm that marginalizes the joint posterior distribution $P(R|\mathbf{Y})$, which has exponential complexity in terms of size of R, i.e., the number of patterns, into posterior distributions for each pattern, i.e., $P(R_i|\mathbf{Y})$. This will reduce the complexity to be linear versus the size of R. There are two types of messages in BP. A message from a variable node to its neighbor constraint node represents its marginal distribution estimate at each iteration. The constraint node combines all the incoming messages from its

variable node neighbors, except for one of the variable nodes in its neighborhood, imposes its constraint and sends it to the variable node which in return updates its estimate. Note that convergence of BP requires a sparse factor graph which would be met for the sparse $\mathbf{A}$.

In Fig. 8.2, we have five types of variable nodes: pattern indicators I, miRNA state variables Q, miRNA concentration nodes X (continuous variable X_i for i^{th} miRNA), measurements Y (variable Y_j for biosensor output j), and the noise terms n. Binary random variables I_i, $i \in \{1, \ldots, , L\}$ are indicator function for the pattern. In other words, $Prob\{I_i = 1\} = Prob\{R_i \text{ present}\}$. Here, L is the total number of patterns of interest (out of 2^M possible patterns). Hence, each I_i is a function $G_i(\cdot)$ of the state of the miRNAs (i.e., those Q_j) that make up the pattern R_i. The binary random variable Q_i in Fig. 8.2 determines the state of the ith miRNA and is initialized with the Bernoulli prior probability η_i.

We use a mixture model consisting of distributions with different means (and possibly variances) to model the concentration of the input miRNAs X. Depending on the state of each miRNA, i.e., Q_i, one of the distributions is chosen to model X_i. In the special binary case, there will be two distributions corresponding to the "high" and "low" state of each input miRNA. We use a Gaussian mixture taking $\mathcal{N}(\mu^l, \sigma_l^2)$ for $Q_i = 0$ and $\mathcal{N}(\mu^h, \sigma_h^2)$ for $Q_i = 1$ where $\mu^l < \mu^h$ and $\sigma_l < \sigma_h$. The mixture parameters are chosen such that the probability of X_i being negative, which is meaningless for an input concentration, approaches zero. We also assume the noise variables to be independent of the signal and have a constant variance σ_0^2. The setup can be extended to accommodate the signal-dependent noise as well. As we will see, these assumptions will allow us to construct short messages in BP by only sending the model parameters.

We also have five types of constraint nodes: Bernoulli priors π on I which depend on the natural prevalence of each pattern, g which represents the constraint between I and the subset of Q that makes up the pattern, and Bernoulli priors η on Q which depends on the natural occurrence of each miRNA. Moreover, ν imposes the conditional mixture model constraint between X and Q, and F imposes the measurement constraints (linear or

nonlinear) between Y and a subset of relevant X in that measurement.

Here, we explain the non-trivial BP messages in Fig. 8.2 that would solve the Bayesian inference problem described. Note that due to the Gaussian mixture model, all the messages are short and can be sent parametrically. In lack of such assumption, the distributions need to be sampled and sent. At the beginning, the variables Q_i and I_j are initialized with their corresponding priors and BP starts from left side of the factor graph. The message passing continues until the change in distributions of I_i is smaller than a fixed threshold. In order to elucidate the mechanism, we focus on nodes X_1 and X_2 and assume the pattern of interest R_1 is observed when both Q_1 and Q_2 are on the "1" state, i.e., $G_1(Q_1, Q_2) = Q_1 \wedge Q_2$. In such a case, the g_1 constraint can be written as

$$g_1(I_1, Q_1, Q_2) = \begin{cases} 1 & \text{for } G_1(Q_1, Q_2) = I_1 = 1 \text{ or } G_1(Q_1, Q_2) = I_1 = 0, \\ 0 & \text{otherwise} \end{cases} \tag{8.10}$$

The message from nodes Q_1 and Q_2 to g_1 represent their corresponding binary distribution. Hence, the message $\lambda_{g_1 \to I_1}$ from g_1 to I_1 would be $\sum_{Q_1, Q_2} g_1(I_1, Q_1, Q_2)P(Q_1)P(Q_2)$, which indicates the probability distribution of I_1 from the perspective of g_1. For $G_1(Q_1, Q_2) = Q_1 \wedge Q_2$, it can be written as

$$\lambda_{g_1 \to I_1}(I_1) = I_1 P(Q_1 = 1)P(Q_2 = 1) + (1 - I_1)(1 - P(Q_1 = 1)P(Q_2 = 1)), \tag{8.11}$$

which can be simply interpreted as $P(I_1 = 1) \propto P(Q_1 = 1)P(Q_2 = 1)$ from the perspective of g_1. Based on this incoming message and its prior π_1, node I_1 updates its posterior distribution. On the other hand, the message from node I_1 to g_1 would only contain the prior information π_1 and hence, the message $\lambda_{g_1 \to Q_2}$ from g_1 to Q_2 would be:

$$\begin{cases} \lambda_{g_1 \to Q_2}(Q_2 = 0) & = & \pi_1(0) \\ \lambda_{g_1 \to Q_2}(Q_2 = 1) & = & \pi_1(1)P(Q_1 = 1) + \pi_1(0)P(Q_1 = 0) \end{cases} . \tag{8.12}$$

The first equation in (8.12), can be explained by the fact that for $Q_2 = 0$, no matter the value of Q_1, the constraint in (8.10) can be only satisfied by having $I_1 = 0$. On the other hand, for $Q_2 = 1$, the constraint can be met by either having $I_1 = Q_1 = 1$ or $I_1 = Q_1 = 0$.

The message from node Q_1 to ν_1 determines the probability by which each of the mixture models governs the state of X_1. The message from X_1 to F_1 sends the mixture model parameters alongside with probability of each. For the case of linear measurements, the constraint message can be formed parametrically as well. For example, consider $Y_1 = X_1 + X_2 + n_1$. Hence, the constraint message sent to X_1 would be $Y_1 - X_2 - n_1$ where Y_1 is a constant, X_2 is conditionally Gaussian, and n_1 is Gaussian noise. Hence, the return message is conditionally Gaussian as well; i.e., $\mathcal{N}(Y_1 - \mu_l, \sigma_l^2 + \sigma_0^2)$ with $P(Q_2 = 0)$, and $\mathcal{N}(Y_1 - \mu_h, \sigma_h^2 + \sigma_0^2)$ with $P(Q_2 = 1)$.

8.4.1 Simulation Results

Here, we study the performance of the algorithm over the data derived by a model, as there is no public real-world data readily available at this moment. As mentioned earlier, the sampling matrix Θ in (8.9) is row/column-wise sparse. Hence, we assume each column $\boldsymbol{\theta}_i$ that corresponds to the universal silencing effect of miRNA$_i$ consists of k randomly chosen nonzero elements from a given distribution (here $\mathcal{N}(0, \sigma_k)$). The positive and negative elements of Θ correspond, respectively, to promotory or inhibitory effect of a miRNA on a particular biosensor's output. In other words, the usual inhibitory effect of a miRNA silencing can be used to promote the production of the output protein through a "double inversion" strategy, whereby the miRNA targets a repressor of the protein. Thus in the absence of the miRNA, the output protein is repressed while increasing the miRNA level depletes the repressor, resulting in increased output protein levels [9, 172].

Note that the location of nonzero elements in *Theta*, chosen randomly here, would have a major effect on the performance of the algorithm. In a more practical setting, following the modularity guidelines in synthetic biology [13], one should choose the optimal sensors for the input miRNAs from a pool of pre-synthesized biosensors such that their concurrent false positive would rarely, if ever, concur.

In order to obtain the performance of BP, we use Monte Carlo simulation by randomly selecting values for the entries of Θ, the concentration μ for miRNAs and also on the
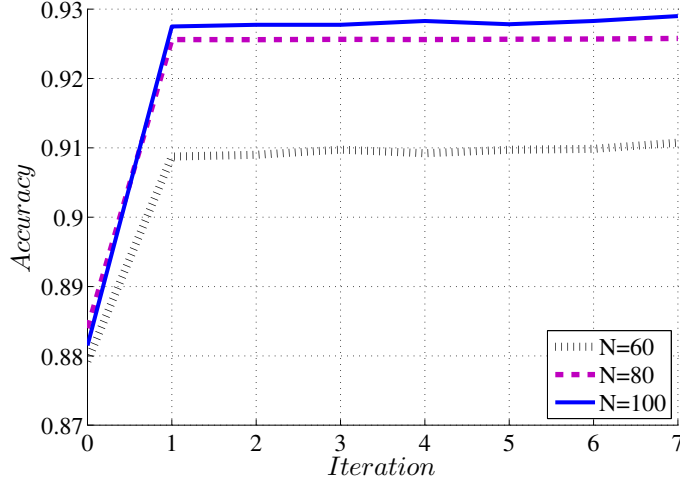
Figure 8.3. BP accuracy versus the number of iterations for different number of biosensors

patterns of interest. We pick $\mathcal{N}(100, 20)$ and $\mathcal{N}(50, 10)$ for the high and low distribution, respectively, in the mixture model for miRNA concentration. Moreover, we fix $k = 3$. To measure the effect of the output noise, we introduce the ratio $r = \frac{\sigma_k^2}{\sigma_0^2}$ which captures the relative variances of Θ and e entries in (8.9). Moreover, we fix the number s of miRNAs in each pattern of interest.

We define accuracy as the percentage of patterns, regular or irregular, that are correctly classified. In Fig. (8.3), we have shown the effect of BP iterations on the detection accuracy for $M = 80$, $r = 1$ and different values of N. Moreover, the number of patterns of interest $L = 10$ and number of miRNAs in each patters is $s = 3$. Note that iteration zero corresponds to the base measure, i.e., initialization of BP with the priors. We observe that BP converges very fast as the factor graph is sparse and lacks short cycles. Moreover, using more biosensors results in higher accuracy but with diminishing gains. Further, since the irregular patterns are quite unlikely, the base prior classifier yields high accuracy.

We define precision as the percentage of detected irregular patterns that are correctly classified. In Fig. (8.4), we have shown the precision versus s for $N = 80$, $r = 1$, $L = 10$, and different values of M. As we observe from the plot, the BP precision decreases linearly with respect to increasing s for which the irregular patterns become more improbable.
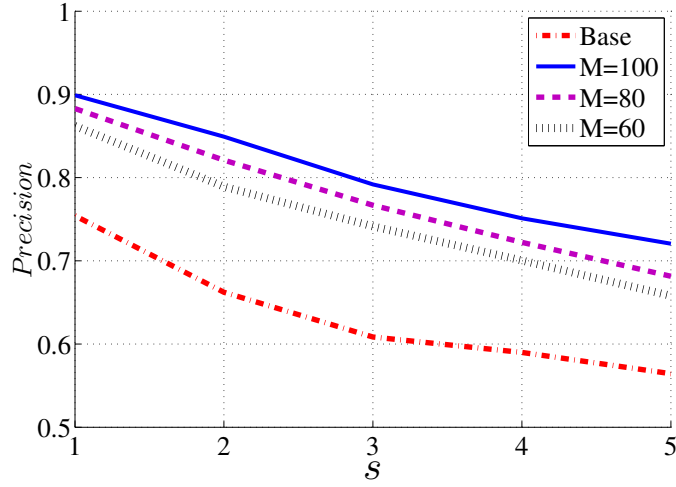
Figure 8.4. Precision versus the number of miRNAs in each pattern for different number of input miRNAs

Moreover, the relative precision advantage of using more biosensors than input miRNAs is more emphasized for larger s. Further, the prior base measure (which can be considered as having $N = 0$) yields comparable precision for small s but falls exponentially afterwards.

We define recall as the percentage of irregular patterns that are detected by the algorithm. In Fig. (8.5), we have shown the recall versus s for $M = 80$, $N = 80$, and $L = 10$, and different values of the noise measure r. As we can see in the plot, the BP recall falls linearly with s whereas the base performance approaches zero exponentially. Moreover, the advantage of using higher values of SNR is diminishing and stops at the point where the BP performance is solely constrained by the interference between the input miRNA. In Fig. (8.6), we have fixed $r = 1$ and shown the recall for different number of input miRNAs M. We observe that unlike the case for accuracy, the advantage of using more biosensors than input miRNAs persists for the recall performance.

In Fig. (8.7), we have shown the effect of number of patterns L on the recall for $M = 80$, $s = 3$, $r = 1$, and different values of N. As we can see in the plot, the recall is almost constant for simultaneous detection of different number of irregular patterns which shows the scalability of using BP over factor graphs.
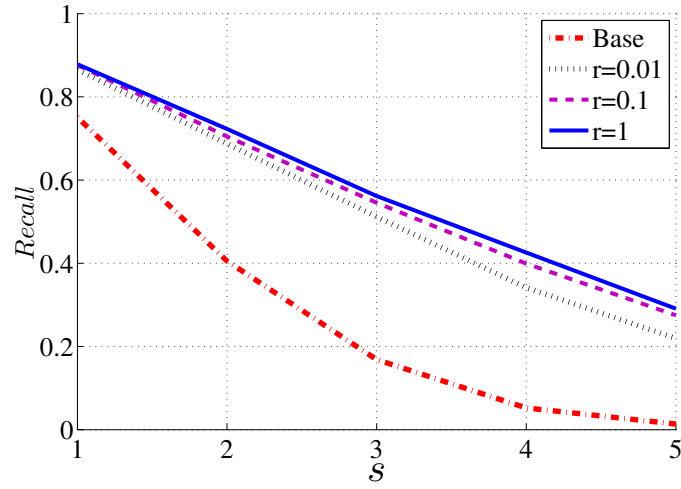
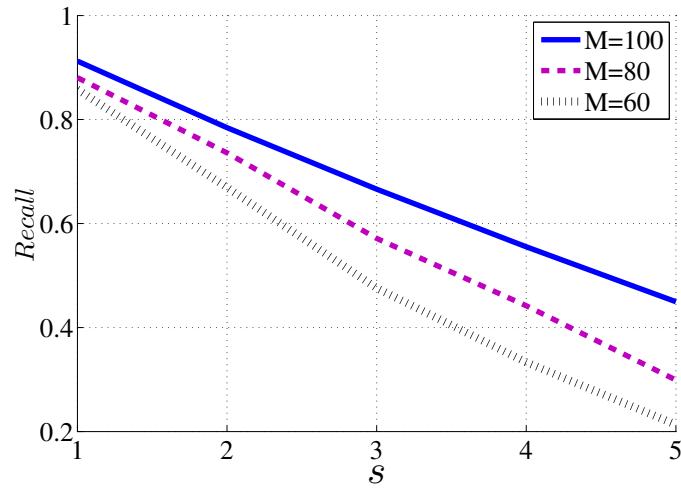**Figure 8.5. Recall versus the number of miRNAs in each pattern for different values of SNR**

Figure 8.6. Recall versus the number of miRNAs in each pattern for different values of input miRNA
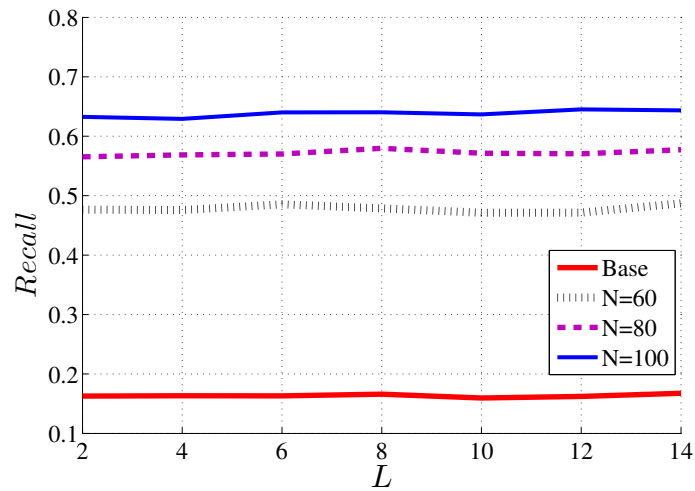

Figure 8.7. Recall versus the number of patterns for different number of biosensors

8.5 Discussion

The general framework described above can be extended in various directions. First is the measurement matrix Θ which was chosen randomly based on some rules. Following the modularity guidelines in synthetic biology [13], one should use a pool of pre-synthesized biosensors in which each circuit may comprise one or more transcripts that are logically combined. Using higher number of transcripts in each sensor would make it more specific and less prone to interference but would be less reusable. Given a library set of the biomarkers, one would be interested in analytically finding the "optimal" subset such that their failure would rarely, if ever, concur. Another problem of interest in this context is to obtain the minimum number of optimally-chosen biomarkers to lower the detection error below a preset threshold.

One can also impose the signal-dependent noise by placing new constraint nodes between n_i and the set of X's that account for the observation Y_i. Further, the effect of using different mixture models such as the exponential mixture, which enforces the non-negative nature of the input concentrations, can be investigated. Note that in such cases, the messages cannot be formed parametrically and would contain the sampled distributions of the continuous variables, e.g., Gibbs sampling method. Hence, messages would be no longer short and the quantization noise may affect the accuracy and convergence of BP. Note that due to both the measurements and pattern constraints, there might be loops in the factor graph which would increase by adding the signal-dependence constraints to the noise nodes. Hence, loopy BP techniques should be investigated [173]. Moreover, the signal-dependence of e has a broader impact as the output samples are not necessarily independent. The effect of such a noise on the robustness of this algorithm should be studied as well.

The sensing model described above can be generalized to work with a nonlinear model for the miRNA silencing action. We derived a nonlinear model in (8.6) and another one has been introduced in [9] for the miRNA silencing action. In the latter, the miRNA effect has

been modeled as

$$
Y = \begin{cases} 1 - e^{-\sum_i \alpha_i \mu_i}(1 - \sum_j e^{-\beta_j \mu_j}) & \text{for } \sum_j e^{-\beta_j \mu_j} < 1, \\ 1 & \text{otherwise} \end{cases} \tag{8.13}
$$

where α_i and β_j are constants corresponding to the silencing and anti-silencing miRNAs. As such, the parameter passing would not be possible even for well-behaving mixture models. Further, nonlinear observation constraints would dramatically increase the message formation complexity.

Finally, we need to measure the performance of the algorithm on real-world data. There have been numerous efforts in gathering a comprehensive miRNA database that could be aggregated to evaluate our algorithm [174–180]. For example, microRNA.org provides miRNA's expression levels at various tissues and miRTarBase is a comprehensive atlas of predicted and validated miRNA-target interactions for different species. Also miR2Disease and miRCancer provide comprehensive collections of miRNA expression profiles in various human cancers and diseases.

8.6   Conclusion

In this chapter, we studied sensor cell arrays in which sensing diversity is introduced by measuring the molecular inputs by using multiple types of sensors. In particular, we studied the problem of detecting irregular patterns over environmental miRNAs via a RNA sensor array. Such irregular patterns have been shown to be indicator of various diseases such as cancer. We formulated the noise and interference in such a sensing system and solved the detection problem via a factor graph. Finally, we used BP to iteratively infer the detected patterns. We showed that the performance of BP depends on parameters such as the number of biosensors and number of miRNAs in each pattern. Moreover, we showed how using BP over the sensor-cell data can improve the recall performance significantly.

CHAPTER 9

CONCLUSION OF THE THESIS

In this dissertation, we investigated molecular communication and sensing via primitive living agents. We analyzed fundamental problems such as capacity, modulation and rate-distortion and proposed algorithms for practical design of communication and sensing systems. Reliability is one of the most important issues in such design. We introduced various methods such as relaying, error-control coding and sensing redundancy to improve the reliability in sensing and communication applications.

In Chapter 1, we introduced the molecular communication and sensing as an alternative for the conventional electromagnetic communication for biological environments. We motivated the research via the related work and presented the important fundamental problems that need to be solved.

In Chapter 2, we presented two models accounting for the uncertainty in estimation of concentration of molecules by the ligand receptors. Using these models, we obtained the rate limit due to the ligand reception. The input capacity-achieving distribution was shown to be highly polarized, i.e., in order to achieve higher rates, the transmitter should mostly produce concentrations which are either low or high. This observation motivates the use of binary symbols in molecular communication.

In Chapter 3, we used the discrete noiseless channel model to obtain the capacity of the diffusion channel for a binary input which is motivated by the results of the previous chapter. We modeled the channel memory with a two-state Markov chain by taking into account the effect of the channel state on the next received bit. We showed that beyond a threshold, increasing the power level is detrimental to the channel memory and has a negative effect on the capacity.

In Chapter 4, we showed how reliable communication can be formed out of collective

behavior of unreliable agents and studied the molecular communication between two populations of bacteria via a diffusion channel. Although, it is aimed at bacteria, the principles developed here can be generalized to analyze the communication of any population of bio entities through molecular signaling in a diffusion channel. The effects of uncertainty in production of molecules, channel parameters and reception process on the overall noise of the communication were studied. We studied the theoretical limits on the information transfer rate in terms of number of bacteria per node, noise level and maximum molecule production levels. Finally, we considered M-ary schemes and analyzed the achievable rates and their error probabilities. We observed that for a fixed number of bacteria per node, reliable communication is not possible for large M, even with arbitrarily increasing the range of the molecular input.

In Chapter 5, we proposed relaying as a means of enhancing reliability in molecular communication. We investigated both the amplify-and-forward and decode-and-forward scenarios. In the first case, we showed that depending on whether the relay uses the same or different type of molecules as the transmitter, relaying would result in expanding the range of the concentration of molecules or increasing the effective number of bacteria in the nodes, respectively. For decode and forward relaying, the relay node decodes the incoming symbol from the transmitter and forwards it to the destination using the same or different type of molecules as the transmitter. In the hetero-type case, we showed how the optimal combining of the outputs would result in improving the reliability and compared the results with the same-type relaying scenario.

In Chapter 6, we studied another method to improve the reliability in MC by introducing error-detection coding schemes that achieve arbitrarily small probability of detection error. We showed the trade-off between the code rate and probability of error for such coding schemes. We obtained the theoretical limits on the rate of such codes and proposed algorithms to find the optimal codewords. We then studied constant-weight codewords, a sub-family of above codes, which meet the molecular communication specific needs in

terms of both the perfect error detection and low complexity.

In Chapter 7, we studied the distortion in a molecular sensor with ligand receptors. We obtained the optimal quantizers and identified two sources of distortion: the random ligand reception and the receiver output quantization. We showed that increasing the number of quantization levels after a certain point has negligible effect on improving the overall distortion where the random observation of the input becomes the dominant source of the distortion. We compared the performance of the optimal random quantizer with a uniform quantizer and the theoretical limit given by the distortion-rate curve. We observed that it is possible to approach the distortion-rate curve in low rates by using large number of receptors but the curves always finally diverge as the optimal quantizer's distortion approaches its asymptotic value which is independent of the rate. We also studied the universal minimax quantizer when the distribution of molecules are not known at the receptors and obtained lower and upper bounds on the distortion of the optimal minimax quantizer

In Chapter 8, we studied RNA sensor arrays to detect irregular patterns over environmental miRNA. Such irregular patterns have been shown to be biomarker of various diseases such as cancer. We presented a probabilistic model for the miRNA silencing to account for the noise and interference. We solved the detection problem via a factor graph and we used BP to iteratively infer the detected patterns.

REFERENCES

[1] B. L. Bassler, "How bacteria talk to each other: regulation of gene expression by quorum sensing.," *Curr Opin Microbiol*, vol. 2, pp. 582–587, Dec 1999.

[2] H. B. Kaplan and E. P. Greenberg, "Diffusion of autoinducer is involved in regulation of the vibrio fischeri luminescence system.," *J. Bacteriol.*, vol. 163, pp. 1210–1214, Sep 1985.

[3] B. K. Hammer and B. L. Bassler, "Quorum sensing controls biofilm formation in vibrio cholerae.," *Mol Microbiol*, vol. 50, pp. 101–104, Oct 2003.

[4] J. Muller, C. Kuttler, and B. A. Hense, "Sensitivity of the quorum sensing system is achieved by low pass filtering.," *Bio Systems*, vol. 92, no. 1, pp. 76–81, 2008.

[5] P. D. Prez and S. J. Hagen, "Heterogeneous response to a quorum-sensing signal in the luminescence of individual," *PLoS ONE*, vol. 5, 11 2010.

[6] D. Galas, P. Wilmes, and K. Wang, "Rna in circulation: sources and functions of extracellular exogenous rna in blood," *Encyclopedia of Metagenomics*, 2014.

[7] V. Kinet, J. Halkein, E. Dirkx, and L. J. De Windt, "Cardiovascular extracellular micrornas: emerging diagnostic markers and mechanisms of cell-to-cell rna communication," *Frontiers in genetics*, vol. 4, 2013.

[8] D. A. Shifrin, M. D. Beckler, R. J. Coffey, and M. J. Tyska, "Extracellular vesicles: communication, coercion, and conditioning," *Molecular biology of the cell*, vol. 24, no. 9, pp. 1253–1259, 2013.

[9] Z. Xie, L. Wroblewska, L. Prochazka, R. Weiss, and Y. Benenson, "Multi-input rnai-based logic circuit for identification of specific cancer cells," *Science*, vol. 333, no. 6047, pp. 1307–1311, 2011.

[10] I. Akyildiz, F. Fekri, R. Sivakumar, C. Forest, and B. Hammer, "Monaco: fundamentals of molecular nano-communication networks," *Wireless Communications, IEEE*, vol. 19, pp. 12 –18, Oct. 2012.

[11] T. Nakano, M. Moore, F. Wei, A. Vasilakos, and J. Shuai, "Molecular communication and networking: Opportunities and challenges," *NanoBioscience, IEEE Transactions on*, vol. 11, pp. 135 –148, June 2012.

[12] C. Myhrvold and P. A. Silver, "Using synthetic rnas as scaffolds and regulators," *Nature structural & molecular biology*, vol. 22, no. 1, pp. 8–10, 2015.

[13] G. M. Church, M. B. Elowitz, C. D. Smolke, C. A. Voigt, and R. Weiss, "Realizing the potential of synthetic biology," *Nature Reviews Molecular Cell Biology*, vol. 15, no. 4, pp. 289–294, 2014.

[14] J. C. Way, J. J. Collins, J. D. Keasling, and P. A. Silver, "Integrating biological redesign: where synthetic biology came from and where it needs to go," *Cell*, vol. 157, no. 1, pp. 151–161, 2014.

[15] A. Einolghozati, M. Sardari, A. Beirami, and F. Fekri, "Data gathering in networks of bacteria colonies: Collective sensing and relaying using molecular communication," in *Computer Communications Workshops (INFOCOM WKSHPS), 2012 IEEE Conference on*, pp. 256–261, 2012.

[16] S. Choudhary and C. Schmidt-Dannert, "Applications of quorum sensing in biotechnology.," *Appl Microbiol Biotechnol*, vol. 86, pp. 1267–1279, May 2010.

[17] T. Danino, O. Mondragn-Palomino, L. Tsimring, and J. Hasty, "A synchronized quorum of genetic clocks.," *Nature*, vol. 463, pp. 326–330, Jan 2010.

[18] M. A. Palacios, E. Benito-Pea, M. Manesse, A. D. Mazzeo, C. N. LaFratta, G. M. Whitesides, and D. R. Walt, "Infobiology by printed arrays of microorganism colonies for timed and on-demand release of messages," *Proceedings of the National Academy of Sciences*, 2011.

[19] M. N. Win, J. C. Liang, and C. D. Smolke, "Frameworks for programming biological function through rna parts and devices," *Chemistry & biology*, vol. 16, no. 3, pp. 298–310, 2009.

[20] E. Andrianantoandro, S. Basu, D. K. Karig, and R. Weiss, "Synthetic biology: new engineering rules for an emerging discipline," *Molecular systems biology*, vol. 2, no. 1, 2006.

[21] A. S. Khalil and J. J. Collins, "Synthetic biology: applications come of age," *Nature Reviews Genetics*, vol. 11, no. 5, pp. 367–379, 2010.

[22] Y. Moritani, S. Hiyama, and T. Suda, "Molecular communication for health care applications," in *Pervasive computing and communications workshops, 2006. PerCom Workshops 2006. Fourth Annual IEEE International Conference on*, pp. 5–pp, IEEE, 2006.

[23] R. A. Freitas, *Nanomedicine, volume I: basic capabilities*. Landes Bioscience Georgetown, TX, 1999.

[24] J. El-Ali, P. K. Sorger, and K. F. Jensen, "Cells on chips," *Nature*, vol. 442, no. 7101, pp. 403–411, 2006.

[25] O. Veiseh, J. W. Gunn, and M. Zhang, "Design and fabrication of magnetic nanoparticles for targeted drug delivery and imaging," *Advanced drug delivery reviews*, vol. 62, no. 3, pp. 284–304, 2010.

[26] A. J. Demello, "Control and detection of chemical reactions in microfluidic systems.," *Nature*, vol. 442, no. 7101, pp. 394–402, 2006.

[27] S. Hiyama, Y. Moritani, T. Suda, R. Egashira, A. Enomoto, M. Moore, and T. Nakano, "Molecular communication," *Journal-Institute of Electronics Information and Communication Engineers*, vol. 89, no. 2, p. 162, 2006.

[28] A. Tamsir, J. J. Tabor, and C. A. Voigt, "Robust multicellular computing using genetically encoded nor gates and chemical 'wires'.," *Nature*, vol. 469, pp. 212–215, Jan 2011.

[29] T. Suda, M. Moore, T. Nakano, R. Egashira, A. Enomoto, S. Hiyama, and Y. Moritani, "Exploratory research on molecular communication between nanomachines," in *Genetic and Evolutionary Computation Conference (GECCO), Late Breaking Papers*, 2005.

[30] J. Philibert, "One and a half century of diffusion: Fick, einstein, before and beyond," *Diffusion Fundamentals*, vol. 2, no. 1, pp. 1–10, 2005.

[31] H. Berg, *Random Walks in Biology*. Princeton, 1977.

[32] M. Pierobon and I. F. Akyildiz, "A physical end-to-end model for molecular communication in nanonetworks," *IEEE Journal of Selected Areas in Communications*, vol. 28, pp. 602–611, May 2010.

[33] B. Atakan and O. B. Akan, "On channel capacity and error compensation in molecular communication," in *Transactions on computational systems biology X*, pp. 59–80, Springer, 2008.

[34] T. Nakano, Y. Okaie, and J.-Q. Liu, "Channel model and capacity analysis of molecular communication with brownian motion," *Communications Letters, IEEE*, vol. 16, no. 6, pp. 797–800, 2012.

[35] A. Einolghozati, M. Sardari, A. Beirami, and F. Fekri, "Capacity of discrete molecular diffusion channels," in *Information Theory Proceedings (ISIT), 2011 IEEE International Symposium on*, pp. 723–727, IEEE, 2011.

[36] M. Pierobon and I. F. Akyildiz, "Capacity of a diffusion-based molecular communication system with channel memory and molecular noise," *Information Theory, IEEE Transactions on*, vol. 59, no. 2, pp. 942–954, 2013.

[37] H. Arjmandi, G. Aminian, A. Gohari, M. Nasiri Kenari, and U. Mitra, "Capacity of diffusion based molecular communication networks over lti-poisson channels," *arXiv preprint arXiv:1410.3988*, 2014.

[38] A. Einolghozati, M. Sardari, and F. Fekri, "Design and analysis of wireless communication systems using diffusion-based molecular communication among bacteria," *Wireless Communications, IEEE Transactions on*, vol. 12, no. 12, pp. 6096–6105, 2013.

[39] A. Noel, K. C. Cheung, and R. Schober, "Improving receiver performance of diffusive molecular communication with enzymes," *arXiv preprint arXiv:1305.1926*, 2013.

[40] R. Mosayebi, H. Arjmandi, A. Gohari, M. Nasiri-Kenari, and U. Mitra, "Receivers for diffusion based molecular communication: Exploiting memory and sampling rate," 2014.

[41] N. Michelusi, S. Pirbadian, M. Y. El-Naggar, and U. Mitra, "A stochastic model for electron transfer in bacterial cables," *Selected Areas in Communications, IEEE Journal on*, vol. 32, no. 12, pp. 2402–2416, 2014.

[42] A. Keramidas, A. J. Moorhouse, P. R. Schofield, and P. H. Barry, "Ligand-gated ion channels: mechanisms underlying ion selectivity," *Progress in Biophysics and Molecular Biology*, vol. 86, no. 2, pp. 161 – 204, 2004.

[43] M. A. Model and G. M. Omann, "Ligand-receptor interaction rates in the presence of convective mass transport," *Biophysical Journal*, vol. 69, no. 5, pp. 1712–1720, 1995.

[44] M. Pierobon and I. F. Akyildiz, "Noise analysis in ligand-binding reception for molecular communication in nanonetworks," *Signal Processing, IEEE Transactions on*, vol. 59, no. 9, pp. 4168–4182, 2011.

[45] M. U. Mahfuz, D. Makrakis, and H. T. Mouftah, "Sampling based optimum signal detection in concentration encoded molecular communication-receiver architecture and performance.," in *BIOSIGNALS*, pp. 372–376, 2013.

[46] A. Einolghozati, M. Sardari, and F. Fekri, "Capacity of diffusion-based molecular communication with ligand receptors," in *Information Theory Workshop (ITW), 2011 IEEE*, pp. 85–89, IEEE, 2011.

[47] M. Tahmasbi and F. Fekri, "On the capacity achieving probability measures for molecular receivers," in *2015 IEEE Information Theory Workshop*, IEEE, 2015.

[48] A. W. Eckford and P. J. Thomas, "Capacity of a simple intercellular signal transduction channel," *arXiv preprint arXiv:1305.2245*, 2013.

[49] D. Kilinc and O. B. Akan, "Receiver design for molecular communication," *Selected Areas in Communications, IEEE Journal on*, vol. 31, no. 12, pp. 705–714, 2013.

[50] I. Llatser, A. Cabellos-Aparicio, M. Pierobon, and E. Alarcón, "Detection techniques for diffusion-based molecular communication," *Selected Areas in Communications, IEEE Journal on*, vol. 31, no. 12, pp. 726–734, 2013.

[51] L.-S. Meng, P.-C. Yeh, K.-C. Chen, and I. F. Akyildiz, "On receiver design for diffusion-based molecular communication," *Signal Processing, IEEE Transactions on*, vol. 62, no. 22, pp. 6032–6044, 2014.

[52] Q. Liu and K. Yang, "Channel capacity analysis of a diffusion-based molecular communication system with ligand receptors," *International Journal of Communication Systems*, 2014.

[53] R. Mosayebi, H. Arjmandi, A. Gohari, M. Nasiri-Kenari, and U. Mitra, "Receivers for diffusion-based molecular communication: Exploiting memory and sampling rate," *Selected Areas in Communications, IEEE Journal on*, vol. 32, no. 12, pp. 2368–2380, 2014.

[54] H. ShahMohammadian, G. G. Messier, and S. Magierowski, "Optimum receiver for molecule shift keying modulation in diffusion-based molecular communication channels," *Nano Communication Networks*, vol. 3, no. 3, pp. 183–195, 2012.

[55] A. Noel, K. C. Cheung, and R. Schober, "Optimal receiver design for diffusive molecular communication with flow and additive noise," *arXiv preprint arXiv:1308.0109*, 2013.

[56] P.-C. Yeh, K.-C. Chen, Y.-C. Lee, L.-S. Meng, P.-J. Shih, P.-Y. Ko, W.-A. Lin, and C.-H. Lee, "A new frontier of wireless communication theory: diffusion-based molecular communications," *Wireless Communications, IEEE*, vol. 19, pp. 28 –35, Oct. 2012.

[57] S. Kadloor and R. S. Adve, "Development of a framework to study a molecular communication system," in *18th International Conf. on Computer Comm. and Networks*, 2009.

[58] L. You, R. S. Cox, R. Weiss, and F. H. Arnold, "Programmed population control by cell–cell communication and regulated killing," *Nature*, vol. 428, no. 6985, pp. 868–871, 2004.

[59] M. J. Doktycz and M. L. Simpson, "Nano-enabled synthetic biology," *Molecular systems biology*, vol. 3, no. 1, p. 125, 2007.

[60] N. Farsad, A. W. Eckford, S. Hiyama, and Y. Moritani, "On-chip molecular communication: analysis and design," *NanoBioscience, IEEE Transactions on*, vol. 11, no. 3, pp. 304–314, 2012.

[61] N. Farsad, N. R. Kim, A. W. Eckford, and C. B. Chae, "Channel and noise models for nonlinear molecular communication systems," *IEEE Journal on Selected Areas in Communications*, vol. 32, pp. 2392–2401, Dec 2014.

[62] A. Einolghozati, M. Sardari, and F. Fekri, "Networks of bacteria colonies: A new framework for reliable molecular communication networking," *Nano Communication Networks*, vol. 7, pp. 17–26, 2015.

[63] A. Einolghozati, M. Sardari, A. Beirami, and F. Fekri, "Consensus problem under diffusion-based molecular communication," in *Information Sciences and Systems (CISS), 2011 45th Annual Conference on*, pp. 1–6, IEEE, 2011.

[64] A. Einolghozati, M. Sardari, and F. Fekri, "Collective sensing-capacity of bacteria populations," in *Information Theory Proceedings (ISIT), 2012 IEEE International Symposium on*, pp. 2959–2963, IEEE, 2012.

[65] A. Einolghozati, M. Sardari, and F. Fekri, "Molecular communication between two populations of bacteria," in *Information Theory Workshop (ITW), 2012 IEEE*, pp. 437–441, IEEE, 2012.

[66] L. Hong, W. Chen, and F. Liu, "Cooperative molecular communication for nanonetwork," in *2014 Sixth International Conference on Ubiquitous and Future Networks (ICUFN)*, 2014.

[67] B. Krishnaswamy and R. Sivakumar, "Source addressing and medium access control in bacterial communication networks," in *Proceedings of the Second Annual International Conference on Nanoscale Computing and Communication*, p. 1, ACM, 2015.

[68] C. Bai, M. S. Leeson, and M. D. Higgins, "Performance of sw-arq in bacterial quorum communications," *Nano Communication Networks*, vol. 6, no. 1, pp. 3–14, 2015.

[69] C. Jiang, Y. Chen, and K. R. Liu, "Nanoscale molecular communication networks: a game-theoretic perspective," *EURASIP Journal on Advances in Signal Processing*, vol. 2015, no. 1, pp. 1–15, 2015.

[70] V. Petrov, S. Balasubramaniam, R. Lale, D. Moltchanov, Y. Koucheryavy, *et al.*, "Forward and reverse coding for chromosome transfer in bacterial nanonetworks," *Nano Communication Networks*, vol. 5, no. 1, pp. 15–24, 2014.

[71] V. Petrov, D. Moltchanov, S. Balasubramaniam, and Y. Koucheryavy, "Incorporating bacterial properties for plasmid delivery in nano sensor networks," *Nanotechnology, IEEE Transactions on*, vol. 14, no. 4, pp. 751–760, 2015.

[72] V. Loscri and A. M. Vegni, "An acoustic communication technique of nanorobot swarms for nanomedicine applications," *NanoBioscience, IEEE Transactions on*, vol. 14, no. 6, pp. 598–607, 2015.

[73] A. M. Ahmed, F. Xia, Q. Yang, H. B. Liaqat, Z. Chen, and T. Qiu, "Poster: bacteria inspired mitigation of selfish users in ad-hoc social networks," in *Proceedings of the*

15th ACM international symposium on Mobile ad hoc networking and computing, pp. 421–422, ACM, 2014.

[74] N. Michelusi, J. Boedicker, M. Y. El-Naggar, and U. Mitra, "A stochastic queuing model of quorum sensing in microbial communities," in *2015 49th Asilomar Conference on Signals, Systems and Computers*, pp. 133–138, IEEE, 2015.

[75] K. Srinivas, A. Eckford, and R. Adve, "Molecular communication in fluid media: The additive inverse gaussian noise channel," *Information Theory, IEEE Transactions on*, vol. 58, pp. 4678 –4692, July 2012.

[76] Y. Tsai, C. Rose, R. Song, and I. Mian, "An additive exponential noise channel with a transmission deadline," in *Information Theory Proceedings (ISIT), 2011 IEEE International Symposium on*, pp. 718 –722, 31 2011-aug. 5 2011.

[77] A. W. Eckford, "Molecular communication: Physically realistic models and achievable information rates." arXiv:0812.1554v1.

[78] A. W. E. Sachin Kadloor, Raviraj S. Adve, "Molecular communication using brownian motion with drift." arXiv:1006.3959v1.

[79] T. Nakano, Y. Okaie, and J.-Q. Liu, "Channel model and capacity analysis of molecular communication with brownian motion," *Communications Letters, IEEE*, vol. 16, no. 6, pp. 797–800, 2012.

[80] H. Li, S. M. Moser, and D. Guo, "Capacity of the memoryless additive inverse gaussian noise channel," *Selected Areas in Communications, IEEE Journal on*, vol. 32, no. 12, pp. 2315–2329, 2014.

[81] R. Song, C. Rose, Y.-L. Tsai, and I. Mian, "Wireless signaling with identical quanta," in *IEEE Wireless Communications and Networking Conference (WCNC)*, 2012.

[82] I. F. Akyildiz, J. M. Jornet, and M. Pierobon, "Nanonetworks: A new frontier in communications," *Communications of the ACM*, vol. 54, pp. 84–89, Nov 2011.

[83] M. S. Kuran, H. B. Yilmaz, T. Tugcu, and I. F. Akyildiz, "Modulation techniques for communication via diffusion in nanonetworks," in *Communications (ICC), 2011 IEEE International Conference on*, 2011.

[84] B. Tepekule, A. E. Pusane, H. B. Yilmaz, and T. Tugcu, "Energy efficient isi mitigation for communication via diffusion," in *Communications and Networking (Black-SeaCom), 2014 IEEE International Black Sea Conference on*, pp. 33–37, IEEE, 2014.

[85] M. E. Ortiz and D. Endy, "Engineered cell-cell communication via dna messaging," *Journal of biological engineering*, vol. 6, no. 1, pp. 1–12, 2012.

[86] A. Aijaz and A.-H. Aghvami, "Error performance of diffusion-based molecular communication using pulse-based modulation," *NanoBioscience, IEEE Transactions on*, vol. 14, no. 1, pp. 146–151, 2015.

[87] H. Arjmandi, A. Gohari, M. N. Kenari, and F. Bateni, "Diffusion-based nanonetworking: A new modulation technique and performance analysis," *Communications Letters, IEEE*, vol. 17, no. 4, pp. 645–648, 2013.

[88] T. Nakano, A. W. Eckford, and T. Haraguchi, *Molecular communication*. Cambridge University Press, 2013.

[89] L. P. Gin and I. F. Akyildiz, "Molecular communication options for long range nanonetworks," *Computer Networks*, vol. 53, no. 16, pp. 2753 – 2766, 2009.

[90] I. Llatser, E. Alarcón, and M. Pierobon, "Diffusion-based channel characterization in molecular nanonetworks," in *Computer Communications Workshops (INFOCOM WKSHPS), 2011 IEEE Conference on*, pp. 467–472, IEEE, 2011.

[91] T. Nakano and J. Shuai, "Repeater design and modeling for molecular communication networks," in *Computer Communications Workshops (INFOCOM WKSHPS), 2011 IEEE Conference on*, pp. 501 –506, April 2011.

[92] B. Atakan and O. B. Akan, "On molecular multiple-access, broadcast, and relay channels in nanonetworks," in *Proceedings of the 3rd International Conference on Bio-Inspired Models of Network, Information and Computing Sytems*, BIONETICS '08, pp. 16:1–16:8, 2008.

[93] A. Einolghozati, M. Sardari, and F. Fekri, "Relaying in diffusion-based molecular communication," in *Information Theory Proceedings (ISIT), 2013 IEEE International Symposium on*.

[94] A. Einolghozati, M. Sardari, and F. Fekri, "Decode and forward relaying in diffusion-based molecular communication between two populations of biological agents," in *Communications (ICC), 2014 IEEE International Conference on*, pp. 3975–3980, IEEE, 2014.

[95] A. Ahmadzadeh, A. Noel, and R. Schober, "Analysis and design of two-hop diffusion-based molecular communication networks," in *Global Communications Conference (GLOBECOM), 2014 IEEE*, pp. 2820–2825, IEEE, 2014.

[96] A. Ahmadzadeh, A. Noel, A. Burkovski, and R. Schober, "Amplify-and-forward relaying in two-hop diffusion-based molecular communication networks," *arXiv preprint arXiv:1504.03738*, 2015.

[97] X. Wang, M. D. Higgins, and M. S. Leeson, "Relay analysis in molecular communications with time-dependent concentration," *Communications Letters, IEEE*, vol. 19, no. 11, pp. 1977–1980, 2015.

[98] M. Farahnak-Ghazani, G. Aminian, M. Mirmohseni, A. Gohari, and M. Nasiri-Kenari, "Physical layer network coding in molecular two-way relay networks," *arXiv preprint arXiv:1604.05680*, 2016.

[99] T. Nakano, T. Suda, Y. Okaie, M. Moore, and A. Vasilakos, "Molecular communication among biological nanomachines: A layered architecture and research issues," 2014.

[100] A. Einolghozati and F. Fekri, "Error detection in diffusion-based molecular communication," in *2015 IEEE International Conference on Communications (ICC)*, pp. 1128–1133, June 2015.

[101] C. Berrou and A. Glavieux, "Near optimum error correcting coding and decoding: Turbo-codes," *Communications, IEEE Transactions on*, vol. 44, no. 10, pp. 1261–1271, 1996.

[102] T. K. Moon, "Error correction coding," *Mathematical Methods and Algorithms. Jhon Wiley and Son*, 2005.

[103] P.-Y. Ko, Y.-C. Lee, P.-C. Yeh, C.-h. Lee, and K.-C. Chen, "A new paradigm for channel coding in diffusion-based molecular communications: Molecular coding distance function," in *Global Communications Conference (GLOBECOM), 2012 IEEE*, pp. 3748–3753, IEEE, 2012.

[104] P.-J. Shih, C.-H. Lee, P.-C. Yeh, and K.-C. Chen, "Channel codes for reliability enhancement in molecular communication," *Selected Areas in Communications, IEEE Journal on*, vol. 31, no. 12, pp. 857–867, 2013.

[105] M. Mahfuz, D. Makrakis, and H. Mouftah, "Performance analysis of convolutional coding techniques in diffusion-based concentration-encoded pam molecular communication systems," *BioNanoScience*, vol. 3, no. 3, pp. 270–284, 2013.

[106] M. Leeson and M. Higgins, "Error correction coding for molecular communications," in *Communications (ICC), 2012 IEEE International Conference on*, pp. 6172–6176, 2012.

[107] A. Einolghozati and F. Fekri, "Analysis of error-detection schemes in diffusion-based molecular communication," *IEEE Journal on Selected Areas in Communications*, vol. 34, pp. 615–624, March 2016.

[108] J. Max, "Quantizing for minimum distortion," *Information Theory, IRE Transactions on*, vol. 6, no. 1, pp. 7–12, 1960.

[109] R. M. Gray and D. L. Neuhoff, "Quantization," *Information Theory, IEEE Transactions on*, vol. 44, no. 6, pp. 2325–2383, 1998.

[110] H. Gish and J. Pierce, "Asymptotically efficient quantizing," *Information Theory, IEEE Transactions on*, vol. 14, no. 5, pp. 676–683, 1968.

[111] J. Morris and V. Vandelinde, "Robust quantization of discrete-time signals with independent samples," *Communications, IEEE Transactions on*, vol. 22, no. 12, pp. 1897–1902, 1974.

[112] W. G. Bath and V. D. VandeLinde, "Robust memoryless quantization for minimum signal distortion," *Information Theory, IEEE Transactions on*, vol. 28, no. 2, pp. 296–306, 1982.

[113] D. Kazakos, "New results on robust quantization," *Communications, IEEE Transactions on*, vol. 31, no. 8, pp. 965–974, 1983.

[114] A. Einolghozati, , and F. Fekri, "Rate-distortion in molecular signal sensing with ligand receptors," in *Information Theory Proceedings (ISIT), 2015 IEEE International Symposium on*, IEEE, 2015.

[115] M. Schena, D. Shalon, R. W. Davis, and P. O. Brown, "Quantitative monitoring of gene expression patterns with a complementary dna microarray," *Science*, vol. 270, no. 5235, pp. 467–470, 1995.

[116] U. R. Müller and D. V. Nicolau, *Microarray technology and its applications*. Springer, 2005.

[117] Z. Wang, M. Gerstein, and M. Snyder, "Rna-seq: a revolutionary tool for transcriptomics," *Nature Reviews Genetics*, vol. 10, no. 1, pp. 57–63, 2009.

[118] F. Rapaport, A. Zinovyev, M. Dutreix, E. Barillot, and J.-P. Vert, "Classification of microarray data using gene networks," *BMC bioinformatics*, vol. 8, no. 1, p. 35, 2007.

[119] A. Hassibi, H. Vikalo, J. L. Riechmann, and B. Hassibi, "Real-time dna microarray analysis," *Nucleic acids research*, vol. 37, no. 20, pp. e132–e132, 2009.

[120] M. A. Khajehnejad, A. G. Dimakis, W. Xu, and B. Hassibi, "Sparse recovery of nonnegative signals with minimal expansion," *Signal Processing, IEEE Transactions on*, vol. 59, no. 1, pp. 196–208, 2011.

[121] W. Dai, M. A. Sheikh, O. Milenkovic, and R. G. Baraniuk, "Compressive sensing dna microarrays," *EURASIP journal on bioinformatics and systems biology*, vol. 2009, no. 1, p. 162824, 2009.

[122] X. Peng, C. L. Wood, E. M. Blalock, K. C. Chen, P. W. Landfield, and A. J. Stromberg, "Statistical implications of pooling rna samples for microarray experiments," *BMC bioinformatics*, vol. 4, no. 1, p. 26, 2003.

[123] C. Sabatti, S. L. Karsten, and D. H. Geschwind, "Thresholding rules for recovering a sparse signal from microarray experiments," *Mathematical biosciences*, vol. 176, no. 1, pp. 17–34, 2002.

[124] J. H. Shih, A. M. Michalowska, K. Dobbin, Y. Ye, T. H. Qiu, and J. E. Green, "Effects of pooling mrna in microarray class comparisons," *Bioinformatics*, vol. 20, no. 18, pp. 3318–3325, 2004.

[125] A. Rao, C. Renumadhavi, M. G. Chandra, and R. Srinivasan, "Compressed sensing methods for dna microarrays, rna interference, and metagenomics," *Journal of Computational Biology*, vol. 22, no. 2, pp. 145–158, 2015.

[126] Y. Prat, M. Fromer, N. Linial, and M. Linial, "Recovering key biological constituents through sparse representation of gene expression," *Bioinformatics*, vol. 27, no. 5, pp. 655–661, 2011.

[127] R. M. Kainkaryam, A. Bruex, A. C. Gilbert, J. Schiefelbein, and P. J. Woolf, "poolmc: Smart pooling of mrna samples in microarray experiments," *BMC bioinformatics*, vol. 11, no. 1, p. 299, 2010.

[128] F. Parvaresh, H. Vikalo, S. Misra, and B. Hassibi, "Recovering sparse signals using sparse measurement matrices in compressed dna microarrays," *Selected Topics in Signal Processing, IEEE Journal of*, vol. 2, no. 3, pp. 275–285, 2008.

[129] T. Elad, E. Benovich, S. Magrisso, and S. Belkin, "Toxicant identification by a luminescent bacterial bioreporter panel: application of pattern classification algorithms," *Environmental science & technology*, vol. 42, no. 22, pp. 8486–8491, 2008.

[130] O.-P. Smolander, A. S. Ribeiro, O. Yli-Harja, and M. Karp, "Identification of β-lactam antibiotics using bioluminescent escherichia coli and a support vector machine classifier algorithm," *Sensors and Actuators B: Chemical*, vol. 141, no. 2, pp. 604–609, 2009.

[131] S. Jouanneau, M.-J. Durand, P. Courcoux, T. Blusseau, and G. Thouand, "Improvement of the identification of four heavy metals in environmental samples by using

predictive decision tree models coupled with a set of five bioluminescent bacteria," *Environmental science & technology*, vol. 45, no. 7, pp. 2925–2931, 2011.

[132] G. Zararsiz, D. Goksuluk, S. Korkmaz, V. Eldem, I. P. Duru, A. Ozturk, and T. Unver, "Classification of rna-seq data via bagging support vector machines," *bioRxiv*, p. 007526, 2014.

[133] A. Einolghozati, J. Zou, A. Abdi, and F. Fekri, "Micro-rna profile detection via factor graphs," in *To appear in the 17th IEEE International workshop on Signal Processing advances in Wireless Communications (SPAWC)*, IEEE, 2016.

[134] Q. Xie and A. R. Barron, "Minimax redundancy for the class of memoryless sources," *IEEE Transactions on Information Theory*, vol. 43, no. 2, pp. 646–657, 1997.

[135] peter J. Thomas, D. J. Spencer, S. K. hampton, P. Park, and J. P. Zurkus, "The diffusion mediated biochemical relay channel," in *17th Annual Conference on Neural Information Processing Systems (NIPS '03)*, 2003.

[136] T. Cover and J. Thomas, *Elements of Information Theory*. Wiley-Interscience, 1990.

[137] C. E. Shannon, "A mathematical theory of communication," *Bell System Technical Journal*, vol. 27, pp. 379–423, 1948.

[138] A. Milton and I. Stegun, *Handbook of Mathematical Functions with Formulas, Graphs, and Mathematical Tables*. New York: Dover, 1964.

[139] B. Krishnaswamy, C. M. Austin, J. P. Bardill, D. Russakow, G. L. Holst, B. K. Hammer, C. R. Forest, and R. Sivakumar, "Time-elapse communication: Bacterial communication on a microfluidic chip," *Communications, IEEE Transactions on*, vol. 61, no. 12, pp. 5139–5151, 2013.

[140] C. Waters and et al., "Control of the type 3 secretion system in vibrio harveyi by quorum sensing through repression of exsa.," *Applied and environmental Biology*, vol. 76, pp. 4996–5004, June 2010.

[141] M. Pierobon and I. Akyildizt, "Diffusion-based noise analysis for molecular communication in nanonetworks," *IEEE Transactions on Signal Processing*, vol. 59, no. 6, June 2011.

[142] P. Haggie and A. Verkman, "Gfp sensors," in *Advanced Concepts in Fluorescence Sensing* (C. Geddes and J. Lakowicz, eds.), vol. 10 of *Topics in Fluorescence Spectroscopy*, pp. 21–40, Springer US, 2005.

[143] C. M. Austin, W. Stoy, P. Su, M. C. Harber, J. P. Bardill, B. K. Hammer, and C. R. Forest, "Modeling and validation of autoinducer-mediated bacterial gene expression in microfluidic environments," *Biomicrofluidics*, vol. 8, no. 3, p. 034116, 2014.

[144] D. G. Brennan, "Linear diversity combining techniques," *Proceedings of the IRE*, vol. 47, no. 6, pp. 1075–1102, 1959.

[145] T. Wang, A. Cano, G. Giannakis, and J. Laneman, "High-performance cooperative demodulation with decode-and-forward relays," *Communications, IEEE Transactions on*, vol. 55, no. 7, pp. 1427–1438, 2007.

[146] A. Nosratinia, T. Hunter, and A. Hedayat, "Cooperative communication in wireless networks," *Communications Magazine, IEEE*, vol. 42, no. 10, pp. 74–80, 2004.

[147] R. W. Yeung, *A first course in information theory*, vol. 1. Springer, 2002.

[148] R. E. Bellman and S. E. Dreyfus, *Applied dynamic programming*. Rand Corporation, 1962.

[149] S. C. Madeira and A. L. Oliveira, "Biclustering algorithms for biological data analysis: a survey," *IEEE/ACM Transactions on Computational Biology and Bioinformatics (TCBB)*, vol. 1, no. 1, pp. 24–45, 2004.

[150] Y. Cheng and G. M. Church, "Biclustering of expression data.," in *Ismb*, vol. 8, pp. 93–103, 2000.

[151] M. Blaum, *Codes for detecting and correcting unidirectional errors*. IEEE Computer Society Press, 1993.

[152] J. M. Berger, "A note on error detection codes for asymmetric channels," *Information and Control*, vol. 4, no. 1, pp. 68–73, 1961.

[153] H. ShahMohammadian, G. Messier, and S. Magierowski, "Blind synchronization in diffusion-based molecular communication channels," *Communications Letters, IEEE*, vol. 17, pp. 2156–2159, November 2013.

[154] P. Mehta, S. Goyal, T. Long, B. L. Bassler, and N. S. Wingreen, "Information processing and signal integration in bacterial quorum sensing.," *Mol Syst Biol*, vol. 5, p. 325, 2009.

[155] T. Fine, "Optimum mean-square quantization of a noisy input (corresp.)," *Information Theory, IEEE Transactions on*, vol. 11, no. 2, pp. 293–294, 1965.

[156] C. E. Shannon, "Coding theorems for a discrete source with a fidelity criterion," *IRE Nat. Conv. Rec*, vol. 4, no. 142-163, p. 1, 1959.

[157] R. E. Blahut, "Computation of channel capacity and rate-distortion functions," *Information Theory, IEEE Transactions on*, vol. 18, no. 4, pp. 460–473, 1972.

[158] A. Abdi, A. Einolghozati, and F. Fekri, "Rate-distortion and optimal minimax quantizer in molecular signal sensing with ligand receptors," *submitted to IEEE Transactions on Molecular, Biological, and Multi-Scale Communications*, 2016.

[159] G. Casella and R. Berger, *Statistical Inference*. Duxbury advanced series in statistics and decision sciences, Thomson Learning, 2002.

[160] C. C. Liu and A. P. Arkin, "The case for rna," *science*, vol. 330, no. 6008, pp. 1185–1186, 2010.

[161] E. Van Rooij, E. N. Olson, *et al.*, "Micrornas: powerful new regulators of heart disease and provocative therapeutic targets," *The Journal of clinical investigation*, vol. 117, no. 117 (9), pp. 2369–2376, 2007.

[162] B. D. Brown, B. Gentner, A. Cantore, S. Colleoni, M. Amendola, A. Zingale, A. Baccarini, G. Lazzari, C. Galli, and L. Naldini, "Endogenous microrna can be broadly exploited to regulate transgene expression according to tissue, lineage and differentiation state," *Nature biotechnology*, vol. 25, no. 12, pp. 1457–1467, 2007.

[163] A. Lichtenstein, "Cancer research: A hurdle race," *Biochemistry (Moscow)*, vol. 5, no. 79, pp. 385–390, 2014.

[164] C. M. Croce, "Oncogenes and cancer," *New England Journal of Medicine*, vol. 358, no. 5, pp. 502–511, 2008.

[165] P. S. Meltzer, "Cancer genomics: small rnas with big impacts," *Nature*, vol. 435, no. 7043, pp. 745–746, 2005.

[166] F. R. Kschischang and B. J. Frey, "Iterative decoding of compound codes by probability propagation in graphical models," *Selected Areas in Communications, IEEE Journal on*, vol. 16, no. 2, pp. 219–230, 1998.

[167] P. F. Felzenszwalb and D. P. Huttenlocher, "Efficient belief propagation for early vision," *International journal of computer vision*, vol. 70, no. 1, pp. 41–54, 2006.

[168] E. Ayday and F. Fekri, "A belief propagation based recommender system for online services," in *Proceedings of the fourth ACM conference on Recommender systems*, pp. 217–220, ACM, 2010.

[169] R. J. Bloom, S. M. Winkler, and C. D. Smolke, "A quantitative framework for the forward design of synthetic mirna circuits," *Nature methods*, vol. 11, no. 11, pp. 1147–1153, 2014.

[170] A. Lichtenstein, "Cancer research: A hurdle race," *Biochemistry (Moscow)*, vol. 5, no. 79, pp. 385–390, 2014.

[171] S. S. Jeffrey, "Cancer biomarker profiling with micrornas," *Nature biotechnology*, vol. 26, no. 4, pp. 400–401, 2008.

[172] Y. Benenson, "Synthetic biology with rna: progress report," *Current opinion in chemical biology*, vol. 16, no. 3, pp. 278–284, 2012.

[173] K. P. Murphy, Y. Weiss, and M. I. Jordan, "Loopy belief propagation for approximate inference: An empirical study," in *Proceedings of the Fifteenth conference on Uncertainty in artificial intelligence*, pp. 467–475, Morgan Kaufmann Publishers Inc., 1999.

[174] H. Dweep, C. Sticht, P. Pandey, and N. Gretz, "mirwalk–database: prediction of possible mirna binding sites by walking the genes of three genomes," *Journal of biomedical informatics*, vol. 44, no. 5, pp. 839–847, 2011.

[175] S. Griffiths-Jones, R. J. Grocock, S. Van Dongen, A. Bateman, and A. J. Enright, "mirbase: microrna sequences, targets and gene nomenclature," *Nucleic acids research*, vol. 34, no. suppl 1, pp. D140–D144, 2006.

[176] D. Betel, M. Wilson, A. Gabow, D. S. Marks, and C. Sander, "The microrna. org resource: targets and expression," *Nucleic acids research*, vol. 36, no. suppl 1, pp. D149–D153, 2008.

[177] B. Xie, Q. Ding, H. Han, and D. Wu, "mircancer: a microrna–cancer association database constructed by text mining on literature," *Bioinformatics*, p. btt014, 2013.

[178] S.-D. Hsu, F.-M. Lin, W.-Y. Wu, C. Liang, W.-C. Huang, W.-L. Chan, W.-T. Tsai, G.-Z. Chen, C.-J. Lee, C.-M. Chiu, *et al.*, "mirtarbase: a database curates experimentally validated microrna–target interactions," *Nucleic acids research*, p. gkq1107, 2010.

[179] X. Wang, "mirdb: a microrna target prediction and functional annotation database with a wiki interface," *Rna*, vol. 14, no. 6, pp. 1012–1017, 2008.

[180] Q. Jiang, Y. Wang, Y. Hao, L. Juan, M. Teng, X. Zhang, M. Li, G. Wang, and Y. Liu, "mir2disease: a manually curated database for microrna deregulation in human disease," *Nucleic acids research*, vol. 37, no. suppl 1, pp. D98–D104, 2009.